UC San Diego
UC San Diego Electronic Theses and Dissertations

Title

Biomimetic nanoparticles for anti-inflammatory therapy

Permalink

https://escholarship.org/uc/item/93n9w2gq

Author

Zhang, Qiangzhe

Publication Date

2020

Peer reviewed|Thesis/dissertation

UNIVERSITY OF CALIFORNIA SAN DIEGO

Biomimetic Nanoparticles for Anti-Inflammatory Therapy

A dissertation submitted in partial satisfaction of
the requirements of the degree
Doctor of Philosophy

in

Nanoengineering

by

Qiangzhe Zhang

Committee in charge:

      Professor Liangfang Zhang, Chair
      Professor Shaochen Chen
      Professor David Gonzalez
      Professor Jesse Jokerst
      Professor Peter Yingxiao Wang

2020

The Dissertation of Qiangzhe Zhang is approved, and it is acceptable in quality and form for

publication on microfilm and electronically:

_____

_____

_____

_____

_____

Chair

University of California San Diego

2020

DEDICATION

This dissertation is dedicated to my family: Fengshou Zhang, Xiaoyan Qiang, Shifang Qiang, Huifang Liu, Xinhai Zhang, and Xiuyun Yang, who nurtured me with all their hearts to be a curious and responsible man. Thank you for blessing me with a loving family to grow up in.

This dissertation is also dedicated to my girlfriend, Yumeng Gu, who inspired me profoundly with her love and positivity during my journey through college and graduate school. Thank you for being an amazing partner and my best friend.

I am forever grateful to have them in my life. All my work would never happen without their support.

EPIGRAPH

"In the end, it's not the years in your life that count. It's the life in your years."
----Abraham Lincoln

TABLE OF CONTENTS

LIST OF FIGURES

LIST OF TABLES

ACKNOWLEDGEMENTS

First and foremost, I would like to thank my PhD advisor, Professor Liangfang Zhang for his guidance and support throughout my undergraduate and graduate journey. His deep understanding of science and charismatic personality convinced me to become a scientist and benefit the society. His constant belief in me since the first day we met has led to many incredible opportunities that transformed me into who I am today. I will always set him as my role model and strive to follow his vision, kindness, and integrity.

I would then like to give special thanks to my mentor, Dr. Weiwei Gao, from whom I have learned so much about life and science. I started working with Dr. Weiwei Gao as an undergraduate research assistant without any lab experience. Over the years, he patiently taught me everything he knew, shaping me into a capable researcher and a decent person in life. I will always emulate his ethics and integrity and remember the hardship and laughter we shared throughout my journey in Zhang lab.

I would also like to thank my labmates, Dr. Hua Gong, Dr. Xiangzhao Ai, Yao Jiang, Jia Zhuang, Yaou Duan, Jiarong Zhou, Joon Ho Park, Maya Holay, Shuyan Wang, Dan Wang, Zhongyuan Guo, Jiyoung Heo, for being such an incredibly creative and inspiring cohort. I feel honored working alongside all of you everyday. In addition, I would like to express my appreciation for all brilliant researchers I have learned from in the past, Drs. Che-Ming Jack Hu, Brian T. Luk, Soracha Thamphiwatana, Pavimol Angsantikul, Ashley Kroll, Diana Dehaini and Yue Zhang, and visiting scholars Wansong Chen, Xinxin Zhang, Xiaoli Wei, Yijie Chen, Fang Chen, Lifen Zhang, Jie Gao, Man Ying, and Danni Ran, for teaching me the way to succeed in research. Finally, I would like to thank all current and past undergraduate lab members for offering

me a chance to relay my understanding of research to them: Xiangyu Chen, Matthew Yu, Nai-Wen Chang, Enhao Ma, Julia Zhou, Zahra Mesrizadeh, and Letitia Horan. Particularly, I would like to thank Xiangyu Chen and Julia Zhou for dedicating considerable amount of their time and effort in the lab, delivering consistent and reliable results for my projects.

In addition, I would like to thank the UCSD Jacobs Scholars Program, UCSD International Center, for recognizing my work and providing funding for my graduate studies.

Last, but not least, I would like to thank UC San Diego, where I have spent almost 10 years of my life, for being an inclusive and progressive campus. Particularly, I am grateful to Dana Jimenez, Ji Song, and Graduate Division staff for providing heartwarming support throughout my graduate study.

Chapter 4.1, in full, is a reprint of the material as it appears in *Angewandte Chemie International Edition*, 2020, Qiangzhe Zhang, Ronnie H. Fang, Weiwei Gao, and Liangfang Zhang. The dissertation author was the primary author of this paper.

Chapter 4.2, in full, is a reprint of the material in preparation for submission to *Nature Biomedical Engineering*, 2020, Qiangzhe Zhang, Julia Zhou, Jiarong Zhou, Ronnie H. Fang, Weiwei Gao, and Liangfang Zhang. The dissertation author was the primary author of this manuscript.

VITA

2015   B.S. in Chemical Engineering, University of California San Diego, U.S.A.

2016   M.S. in NanoEngineering, University of California San Diego, U.S.A.

2020   Ph.D. in NanoEngineering, University of California San Diego, U.S.A.

PUBLICATIONS

1. <u>Zhang, Q.</u>; Fang, R.; Gao, W.; Zhang, L.* "A biomimetic nanoparticle to 'lure and kill' phospholipase A2", *Angewandte Chemie International Edition* 2020, doi: 10.1002/anie.202002782.

2. <u>Zhang, Q.</u>; Gong, H.; Gao, W.; Zhang, L.* "Recent progress in capturing and neutralizing inflammatory cytokines", *CCS Chemistry* 2020, in press.

3. Zhuang, J.; Gong, H.; Zhou, J.; <u>Zhang, Q.</u>; Gao, W.; Fang, R.; Zhang, L.* "Targeted gene silencing in vivo by platelet membrane-coated metal-organic framework nanoparticles", *Science Advances* 2020, *6*, eaaz6108.

4. Zhang, Y.; Miyamoto, Y.; Ihara, S.; Yang, J.; Zuill, D.; Angsantikul, P.; <u>Zhang, Q.</u>; Gao, W.; Zhang, L.*; Eckmann, L. "Composite thermoresponsive hydrogel with auranofin-loaded nanoparticles for topical treatment of vaginal trichomonad infection", *Advanced Therapeutics* 2019, *2*, 1900157.

5. Zhang, F.; Zhuang, J.; Estaban-Fernández de Avila, B.; Tang, S.; <u>Zhang, Q.</u>; Fang, R.; Zhang, L.*; Wang, J. "A nanomotor-based active delivery system for intracellular oxygen transport", *ACS Nano* 2019, *13*(10), 11996-12005.

6. Zhang, Y.; Chen, Y.; Lo, C.; Zhuang, J.; Angsantikul, P.; <u>Zhang, Q.</u>; Wei, X.; Zhou, Z.; Obonyo, M.; Fang, R. H.; Gao, W.; Zhang, L.* "Inhibition of pathogen invasion by bacterial outer membrane-coated nanoparticles", *Angewandte Chemie International Edition* 2019, *58*, 11404-11408.

7. Wei, X.; Ran, D.; Campeau, A.; Xiao, C.; Zhou, J.; Dehaini, D.; Jiang, Y.; Kroll, A.; <u>Zhang, Q.</u>; Gao, W.; Gonzalez, D.; Fang, R. H.; Zhang, L.* "Multiantigenic nanotoxoid for antivirulence vaccination against antibiotic-resistant gram-negative bacteria", *Nano Letters* 2019, *19*, 4760-4769.

8. Gong, H.; Chen, F.; Huang, Z.; Gu, Y.; <u>Zhang, Q.</u>; Chen, Y.; Zhang, Y.; Zhuang, J.; Cho, Y.-K.; Fang, R. H.; Gao, W.; Xu, S.; Zhang, L.* "Biomembrane-modified field effect transistors for sensitive and quantitative detection of biological toxins and pathogens", *ACS Nano* 2019, *13* (3), 3714-3722.

9. <u>Zhang, Q.</u>; Dehaini, D.; Zhang, Y.; Zhou, J.; Chen, X.; Zhang, L.; Fang, R. H.; Gao, W.; Zhang, L.* "Neutrophil membrane-coated nanoparticles inhibit synovial inflammation and alleviate joint damage in inflammatory arthritis", *Nature Nanotechnology* 2018, *13*, 1182-1190.
Highlighted: *Nature Nanotechnology* 2018, *13*, 1098-1099 (News and Views)
                 Nature Reviews Rheumatology 2018, *14*, 622.
                 Science Translational Medicine 2018, *10 (459)*, eaav0341.

10. Kim, T.; <u>Zhang, Q.</u>; Li, J.; Zhang, L.; Jokerst, J.* "A gold/silver hybrid nanoparticle for treatment and photoacoustic imaging of bacterial infection", *ACS Nano* 2018, *12*, 5615-5625.

11. Angsantikul, P.; Thamphiwatana, S.; <u>Zhang, Q.</u>; Spiekermann, K.; Zhuang, J.; Fang, R.; Gao, W.; Obonyo, M.; Zhang, L.* "Coating nanoparticles with gastric epithelial cell membrane for targeted antibiotic delivery against Helicobacter pylori infection", *Advanced Therapeutics* 2018, *1*, 1800016.

12. Gao, W.; Chen, Y.; Zhang, Y.; <u>Zhang, Q.</u>; Zhang, L.* "Nanoparticle-based local antimicrobial drug delivery", *Advanced Drug Delivery Reviews* 2017, *127*, 46-57.

13. Zhang, X.; Angsantikul, P.; Ying M.; Zhuang, J.; <u>Zhang, Q.</u>; Wei, X.; Jiang, Y.; Zhang, Y.; Dehaini, D.; Chen, M.; Chen, Y.; Gao, W.; Fang, R.; Zhang, L.* "Remote loading of small molecule therapeutics into cholesterol-enriched cell membrane-derived vesicles", *Angewandte Chemie International Edition* 2017, *56*, 14075-14079.

14. Thamphiwatana, S.; Angsantikul, P.; Escajadillo, T.; <u>Zhang, Q.</u>; Olsan, J.; Luk, B.; Zhang, S.; Fang, R.; Gao, W.; Nizet, V.; Zhang, L.* "Macrophage-like nanoparticles concurrently absorbing endotoxins and proinflammatory cytokines for sepsis management", *Proceedings of the National Academy of Sciences* 2017, *114*, 11488-11493.

15. Chen, W.; <u>Zhang, Q.</u>; Luk, B.; Fang, R.; Liu, Y.; Gao, W.; Zhang, L.* "Coating nanofiber scaffolds with beta-cell membrane and promote cell proliferation and function", *Nanoscale* 2016, *8*, 10364-10370.

16. Gao, W.; Zhang, Y.; <u>Zhang, Q.</u>; Zhang, L.* "Nanoparticle-hydrogel: A hybrid biomaterial system for localized drug delivery", *Annals of Biomedical Engineering* 2016, *44*, 2049-2061.

17. Wang, F.; Gao, W.; Thampiwatana, S.; Luk, B.; Angsantikul, P.; <u>Zhang, Q.</u>; Hu, C-M.; Fang, R.; Copp, J.; Pornpattananangkul, D.; Lu, W.; Zhang, L.* "Hydrogel retaining toxin-absorbing nanosponges for local treatment of methicillin-resistant Staphylococcus aureus infection", *Advanced Materials* 2015, *27*, 3437-3443.

18. Gao, W.; Fang, R.; Thamphiwatana, S.; Luk, B.; Li, J.; Angsantikul, P.; <u>Zhang, Q.</u>; Hu, C-M.; Zhang, L.* "Modulating Anti-bacterial Immunity via Bacterial Membrane-coated

Nanoparticles", *Nano Letters* 2015, *15*, 1403-1409.

19. Thamphiwatana, S.; Gao, W.; Pornpattananangkul, D.; <u>Zhang, Q.;</u> Fu, V.; Li, J.; Li, J.; Obonyo, M.; <u>Zhang, L.*</u> "Phospholipase A2-responsive antibiotic delivery via nanoparticle-stabilized liposomes for the treatment of bacterial infection", *Journal of Materials Chemistry B* 2014, *2*, 8201-8207.

20. Gao, W.: Vecchio, D.; Li, J.; Zhu, J.; <u>Zhang, Q.;</u> Fu, V.; Li, J.; Thamphiwatana, S.; Lu, D.; Zhang, L.* "Hydrogel containing nanoparticle-stabilized liposomes for topical antimicrobial delivery", *ACS Nano* 2014, *8*, 2900-2907.

ABSTRACT OF THE DISSERTATION

Biomimetic Nanoparticles for Anti-Inflammatory Therapy

by

Qiangzhe Zhang

Doctor of Philosophy in NanoEngineering

University of California San Diego, 2020

Professor Liangfang Zhang, Chair

Nanomedicine is a flourishing scientific field involving the design and control of matter on the nanometer scale for therapeutic use. One emerging avenue within the nanomedicine field is biodetoxification-based therapy, in which nano-sized structures are used to capture and retain biotoxins that would otherwise attack host cells, cause cellular damage, and trigger damage-

associated signaling pathways to propagate diseases. Particularly, inflammation is a biological process that involves complex signaling networks and disease-specific cellular responses, posing significant challenge for designing medicine with high specificity and potency. To this end, the design flexibility of nanoparticle size and surface modification, and unique particle-cell interaction at the nanoscale can lead to novel and efficacious routes for anti-inflammatory therapy.

Herein, we discuss the new generations of cell membrane-coated nanoparticles specifically tailored for biodetoxification-based anti-inflammatory therapy. Firstly, recent advances in neutralizing inflammatory cytokine will be discussed. The second portion of this dissertation will present neutrophil membrane-coated nanoparticle (neutrophil-NP) for therapeutic treatment of inflammatory arthritis. Neutrophil-NPs targeted and penetrated into the inflamed tissue, and effectively neutralized inflammatory cytokines. The third portion will cover the development of macrophage membrane-coated nanoparticle for neutralization of bacterial endotoxin and inflammatory cytokines, and management of bacterial sepsis. Finally, we will focus on the design of a unique 'lure and kill' nanoparticle for effective inhibition of phospholipase A2 (PLA2). The cell membrane works synergistically with a PLA2 attractant to 'lure' PLA2 for attack, then the PLA2 inhibitor in the cell membrane further 'kills' the enzyme. With effective inhibition of venomous PLA2, these nanoparticles further demonstrated strong inhibitory activity against PLA2 and attenuation of the inflammatory cascade during acute pancreatitis progression.

This dissertation will serve as a paradigm for rational design of cell membrane-coated nanoparticles for therapeutic treatment of inflammatory disorders. By tapping into the biological challenges associated with anti-inflammatory therapy, cell membrane-coated nanoparticles can be tailored towards its designated biological target. By harnessing the design flexibility, this

nanotechnology holds great potential to be developed into a class of drug-free anti-inflammatory

nanomedicine that will be extraordinarily valuable for biomedical researchers and clinicians alike.

Chapter 1

Introduction

1.1 Introduction

Inflammation is a vital and dynamic process of the immune system in response to injury and infection.[1, 2] In this process, inflammatory cytokines secreted by immune cells play vital roles in upregulating immune reactions that drive the immune system to remove harmful stimuli, restore tissue homeostasis, and initiate the healing process.[3] However, when the production of inflammatory cytokines becomes excessive, inflammation remains unresolved and inflammatory disorders arise.[4] For example, pathological 'cytokine storm' occurs in sepsis as a result of uncontrolled inflammatory responses to bacterial infections, which contributes to the high morbidity and mortality of the disease.[5, 6] In the process of wound healing, an uncontrolled cytokine production by the immune cells can lead to destruction of the wound tissue and promote further infiltration of the immune cells, which together perpetuate a vicious circle of chronic inflammation.[7, 8] Moreover, in the case of inflammatory arthritis, an elevated level of various inflammatory cytokines are responsible for aggravating and sustaining joint inflammation, leading to long-standing synovitis, bone destruction, and ultimately joint dysfunction.[9, 10]

The essential roles played by inflammatory cytokines in numerous disorders have motivated the development of therapeutic agents aiming to attenuate their bioactivity through various mechanisms.[11, 12] For instance, some therapeutic agents directly bind with cytokines for neutralization, whereas others bind with cognate receptors on the target cell surface to block their interaction with incoming cytokines.[13] Some agents induce the internalization or downregulation of cytokine receptors of the target cells, therefore restricting cytokine-triggered cell activation.[14] In addition, compounds that induce the clearance of the target cells are also used to reduce the overall cytokine response.[15] In general, anti-cytokine agents that directly capture and neutralize cytokines can avoid interactions with cytokine receptors on the target cells

2

and thus are less likely to be internalized and cleared by the target cells. Moreover, capturing and neutralizing free cytokines instead of targeting cell receptors also reduces the transmission of intracellular signals, which may elicit adverse events such as transient cytokine release and mitogenic activity.[16] Overall, these therapeutic advantages make anti-cytokine agents directly capturing and neutralizing inflammatory cytokines a highly attractive approach for the treatment of various inflammatory disorders.

In this article, we review recent progress in developing cytokine-neutralizing agents with a focus on platform technologies that directly capture and neutralize inflammatory cytokines (**Figure 1.1**). Based on their mechanisms of action, some anti-cytokine agents are 'monoplex', which bind with a specific cytokine for neutralization. In this category, cytokine-neutralizing antibodies represent the most dominant and rapidly growing class of anti-cytokine therapeutics. We provide a thorough review of cytokine-neutralizing antibodies currently in clinical use. In addition to free antibodies, biomaterial-conjugated antibodies are emerging with unique applications through their altered pharmacokinetic profiles and biodistribution *in vivo*. In contrast to monoplex platforms, 'multiplex' anti-cytokine agents are able to concurrently neutralize multiple cytokines that reflect the multiplexity of the cytokine targets in diseases. In this category, two emerging technologies include glycosaminoglycan (GAG)-containing biomaterials and cell membrane-coated nanoparticles. The former mimic the intracellular matrix for dynamic cytokine binding and neutralization and the latter harness natural cell membranes as broad-spectrum cytokine-neutralizing agents. Herein, we review recent progress in the rational design of each anti-cytokine platform and discuss its application by highlighting the material structure–function relationship. Overall, we believe that therapeutic platforms featuring potent, dynamic, and safe

cytokine neutralization ability are of great importance and potential for effective treatment of inflammatory diseases.
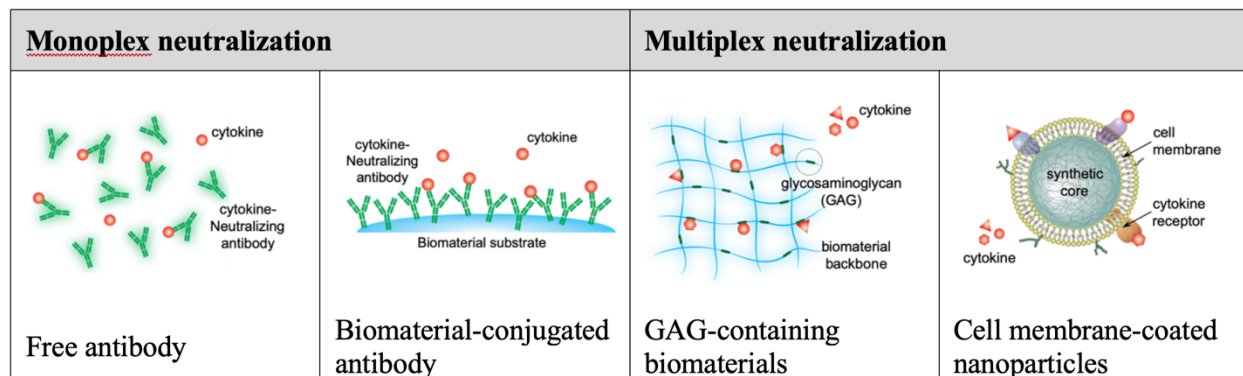
Figure 1.1. Major therapeutic platforms that directly capture and neutralize inflammatory cytokines. Monoplex platforms such as cytokine-neutralizing antibodies and antibodies conjugated with biomaterials are designed primarily with one specific cytokine as the target. Meanwhile, multiplex platforms such as glycosaminoglycan (GAG)-containing biomaterials and cell membrane-coated nanoparticles are designed for concurrently neutralizing multiple cytokines that reflect the multiplexity of cytokines involved in inflammatory diseases.

1.2 Therapeutic antibodies for monoplex cytokine neutralization

1.2.1 Free antibodies

In 1998, infliximab (Remicade) became the first antibody approved for the treatment of inflammatory disorders. Infliximab is a chimeric antibody consisting of human constant domains and mouse variable domains and it specifically binds with tumor necrosis factor (TNF) and thus blocks its bioactivity.[17] Over the next two decades following infliximab approval, the market of cytokine-neutralizing antibodies has grown significantly, with 18 monoclonal antibody products targeting various inflammatory cytokines currently approved by the US Food and Drug Administration (FDA) (**Table 1.1**).

Table 1.1. Cytokine-neutralizing antibodies in clinical use.

Target	Name	Trade name	Antibody format	Approved indications	Year of approval
TNF-α	Infliximab	Remicade	Chimeric TNF-α-specific antibody	Crohn's disease, rheumatoid arthritis, ankylosing spondylitis, psoriatic arthritis, ulcerative colitis, plaque psoriasis	1998
	Etanercept	Enbrel	Human TNFR2-Fc fusion protein	Rheumatoid arthritis, juvenile idiopathic arthritis, psoriatic arthritis, ankylosing spondylitis, plaque psoriasis	1998
	Adalimumab	Humira	Human TNF-α-specific antibody	Rheumatoid arthritis, psoriatic arthritis, ankylosing spondylitis, Crohn's disease, chronic plaque psoriasis, juvenile idiopathic arthritis, ulcerative colitis, hidradenitis suppurativa, uveitis	2002
	Certolizumab pegol	Cimzia	PEGylated Fab domain of humanized TNF-α antibody	Crohn's disease, rheumatoid arthritis, psoriatic arthritis, ankylosing spondylitis	2006
	Golimumab	Simponi	Human TNF-α-specific antibody	Rheumatoid arthritis, psoriatic arthritis, ankylosing spondylitis, ulcerative colitis	2009
IL-6	Tocilizumab	Actemra / RoActemra	Humanized IL-6R-specific antibody	Rheumatoid arthritis, juvenile idiopathic arthritis, giant cell arteritis, CAR T cell-induced cytokine release syndrome	2010
	Siltuximab	Sylvant	Chimeric IL-6-specific antibody	Multicentric Castleman's disease	2014
IL-17	Secukinumab	Cosentyx	Human IL-17-specific antibody	Plaque psoriasis, ankylosing spondylitis, psoriatic arthritis	2015
	Ixekizumab	Taltz	Humanized IL-17-specific antibody	Plaque psoriasis, psoriatic arthritis, ankylosing spondylitis	2016
	Broadalumab	Siliq	Human IL-17R-specific antibody	Plaque psoriasis	2017
IL-23	Ustekinumab	Stelara	Human IL-12/23-specific antibody	Psoriasis, psoriatic arthritis, Crohn's disease, plaque psoriasis, ulcerative colitis	2009
	Guselkumab	Tremfya	Human IL-23-specific antibody	Plaque psoriasis	2017
	Tildrakizumab	Ilumya	Humanized IL-23-specific antibody	Plaque psoriasis	2018
	Risankizumab	Skyrizi	Humanized IL-23-specific antibody	Plaque psoriasis	2019
IL-1	Canakinumab	Ilaris	Human IL-1β-specific antibody	Cryopyrin-associated periodic syndrome (CAPS), juvenile idiopathic arthritis, periodic fever syndrome	2009
IFN-γ	Emapalumab	Gamifant	Human IFN-γ-specific antibody	Primary hemophagocytic lymphohistiocytosis	2018
IL-5	Mepolizumab	Nucala	Humanized IL-5-specific antibody	Severe asthma, eosinophilic granulomatosis with polyangiitis	2015
	Reslizumab	Cinqair	Humanized IL-5-specific antibody	Severe asthma	2016

Among these approved products, chimeric antibodies were produced in genetically modified mouse hybridoma cells that secreted antibodies carrying the human constant domains.[18] The resulting antibodies displayed improved half-life and reduced immune response compared to unmodified antibodies with the mouse constant domain.[19] Later, humanized antibodies were generated by fusing the complementarity-determining regions of mouse antibody onto a human IgG framework and subsequently expressed in hybridoma cells.[20] This engineering approach reduced the incidences of anti-antibody response in patients compared to those receiving the chimeric antibodies.[21] More recently, fully human antibodies consisting of entirely human sequences were produced from transgenic mice expressing the human IgG germlines as opposed to the normal murine germlines. Alternatively, fully human antibodies were also generated through a library of bacteriophages each expressing a fragment of the human antibody to transfect bacterial cells.[22] The improved half-life and reduced percentage of immune response in human patients led to wide clinical success of fully human antibodies.[17] Meanwhile, a few antibody-like molecules have been developed for cytokine neutralization. For example, etanercept was engineered by fusion of a human tumor necrosis factor receptor 2 (TNFR2) immune adhesin onto the Fc domain of human IgG framework. The TNF receptor domain could neutralize both TNF-α and TNF-β, while the human IgG Fc domain reduced immunogenicity of the molecule.[23] In addition, certolizumab pegol adopted a chemical conjugation approach to functionalizing a humanized Fab fragment with polyethylene glycol (PEG) to improve the half-life of the antibody fragment.[24] Overall, cytokine-neutralizing antibodies constitute a flourishing family of compounds for the treatment of various inflammatory diseases.

As the cytokine-neutralizing antibodies continue to be a mainstay of therapeutic options, antibody technologies are evolving.[17, 25] There are tremendous research efforts ongoing to

further improve the performance of existing antibodies or to develop new antibodies for disease treatment. One active research area is to develop engineering approaches to prolonging the circulation half-lives of the antibodies.[26] Among various factors that affect circulation, the primary determinant is antibody binding with neonatal Fc receptor (FcRn), which rescues the antibody from lysosomal degradation and therefore promotes their recycling.[27] As a result, molecular characteristics such as pH-dependence, isoelectric property, and glycosylation have been used as design cues to generate novel antibody variants so that IgG-FcRn binding can be modulated to enhance half-life.[28] Such approaches can potentially reduce the dosage, dosing frequency, and eventually the cost of anti-cytokine treatments. Another research area lies in new antibody designs to enhance or diversify antigen-binding activity. In this perspective, bispecific antibodies that can simultaneously bind to two distinct antigens or epitopes have gained significant interests.[29] Such dual specificity has allowed antibodies to target specific tissues of inflammation for onsite cytokine neutralization.[30] The dual specificity has also been used to concurrently neutralize two cytokines, therefore inhibiting nonoverlapping proinflammatory functions for enhanced efficacy.[31] The third active research area is on product development of antibody, which increasingly emphasizes risk assessment at early stage instead of late stage.[32] In this perspective, high throughput experimental screening such as phage display have been combined with computational algorithms to predict and enhance 'developable' properties of the antibody candidates regarding manufacturing feasibility, stability in storage, and absence of off-target reactivity.[33] Overall, cytokine-neutralizing antibodies offer exciting opportunities for treating inflammatory diseases and are expected to generate long-lasting therapeutic impact.

1.2.2 Biomaterial-conjugated antibodies

One limiting factor of free antibodies stems from their dose-limiting side effects associated with the non-selective biodistribution. To address this limitation, antibodies have been increasingly conjugated with biomaterials to alter their *in vivo* pharmacokinetics and biodistribution for favorable therapeutic index. In addition, the biomaterial conjugation could also expand the use of antibodies to areas where free antibodies were unable to access. These benefits have led to cytokine-neutralizing antibodies conjugated with various biomaterial platforms including polymers, hydrogels, and nanoparticles for a wide range of biomedical applications (**Figure 1.2**).
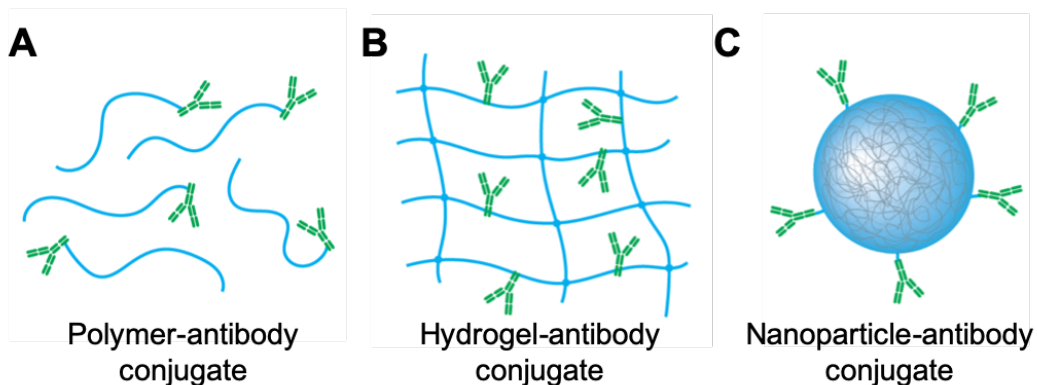
Figure 1.2. Schematic illustration of biomaterial platforms made from (A) polymers, (B) hydrogels, and (C) nanoparticles in conjugation with antibodies for cytokine capture and neutralization.

Conjugation with polymers can increase the molecular weight of the antibodies and limit their diffusion rate when administered to tissues, making the conjugates ideal for localized treatment of inflammatory conditions.[34] For example, anti-TNF-α and anti-IL-1β were conjugated with high molecular weight hyaluronic acid (HA) and used as a topical treatment for burn injury.[35] Compared to free antibodies, HA significantly increased the antibody residence time in the superficial region following the burn injury. In a rodent model of deep partial-thickness burns, the conjugates were effective in attenuating the acute inflammation and reducing the secondary necrosis. This was further validated by the fact that much less immune cells infiltrated

into the region where the polymer-antibody conjugates were retained. Notably, in polymer-antibody conjugates, the polymer backbone could affect the antibody-cytokine binding affinity depending on the use of polymers. For example, anti-IL-1β conjugated with HA or carboxymethylcellulose (CMC) showed an association kinetics comparable to that of the free antibody. However, the captured cytokines dissociated three times more slowly from the HA conjugates than from the CMC conjugates.[36] Such differential dissociation was likely due to the conformational changes of the polysaccharide as a function of antigen binding. In addition to polymer backbone, the size of cytokine targets would also affect the binding kinetics. For example, anti-TNF-α conjugated to CMC or HA both showed reduced adsorption and desorption of TNF-α when compared to free antibody. TNF-α has a molecular weight three times larger than IL-1β, which might become a determining factor in binding events and outperform the effect from the polymer backbone.

Conjugation of cytokine-neutralizing antibodies with hydrogels is another approach of modulating local inflammation while minimizing the systemic side effects associated with free antibodies. One popular application of such conjugates is to treat burn injury, where the injury progression is driven by local inflammatory cytokines through complex cascades.[37] HA hydrogel conjugated with anti-TNF-α significantly reduced the development of necrotic tissue in a rat partial-thickness burn model.[38] With the same model, the free antibody was shown to inhibit macrophage infiltration in the periphery but not at the surface, while the conjugated antibody was able to hinder macrophage infiltration at both the periphery and the surface.[39] Measurements of local antibody concentration showed that the increased antibody residence time in the superficial region strongly correlated with the pattern of inflammatory cell infiltrate in the tissue.[40] These results together demonstrated the benefit of antibody-hydrogel conjugates for

localized treatment. To study the effect of hydrogel crosslinking, anti-IL-1β and anti-TNF-α were conjugated with HA hydrogels and applied for the treatment of burn wound.[41] Intriguingly, the hydrogels were shown to bind with and neutralize cytokines *in vitro*. However, they were unable to reduce the inflammation *in vivo*. The lack of efficacy *in vivo* was attributed to the high density of the hydrogel cross-linking, which limited cytokine diffusion into the gel matrix and diminished the neutralization efficacy. This result suggests that when designing the conjugates, hydrogel crosslinking density needs to be optimized to maintain gel-like properties while maximizing cytokine influx for effective neutralization. Meanwhile, tuning residence time of cytokine-neutralizing antibodies can be an effective strategy in regulating the inflammatory response associated with acute injuries.

Cytokine-neutralizing antibodies can also be conjugated to nanoparticles for benefits including enhanced stability, specific targeting, and prolonged retention after local injection. For example, to neutralize inflammatory cytokines in arthritic joints, nanoparticles made from crosslinked chitosan and HA were conjugated with anti-IL-6 antibodies (**Figure 1.3**).[42] In this study, carbocyclic groups of the antibodies reacted specifically with the amine groups at the nanoparticle surface. The nanoparticle-antibody conjugates exhibited a stronger inhibition of macrophage activation and the effect lasted longer when compared to free anti-IL-6 antibody. The benefit was attributed to the antibody immobilization on the nanoparticles, which reduced their degradation. In another study for the treatment of acute temporal lobe epilepsy (TLE), superparamagnetic iron oxide nanoparticles were coated with polyethylene glycol (PEG) and then conjugated with anti- IL-1β antibody.[43] The resulting nanoparticle-antibody conjugates not only enhanced the neuroprotective effect in an acute rat model of TLE through IL-1β neutralization, but also targeted the magnetic nanoparticles to the astrocytes and neurons in epileptogenic tissues,

leading to a higher T2 sensitivity in magnetic resonance imaging than nanoparticles without antibody conjugation.

Figure 1.3. (A) Schematics of nanoparticles made from crosslinked chitosan and hyaluronic acid, followed by conjugation with anti-IL-6 antibodies. (B) Schematic functions of the nanoparticles in neutralizing IL-6 and reducing the inflammation in the synovial fluid. (C) *In vitro* efficacy of the nanoparticles in reducing IL-6 production from human articular chondrocytes stimulated with macrophage conditioned medium. Ctr: cells without stimulation nor treatment; No treat: stimulated cells but without treatment; NPs-Ab: stimulated cells treated with nanoparticles; Ab: stimulated cells treated with soluble antibodies. Reproduced with permission from ref 42. Copyright 2018 American Chemical Society.

1.2.3 Biomimetic platforms for multiplex cytokine neutralization

1.2.3.1 Glycosaminoglycan-functionalized hydrogels and nanoparticles

Extracellular matrix glycosaminoglycans (GAGs), such as heparan sulfate and heparin, are known to bind with a diverse range of cytokines primarily through electrostatic interactions between the positively charged amino acid residues of the cytokines and the negatively charged sulfate groups on the GAGs.[44] By varying the GAG composition, concentration, and sulfation degree, the extracellular matrix is able to modulate cytokine transport within the matrix and influence the bioactivity of the cytokines.[45] Such dynamic binding interactions have recently inspired the use of GAGs as cytokine-scavenging component to construct biomaterials for

11

capturing and neutralizing inflammatory cytokines. With the capability of modulating complex binding events and inhibiting multiple cytokines, these biomimetic materials have become a unique multiplex cytokine neutralizing platform.

GAG-based hydrogels have been synthesized to trap cytokines within tissues and thus to attenuate inflammation in chronic wounds. In one design, hydrogels were made with various desulfated heparin derivatives and cross-linked with star-shaped PEG (starPEG, **Figure 1.4**).[46] These hydrogels were able to neutralize the chemoattractant function of monocyte chemoattractant protein-1 (MCP-1) and IL-8 *in vitro* and *in vivo* when applied onto excisional wounds. This sequestration effect resulted in significantly reduced influx of immune cells into the wound. Mechanistic studies showed no binding of the less heparin-affine cytokines TNF-α, IL-1β, and IL-6 by the hydrogels, whereas chemotactic factors such as macrophage inflammatory protein 1 (MIP-1)α, MIP-1β, and epithelial neutrophil-activating protein 78 (ENA-78) interacted with the GAG-based hydrogels. Nevertheless, as a secondary effect of the reduced influx of immune cells into the wound, the overall expression of inflammatory cytokines and chemokines such as TNF-α, IL-1β, growth-regulated oncogene-α (GRO-α), and MCP-1 was also diminished. Furthermore, the capacity of the hydrogels to capture MCP-1 and IL-8 decreased as the sulfation degree of the matrix decreased. The results from this study are consistent with another study showing that the binding of strongly charged cytokines correlated with the integral space charge density of the hydrogel, while the binding of weakly charged cytokines was governed by the GAG sulfation pattern.[47] Overall, the GAG-based hydrogel was beneficial for wound healing by decreasing inflammatory signaling, leading ultimately to enhanced granulation tissue maturation, vascularization, and re-epithelialization.
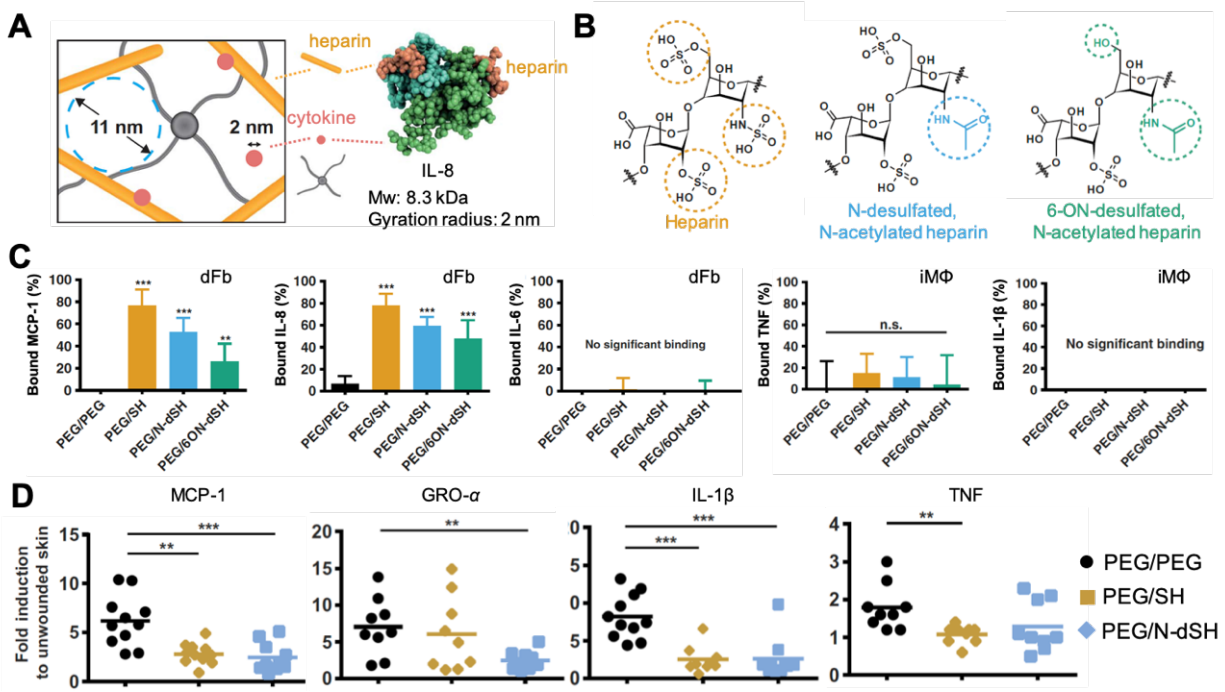
Figure 1.4. (A) Schematics of hydrogel scaffolds formed by cross-linking of starPEG and different heparin derivatives (starPEG-GAG hydrogels). The hydrogel mesh size (11 nm) and gyration radius (2 nm) of IL-8 are also depicted. (B) Structures of native heparin (SH) and selectively desulfated heparin derivatives including N-desulfated, N-acetylated heparin (N-dSH), and 6-ON-desulfated N-acetylated heparin (6ON-dSH). (C) Characterization of starPEG-GAG hydrogels binding with cell-derived MCP-1 and IL-8. Conditioned medium derived from human activated dermal fibroblast (dFb) or inflammatory macrophage (iMΦ) was incubated with the different hydrogels. After 24 hours, the remaining cytokines were quantified by ELISA, and the amounts of hydrogel-bound cytokines were calculated. Bars represent mean ± SD of data from four dFb and seven iMΦ donors. (D) Characterization of starPEG-GAG hydrogels in inhibiting inflammation during wound healing in mice. Wounds on the backs of C57BL/6 wild-type mice were inflicted by 6-mm punch biopsy and treated with hydrogel discs for 5 days. RNA was isolated from whole wound tissue, gene expression was analyzed, and expression was calculated and compared to unwounded skin. Each symbol represents one wound. Bars represent means ± SD. ANOVA with multiple comparisons versus PEG/PEG using Bonferroni t test or Dunnett's method: ***$P \leq 0.001$, **$P \leq 0.01$, *$P \leq 0.05$ (B and C). Unpaired t test: **$P \leq 0.01$, *P ≤ 0.05. Reproduced with permission from ref 46. Copyright 2017 American Association for the Advancement of Science.

Various nanoparticle formulations using GAGs as building blocks have also been developed for cytokine neutralization. For example, heparins conjugated with D-erythro-sphingosine showed a lipid-like structure and self-assembled into stable nanoparticles that suppressed the production of inflammatory cytokines including TNF-α, IL-6, and IL-1β in lipopolysaccharides (LPS)-stimulated macrophages much more strongly than native heparin.[48] The initial success also motivated the development of conjugates with a series of GAG derivatives including chondroitin sulfate (CS), HA, and low-molecular-weight heparin (LH). Such rationale design allowed for studies on the

relationship of conjugate structure and their anti-inflammatory activity, which revealed a critical role played by the degree of sulfation in determining the anti-inflammatory activity. [49] In another study, heparin-based nanogels were embedded in HA hydrogel, which exerted dual functions for the repair of brain tissue following stroke; loading VEGF for delivery to the brain followed by binding and decreasing brain levels of stroke-induced TNF-α directly at the lesion site.[50, 51] Heparin nanoparticles sequestered cytokines, reduced astrocytic scar formation, and ultimately promoted tissue repair after the stroke. Heparin was also mixed with oppositely charged chitosan oligosaccharide to form stable nanoparticles with diameters in the range of 100 to 200 nm.[52] These nanoparticles were able to bind with cytokines such as the stromal cell-derived factor 1α (SDF-1α) and VEGF while preserving their bioactivity. In another design, nanoparticles were constructed with a layer-by-layer approach; first depositing polylysine onto negatively charged polylactic acid cores, followed by depositing of a heparin shell onto the positively charged core (**Figure 1.5**).[53] The nanoparticles were further conjugated with fragments of C-C chemokine receptor type 5 (CCR5) responsible for inhibiting the CCR5 ligand-mediated leukocyte adhesion. In the study, only the combination in one "nano-trap" of heparin and CCR5 fragments imparted the strongest anti-adhesion effect in blocking the adhesion of monocyte to human umbilical vein endothelial cells (HUVECs).
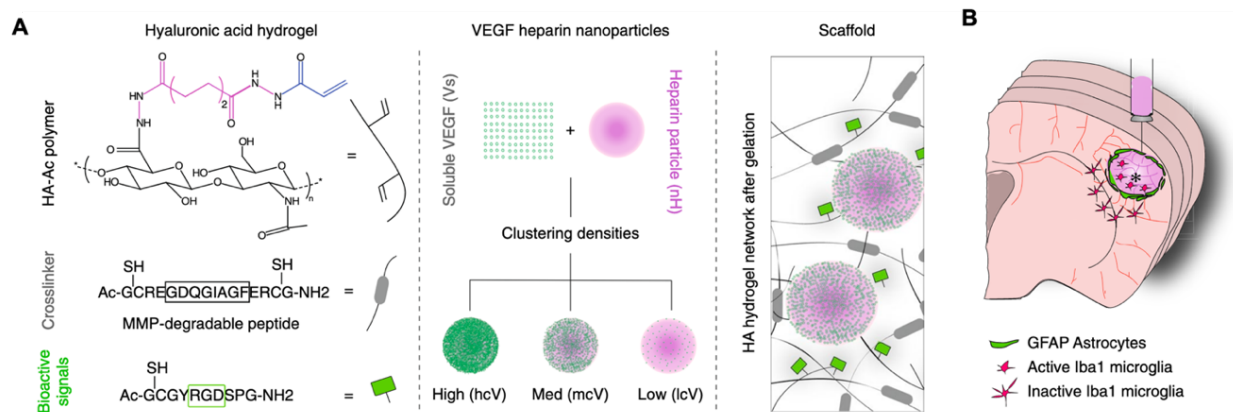
Figure 1.5. The development of an injectable hydrogel for tissue repair after stroke. (A) The hydrogel was composed of hyaluronic acid and heparin nanoparticles with VEGF clusters of varying densities. (B) Illustration of a stroke cavity within the brain, indicating the presence of astrocytes and microglia. The hydrogel containing the therapeutics was injected directly into the brain tissue cavity. Reproduced with permission from ref 51. Copyright 2017 Springer Nature Limited.

1.2.3.2 Cell membrane-coated nanoparticles

Recently, the extremely rich biological functions of cellular membranes have inspired the development of cell membrane-coated nanoparticles by wrapping natural cell membranes onto synthetic nanoparticle cores. Such top-down biomimicry allows these nanoparticles to harness cell-like functions for multifaceted biointerfacing.[54, 55] Among their emerging applications, mimicking the source cells to bind with inflammatory cytokines for neutralization has attracted much attention. By displaying the exact antigenic profile as the source cell, these cell-like nanoparticles neutralize cytokines without the need of identifying individual targets. More importantly, by acting as the decoys of the target cells, these cell membrane-coated nanoparticles capture cytokines by precisely mapping the complexity and multiplicity of cytokine-cell receptor binding in disease pathology. With these advantages, cell membrane-coated nanoparticles have emerged as a unique function-driven and multiplex cytokine neutralizing platform.

Macrophage membrane-coated nanoparticles (denoted 'MΦ-NPs') was first developed and tested for the management of sepsis (**Figure 1.6**).[56] MΦ-NPs possess an antigenic exterior

identical to the source macrophage cells, thus inheriting their capability of capturing endotoxins through the pattern recognition receptor CD14 present on the macrophage membrane. In addition, MΦ-NPs act as decoys to bind with inflammatory cytokines, hence inhibiting their ability to potentiate downstream pathological cytokine storm largely responsible for sepsis-induced lethality. These two functionalities together enable effective intervention during uncontrolled immune activation, providing a powerful therapeutic intervention for the management of sepsis. *In vitro* studies showed that MΦ-NPs neutralized not only endotoxins but also inflammatory cytokines that otherwise potentiating the sepsis cascade. In a mouse *Escherichia coli* bacteremia model, treatment with MΦ-NPs reduced inflammatory cytokine levels, inhibited bacterial dissemination, and ultimately conferred a significant survival advantage to infected mice. Overall, MΦ-NPs take advantage of the common functionality of endotoxin binding to macrophage cells, allowing for a universal neutralization approach across different Gram-negative bacterial genus, species, and strains. The top-down fabrication of MΦ-NPs effectively replicates endotoxin-binding motifs on the target cells that are otherwise difficult to identify, purify, and conjugate. Coating macrophage membranes onto nanoparticle surfaces significantly increases the surface-to-volume ratio of given membrane materials, which is critical for efficient endotoxin neutralization.
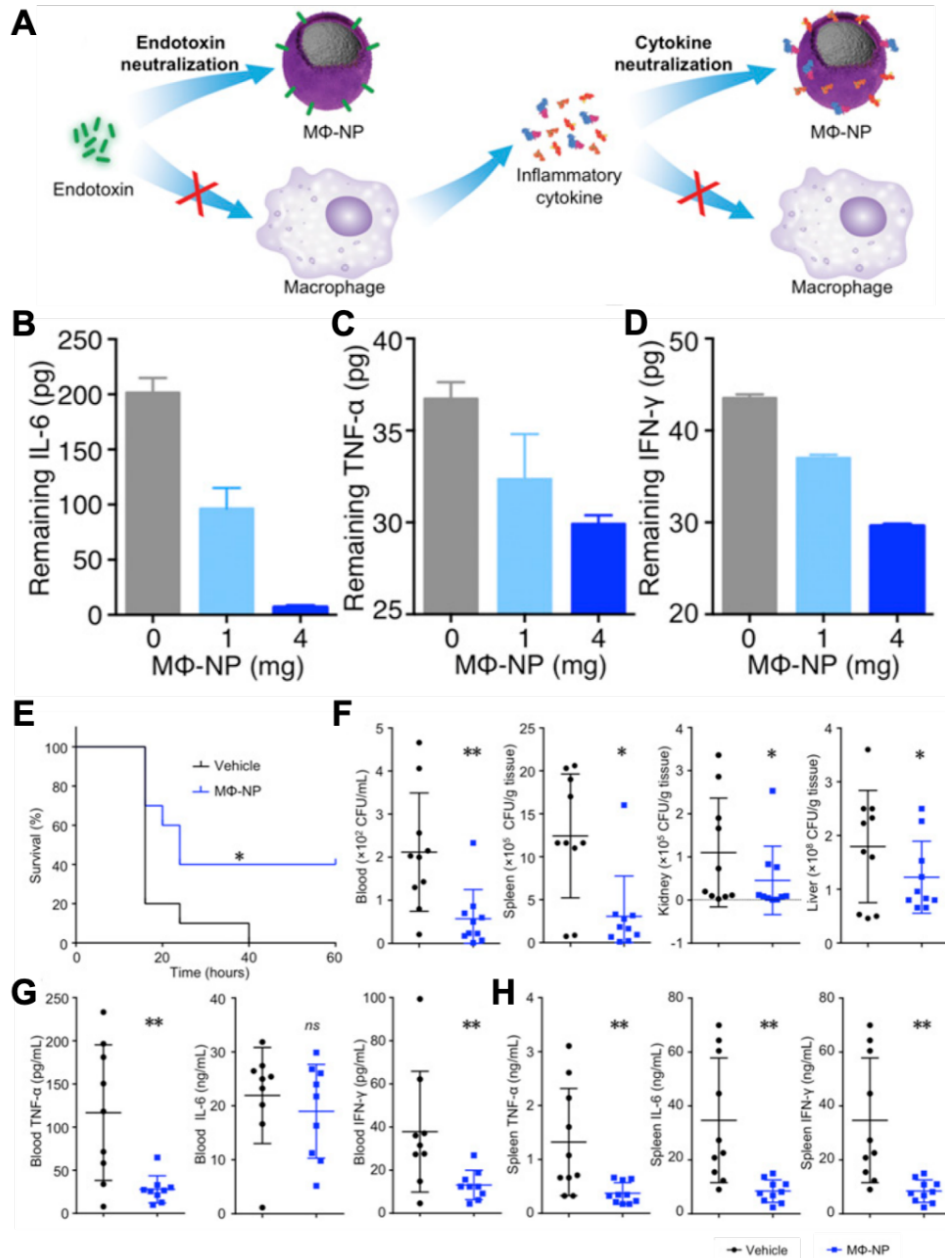
Figure 1.6. (A) Schematic illustration of using MΦ-NPs to neutralize endotoxins and inflammatory cytokines as a two-step process for sepsis management. (B-D) In vitro removal of inflammatory cytokines by MΦ-NPs, including (B) IL-6, (C) TNF-α, and (D) IFN-γ. (E-H) In vivo therapeutic efficacy of MΦ-NPs evaluated with a mouse bacteremia model. (E) Survival curve of mice with bacteremia after treatment with MΦ-NPs (n = 10). (F) Bacterial enumeration in blood, spleen, kidney, and liver at 4 h after MΦ-NPs were intraperitoneally injected. (G and H) Inflammatory cytokines, including IL-6, TNF-α, and IFN-γ, from the blood and spleen were quantified with a cytometric bead array (ns, not significant; *P ≤ 0.05, **P ≤ 0.01). Reproduced with permission from ref 56. Copyright 2017 National Academy of Sciences.

As another example, neutrophil membrane-coated nanoparticles (denoted 'neutrophil-NPs')

were developed as an anti-inflammatory strategy to treat rheumatoid arthritis (RA) (**Figure**

17

1.7).[57] Inflammation and damage in RA are mediated by the influx of an immune cell mixture into the synovial joint space.[58] Among them, neutrophils play central roles in initiating and perpetuating RA progression. Neutrophil-NPs inherit the antigenic exterior and associated membrane functions of the source cells. They were shown to neutralize hallmark cytokines including IL-1β and TNF-α that would otherwise activate and recruit neutrophils to potentiate RA progression. Through the neutralization, neutrophil-NPs effectively suppressed synovial inflammation and inhibited chondrocyte activation and apoptosis. Furthermore, neutrophil-NPs also mimicked the natural adhesion between neutrophils and chondrocytes, which subsequently enhanced their penetration into the cartilage matrix for chondrocyte targeting. Neutrophil-NPs injected into mice with collagen-induced arthritis and a human transgenic mouse model of arthritis showed significant therapeutic efficacy by ameliorating joint damage and suppressing overall arthritis severity. The promising results of using neutrophil-NPs for the treatment of RA suggest that coating cell membrane for biomaterial functionalization can lead to effective broad-spectrum cytokine neutralization for the treatment of inflammatory disorders.
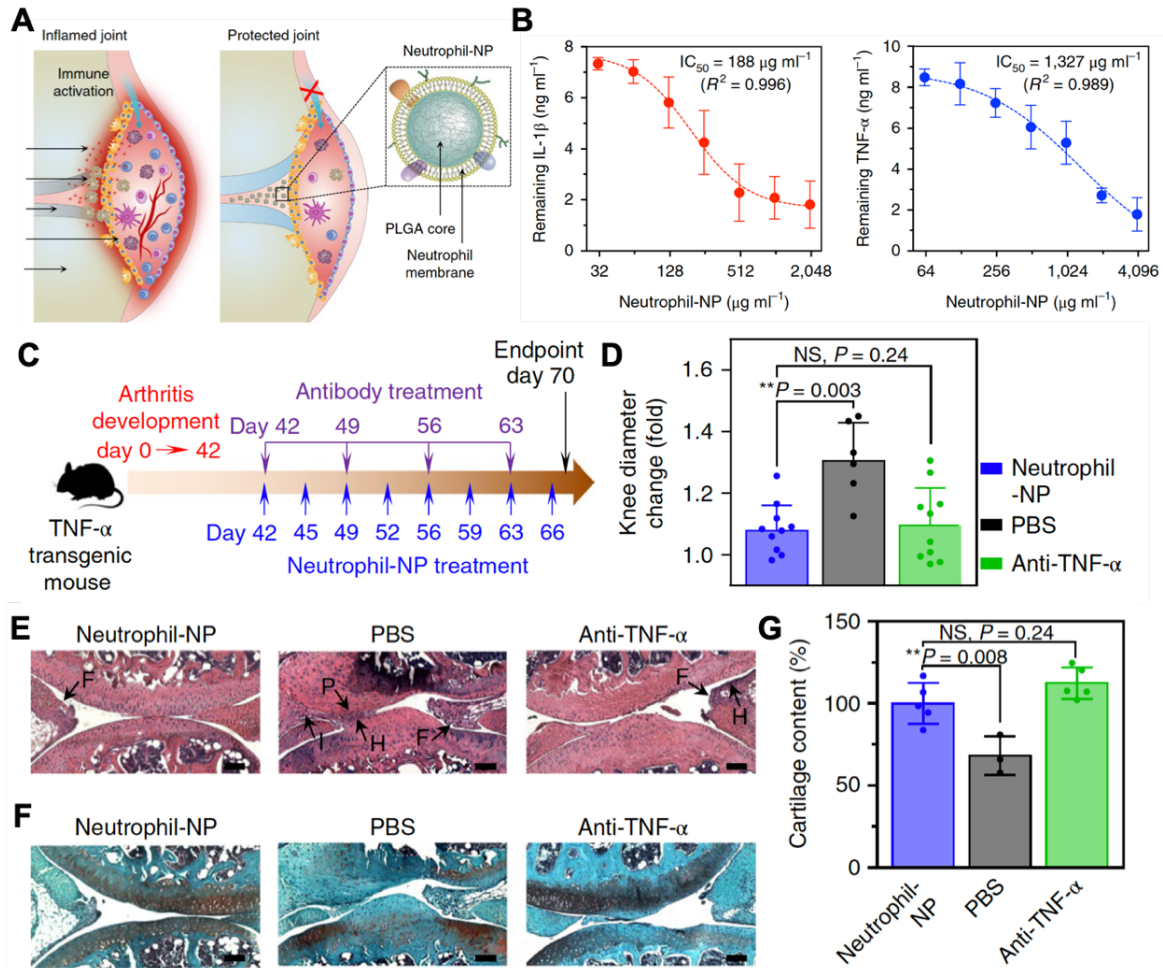
Figure 1.7. (A) Schematics of neutrophil-NPs designed for suppressing synovial inflammation and ameliorating joint destruction in inflammatory arthritis. Neutrophil-NPs were constructed by wrapping polymeric cores in natural human neutrophil membranes. (B) Binding capacity of human neutrophil-NPs with IL-1β (left) and TNF-α (right). (C) The study protocol of using neutrophil-NPs to treat inflammatory arthritis in a human TNF-α transgenic mouse model. (D) Change of hind knee diameter on day 70 compared to that on day 0. (E, F) Representative images of H&E staining (E) and safranin-O staining (F) of knee sections from mice treated with neutrophil-NPs, PBS or anti-TNF-α antibody. Scale bars, 100 μm. F, synovial membrane fibrillation; H, synovium hyperplasia; I, immune cell infiltration; P, pannus formation. (G) Cartilage content was quantified from safranin-O-stained sections of mice treated in different groups. Statistical analysis was performed using one-way ANOVA with Dunnett's post hoc analysis. Data presented as means ± s.d. *$P \leq 0.05$, **$P \leq 0.01$, ***$P \leq 0.001$. Reproduced with permission from ref 57. Copyright 2018 Springer Nature Limited.

Since its initial development, cell membrane coating technology in general has made tremendous progress. A diverse range of cell-like functions are now available on-demand by choosing membranes from appropriate source cells. Additional functions can be achieved by modifying the substrates with different materials or dimensions. Cell membrane-coated

nanoparticles are also increasingly combined with other biomaterials for synergistic functions. Overall, the cell membrane coating technology holds great promise for innovative therapeutics including anti-cytokine therapy.

1.4 Summary and outlook

The capture and neutralization of inflammatory cytokines have been shown effective in treating various inflammatory disorders. To enhance the efficacy of anti-cytokine therapy, biomaterials have been increasingly explored. Herein, we highlighted three distinct approaches to functionalizing synthetic biomaterials toward potent and safe cytokine neutralization: (1) conjugation of cytokine-neutralizing antibodies to biomaterials, (2) integration of glycosaminoglycan building blocks to biomaterial networks, and (3) use of natural cell membranes for broad-spectrum cytokine neutralization. Significant progress has been made in these areas, generating a variety of anti-cytokine platforms including polymer conjugates, hydrogels, and nanoparticles. These research outcomes have offered promising opportunities in advancing anti-cytokine therapeutics.

Toward future development, new strategies are emerging to improve biomaterial-based cytokine capture and neutralization. For example, synthetic polymeric nanoparticles have been engineered with binding affinity for specific protein targets, offering potential alternatives to biological binding ligands such as antibodies. These nanoparticles have been used to capture animal venoms, bacterial toxins, and recently cytokines for suppressing tumor angiogenesis.[59-62] Other affinity moieties such as aptamers have also been integrated with biomaterials as robust and cost-effective alternatives to antibodies for cytokine capture.[63, 64] Overall, we anticipate that combining biomaterials with cytokine capture and neutralization functionality will become a versatile approach for the treatment of various diseases including inflammatory disorders.

Chapter 1, in full, is a reprint of the material as it appears in *CCS Chemistry*, 2020, Qiangzhe Zhang, Hua Gong, Weiwei Gao, and Liangfang Zhang. The dissertation author was the primary author of this paper.

1.5 References

1.   Gupta, S.C., Kunnumakkara, A.B., Aggarwal, S., and Aggarwal, B.B., *Inflammation, a Double-Edge Sword for Cancer and Other Age-Related Diseases.* Frontiers in Immunology, 2018. **9**: p. 2160.

2.   Sugimoto, M.A., Sousa, L.P., Pinho, V., Perretti, M., and Teixeira, M.M., *Resolution of inflammation: what Controls its Onset?* Frontiers in Immunology, 2016. **7**: p. 160.

3.   Hanada, T. and Yoshimura, A., *Regulation of cytokine signaling and inflammation.* Cytokine & Growth Factor Reviews, 2002. **13**(4-5): p. 413-421.

4.   Tabas, I. and Glass, C.K., *Anti-Inflammatory Therapy in Chronic Disease: Challenges and Opportunities.* Science, 2013. **339**(6116): p. 166-172.

5.   Cavaillon, J.M., Adib-Conquy, M., Fitting, C., Adrie, C., and Payen, D., *Cytokine cascade in sepsis.* Scandinavian Journal of Infectious Diseases, 2003. **35**(9): p. 535-544.

6.   Chousterman, B.G., Swirski, F.K., and Weber, G.F., *Cytokine storm and sepsis disease pathogenesis.* Seminars in Immunopathology, 2017. **39**(5): p. 517-528.

7.   Efron, P.A. and Moldawer, L.L., *Cytokines and wound healing: The role of cytokine and anticytokine therapy in the repair response.* Journal of Burn Care & Rehabilitation, 2004. **25**(2): p. 149-160.

8.   Feng, Y., Sanders, A.J., Morgan, L.D., Harding, K.G., and Jiang, W.G., *Potential roles of suppressor of cytokine signaling in wound healing.* Regenerative Medicine, 2016. **11**(2): p. 193-209.

9.   Burmester, G.R., Feist, E., and Doerner, T., *Emerging cell and cytokine targets in rheumatoid arthritis.* Nature Reviews: Rheumatology, 2014. **10**(2): p. 77-88.

10.   Noack, M. and Miossec, P., *Selected cytokine pathways in rheumatoid arthritis.* Seminars in Immunopathology, 2017. **39**(4): p. 365-383.

11.   Dinarello, C.A., *Anti-inflammatory Agents: Present and Future.* Cell, 2010. **140**(6): p. 935-950.

12.   Kopf, M., Bachmann, M.F., and Marsland, B.J., *Averting inflammation by targeting the cytokine environment.* Nature Reviews: Drug Discovery, 2010. **9**(9): p. 703-718.

13.   Schreiber, G. and Walter, M.R., *Cytokine-receptor interactions as drug targets.* Current Opinion in Chemical Biology, 2010. **14**(4): p. 511-519.

14.   MacGlashan, D.W., *Endocytosis, recycling, and degradation of unoccupied Fc epsilon RI in human basophils.* Journal of Leukocyte Biology, 2007. **82**(4): p. 1003-1010.

15.   Guttman-Yassky, E., Vugmeyster, Y., Lowes, M.A., Chamian, F., Kikuchi, T., Kagen, M., Gilleaudeau, P., Lee, E., Hunte, B., Howell, K., Dummer, W., Bodary, S.C., and Krueger, J.G., *Blockade of CD11a by efalizurnab in psoriasis patients induces a unique state of T-cell hyporesponsiveness.* Journal of Investigative Dermatology, 2008. **128**(5): p. 1182-1191.

16.   Chatenoud, L., *Anti-CD3 antibodies: towards clinical antigen -specific immunomodulation.* Current Opinion in Pharmacology, 2004. **4**(4): p. 403-407.

17.   Chan, A.C. and Carter, P.J., *Therapeutic antibodies for autoimmunity and inflammation.* Nature Reviews Immunology, 2010. **10**(5): p. 301-316.

18.   Knight, D.M., Trinh, H., Le, J.M., Siegel, S., Shealy, D., McDonough, M., Scallon, B., Moore, M.A., Vilcek, J., Daddona, P., and Ghrayeb, J., *Construction and initial characterization of a mouse-human chimeric anti-TNF antibody.* Molecular Immunology, 1993. **30**(16): p. 1443-1453.

19.   Modjtahedi, H., Ali, S., and Essapen, S., *Therapeutic application of monoclonal antibodies in cancer: advances and challenges.* British Medical Bulletin, 2012. **104**(1): p. 41-59.

20.   Queen, C., Schneider, W.P., Selick, H.E., Payne, P.W., Landolfi, N.F., Duncan, J.F., Avdalovic, N.M., Levitt, M., Junghans, R.P., and Waldmann, T.A., *A humanized antibody that binds to the interleukin-2 receptor.* Proceedings of the National Academy of Sciences of the United States of America, 1989. **86**(24): p. 10029-10033.

21.   Hwang, W.Y.K. and Foote, J., *Immunogenicity of engineered antibodies.* Methods, 2005. **36**(1): p. 3-10.

22.   Presta, L.G., *Engineering of therapeutic antibodies to minimize immunogenicity and optimize function.* Advanced Drug Delivery Reviews, 2006. **58**(5-6): p. 640-656.

23.   Hassett, B., Singh, E., Mahgoub, E., O'Brien, J., Vicik, S.M., and Fitzpatrick, B., *Manufacturing history of etanercept (Enbrel((R))): Consistency of product quality through major process revisions.* Mabs, 2018. **10**(1): p. 159-165.

24.   Deeks, E.D., *Certolizumab Pegol: A Review in Inflammatory Autoimmune Diseases.* Biodrugs, 2016. **30**(6): p. 607-617.

25.   Carter, P.J. and Lazar, G.A., *Next generation antibody drugs: pursuit of the 'high-hanging fruit'.* Nature Reviews Drug Discovery, 2018. **17**(3): p. 197-223.

26.   Leipold, D. and Prabhu, S., *Pharmacokinetic and Pharmacodynamic Considerations in the Design of Therapeutic Antibodies.* Cts-Clinical and Translational Science, 2019. **12**(2): p. 130-139.

27.   Roopenian, D.C., Christianson, G.J., Sproule, T.J., Brown, A.C., Akilesh, S., Jung, N., Petkova, S., Avanessian, L., Choi, E.Y., Shaffer, D.J., Eden, P.A., and Anderson, C.L., *The MHC class I-like IgG receptor controls perinatal IgG transport, IgG homeostasis, and fate of IgG-Fc-coupled drugs.* Journal of Immunology, 2003. **170**(7): p. 3528-3533.

28.   Kang, T.H. and Jung, S.T., *Boosting therapeutic potency of antibodies by taming Fc domain functions.* Experimental and Molecular Medicine, 2019. **51**: p. 138.

29.   Labrijn, A.F., Janmaat, M.L., Reichert, J.M., and Parren, P., *Bispecific antibodies: a mechanistic review of the pipeline.* Nature Reviews Drug Discovery, 2019. **18**(8): p. 585-608.

30.   Nosenko, M.A., Atretkhany, K.S.N., Mokhonov, V.V., Efimov, G.A., Kruglov, A.A., Tillib, S.V., Drutskaya, M.S., and Nedospasov, S.A., *VHH-Based Bispecific Antibodies Targeting Cytokine Production.* Frontiers in Immunology, 2017. **8**: p. 1073.

31.   Xu, T.S., Ying, T.L., Wang, L.L., Zhang, X.D.H., Wang, Y., Kang, L.S., Huang, T., Cheng, L., Wang, L.P., and Zhao, Q., *A native-like bispecific antibody suppresses the inflammatory cytokine response by simultaneously neutralizing tumor necrosis factor-alpha and interleukin-17A.* Oncotarget, 2017. **8**(47): p. 81860-81872.

32.   Jain, T., Sun, T.W., Durand, S., Hall, A., Houston, N.R., Nett, J.H., Sharkey, B., Bobrowicz, B., Caffry, I., Yu, Y., Cao, Y., Lynaugh, H., Brown, M., Baruah, H., Gray, L.T., Krauland, E.M., Xu, Y.D., Vasquez, M., and Wittrup, K.D., *Biophysical properties of the clinical-stage antibody landscape.* Proceedings of the National Academy of Sciences of the United States of America, 2017. **114**(5): p. 944-949.

33.   Almagro, J.C., Pedraza-Escalona, M., Arrieta, H.I., and Perez-Tapia, S.M., *Phage Display Libraries for Antibody Therapeutic Discovery and Development.* Antibodies, 2019. **8**(3): p. 44.

34.   Washburn, N.R., Prata, J.E., Friedrich, E.E., Ramadan, M.H., Elder, A.N., and Sun, L.T., *Polymer-conjugated inhibitors of tumor necrosis factor-α for local control of inflammation.* Biomatter, 2013. **3**: p. e25597.

35.   Friedrich, E.E., Sun, L.T., Natesan, S., Zamora, D.O., Christy, R.J., and Washburn, N.R., *Effects of hyaluronic acid conjugation on anti-TNF-alpha inhibition of inflammation in burns.* Journal of Biomedical Materials Research Part A, 2014. **102**(5): p. 1527-1536.

36.   Sun, L.A.T., Buchholz, K.S., Lotze, M.T., and Washburn, N.R., *Cytokine Binding by Polysaccharide-Antibody Conjugates.* Molecular Pharmaceutics, 2010. **7**(5): p. 1769-1777.

37.   Shupp, J.W., Nasabzadeh, T.J., Rosenthal, D.S., Jordan, M.H., Fidler, P., and Jeng, J.C., *A Review of the Local Pathophysiologic Bases of Burn Wound Progression.* Journal of Burn Care & Research, 2010. **31**(6): p. 849-873.

38.   Sun, L.T., Friedrich, E., Heuslein, J.L., Pferdehirt, R.E., Dangelo, N.M., Natesan, S., Christy, R.J., and Washburn, N.R., *Reduction of burn progression with topical delivery of (antitumor necrosis factor-alpha)-hyaluronic acid conjugates.* Wound Repair and Regeneration, 2012. **20**(4): p. 563-572.

39.   Friedrich, E.E., Azofiefa, A., Fisch, E., and Washburn, N.R., *Local Delivery of Antitumor Necrosis Factor-alpha Through Conjugation to Hyaluronic Acid: Dosing Strategies and Early Healing Effects in a Rat Burn Model.* Journal of Burn Care & Research, 2015. **36**(2): p. E90-E101.

40.   Friedrich, E.E. and Washburn, N.R., *Transport patterns of anti-TNF-alpha in burn wounds: Therapeutic implications of hyaluronic acid conjugation.* Biomaterials, 2017. **114**: p. 10-22.

41.   Sun, L.T., Bencherif, S.A., Gilbert, T.W., Lotze, M.T., and Washburn, N.R., *Design principles for cytokine-neutralizing gels: Cross-linking effects.* Acta Biomaterialia, 2010. **6**(12): p. 4708-4715.

42.   Lima, A.C., Cunha, C., Carvalho, A., Ferreira, H., and Neves, N.M., *Interleukin-6 Neutralization by Antibodies Immobilized at the Surface of Polymeric Nanoparticles as a Therapeutic Strategy for Arthritic Diseases.* ACS Applied Materials & Interfaces, 2018. **10**(16): p. 13839-13850.

43.   Fu, T.T., Kong, Q.X., Sheng, H.Q., and Gao, L.Y., *Value of Functionalized Superparamagnetic Iron Oxide Nanoparticles in the Diagnosis and Treatment of Acute Temporal Lobe Epilepsy on MRI.* Neural Plasticity, 2016. **2016**: p. 2412958.

44.   Campo, G.M., Avenoso, A., Campo, S., D'Ascola, A., Traina, P., Sama, D., and Calatroni, A., *Purified human plasma glycosaminoglycans reduced NF-kappa B activation, pro-inflammatory cytokine production and apoptosis in LPS-treated chondrocytes.* Innate Immunity, 2008. **14**(4): p. 233-246.

45.   Coombe, D.R., *Biological implications of glycosaminoglycan interactions with haemopoietic cytokines.* Immunology and Cell Biology, 2008. **86**(7): p. 598-607.

46.   Lohmann, N., Schirmer, L., Atallah, P., Wandel, E., Ferrer, R.A., Werner, C., Simon, J.C., Franz, S., and Freudenberg, U., *Glycosaminoglycan-based hydrogels capture*

inflammatory chemokines and rescue defective wound healing in mice. Science Translational Medicine, 2017. **9**(386): p. eaai9044.

47.   Freudenberg, U., Atallah, P., Limasalea, Y.D.P., and Werner, C., *Charge-tuning of glycosaminoglycanbased hydrogels to program cytokine sequestration.* Faraday Discussions, 2019. **219**: p. 244-251.

48.   Babazada, H., Yamashita, F., Yanamoto, S., and Hashida, M., *Self-assembling lipid modified glycol-split heparin nanoparticles suppress lipopolysaccharide-induced inflammation through TLR4-NF-κB signaling.* Journal of Controlled Release, 2014. **194**: p. 332-340.

49.   Yanamoto, S., Babazada, H., Sakai, S., Higuchi, Y., Yamashita, F., and Hashida, M., *Anti-inflammatory Effect of Self-assembling Glycol-Split Glycosaminoglycan-Stearylamine Conjugates in Lipopolysaccharide-Stimulated Macrophages.* Biological & Pharmaceutical Bulletin, 2017. **40**(4): p. 540-545.

50.   Nih, L.R., Gojgini, S., Carmichael, S.T., and Segura, T., *Dual-function injectable angiogenic biomaterial for the repair of brain tissue following stroke.* Nature Materials, 2018. **17**(7): p. 642-651.

51.   Tuladhar, A. and Shoichet, M.S., *Biomaterials driving repair after stroke.* Nature Materials, 2018. **17**(7): p. 573-574.

52.   Wang, B., Tan, I., Deng, D.P., Lu, T., Zhou, C.W., Li, Z.K., Tang, Z.J., Wu, Z.S., and Tang, H., *Novel stable cytokine delivery system in physiological pH solution: chitosan oligosaccharide/heparin nanoparticles.* International Journal of Nanomedicine, 2015. **10**: p. 3417-3427.

53.   Guryanov, I., Cipriani, S., Fiorucci, S., Zashikhina, N., Marchiano, S., Scarpelli, P., Korzhikov-Vlakh, V., Popova, E., Korzhikova-Vlakh, E., Biondi, B., Formaggio, F., and Tennikova, T., *Nanotraps with biomimetic surface as decoys for chemokines.* Nanomedicine: Nanotechnology, Biology, and Medicine, 2017. **13**(8): p. 2575-2585.

54.   Hu, C.M.J., Zhang, L., Aryal, S., Cheung, C., Fang, R.H., and Zhang, L., *Erythrocyte membrane-camouflaged polymeric nanoparticles as a biomimetic delivery platform.* Proceedings of the National Academy of Sciences of the United States of America, 2011. **108**(27): p. 10980-10985.

55.   Fang, R.H., Kroll, A.V., Gao, W., and Zhang, L., *Cell Membrane Coating Nanotechnology.* Advanced Materials, 2018. **30**(23): p. 1706759.

56.   Thamphiwatana, S., Angsantikul, P., Escajadillo, T., Zhang, Q.Z., Olson, J., Luk, B.T., Zhang, S., Fang, R.H., Gao, W., Nizet, V., and Zhang, L., *Macrophage-like nanoparticles concurrently absorbing endotoxins and proinflammatory cytokines for sepsis management.*

Proceedings of the National Academy of Sciences of the United States of America, 2017. **114**(43): p. 11488-11493.

57. Zhang, Q.Z., Dehaini, D., Zhang, Y., Zhou, J.L., Chen, X.Y., Zhang, L., Fang, R.H., Gao, W., and Zhang, L., *Neutrophil membrane-coated nanoparticles inhibit synovial inflammation and alleviate joint damage in inflammatory arthritis.* Nature Nanotechnology, 2018. **13**(12): p. 1182-1190.

58. Tak, P.P., Smeets, T.J.M., Daha, M.R., Kluin, P.M., Meijers, K.A.E., Brand, R., Meinders, A.E., and Breedveld, F.C., *Analysis of the synovial cell infiltrate in early rheumatoid synovial tissue in relation to local disease activity.* Arthritis and Rheumatism, 1997. **40**(2): p. 217-225.

59. O'Brien, J., Lee, S.H., Onogi, S., and Shea, K.J., *Engineering the Protein Corona of a Synthetic Polymer Nanoparticle for Broad-Spectrum Sequestration and Neutralization of Venomous Biomacromolecules.* Journal of the American Chemical Society, 2016. **138**(51): p. 16604-16607.

60. Liu, M.M., Huang, R., Weisman, A., Yu, X.Y., Lee, S.H., Chen, Y.L., Huang, C., Hu, S.H., Chen, X.H., Tan, W.F., Liu, F., Chen, H., and Shea, K.J., *Synthetic Polymer Affinity Ligand for Bacillus thuringiensis (Bt) CryI Ab/Ac Protein: The Use of Biomimicry Based on the Bt Protein-Insect Receptor Binding Mechanism.* Journal of the American Chemical Society, 2018. **140**(22): p. 6853-6864.

61. Koide, H., Yoshimatsu, K., Hoshino, Y., Lee, S.H., Okajima, A., Ariizumi, S., Narita, Y., Yonamine, Y., Weisman, A.C., Nishimura, Y., Oku, N., Miura, Y., and Shea, K.J., *A polymer nanoparticle with engineered affinity for a vascular endothelial growth factor (VEGF(165)).* Nature Chemistry, 2017. **9**(7): p. 715-722.

62. Koide, D.H., Yoshimatsu, K., Hoshino, Y., Ariizumi, S., Okishima, A., Ide, T., Egami, H., Hamashima, Y., Nishimura, Y., Kanazawa, H., Miura, Y., Asai, T., Oku, N., and Shea, K.J., *Sequestering and inhibiting a vascular endothelial growth factor in vivo by systemic administration of a synthetic polymer nanoparticle.* Journal of Controlled Release, 2019. **295**: p. 13-20.

63. Tuleuova, N., Jones, C.N., Yan, J., Ramanculov, E., Yokobayashi, Y., and Revzin, A., *Development of an Aptamer Beacon for Detection of Interferon-Gamma.* Analytical Chemistry, 2010. **82**(5): p. 1851-1857.

64. Hao, Z., Wang, Z.R., Li, Y.J., Zhu, Y.B., Wang, X.J., De Moraes, C.G., Pan, Y.L., Zhao, X.Z., and Lin, Q., *Measurement of cytokine biomarkers using an aptamer-based affinity graphene nanosensor on a flexible substrate toward wearable applications.* Nanoscale, 2018. **10**(46): p. 21681-21688.

Chapter 2

Neutrophil membrane-coated nanoparticles suppress synovial inflammation and ameliorate joint destruction in inflammatory arthritis

2.1 Introduction

Rheumatoid arthritis (RA) is a widespread and devastating autoimmune disease characterized by systemic inflammation that causes progressive joint damage and disability.[1, 2] The precise cause of RA remains elusive and current treatment are primarily targeting inflammatory response.[3] Although there has been success, especially with the use of biologics that inhibit tumor necrosis factor alpha (TNF-α) and interleukin (IL)-1, existing approaches carry considerable limitations.[4, 5] In particular, pathological inflammation in RA is orchestrated by a large number of molecules.[6, 7] Inhibition of one or a few may not be adequate to halt or reverse disease progression.[8, 9] Indeed, under current treatment regimens, RA remains poorly controlled in up to 30% of patients and only a minor proportion of patients reach sustained clinical remission.[10, 11] Moreover, due largely to the multiplicity of cytokine targets, the toxicity of cytokine-inhibition remains highly unpredictable, causing substantial adverse effects and safety concerns.[12] Therefore, alternative anti-inflammatory approaches that overcome the complexity and heterogeneity of the inflammatory network are highly desirable for effective RA treatment.[13]

Recently, the rapid advance of nanomedicine has led to the development of cell membrane-coated nanoparticles as an emerging therapeutic platform.[14, 15] Made by the fusion of natural cell membranes onto synthetic cores, these nanoparticles inherit the antigenic profile of the source cells, enabling them to act as decoys that can absorb and neutralize pathological molecules regardless of their structural specificity.[14] For example, nanoparticles coated with the membrane of red blood cells (RBC-NPs) have demonstrated the ability to bind bacterial pore-forming toxins [14] and pathological autoantibodies,[16] diverting them away from and preventing their attack of healthy RBCs. Furthermore, macrophage membrane-coated nanoparticles have shown the ability to bind and neutralize endotoxins that would otherwise trigger immune activation.[17]

The advancement of cell membrane-coated nanoparticles in biodetoxification, particularly their unique capability of neutralizing pathological targets that are heterogeneous and complex in nature, inspired us to develop these nanoparticles as a novel anti-inflammatory strategy to address the aforementioned challenges facing current RA treatment. Joint inflammation and damage in RA are mediated by the influx of an innate and adaptive immune cell mixture into the synovial joint space.[18] Among them, neutrophils play an important role because of their actions in resolving inflammation and repairing tissues damages.[19] Neutrophils have been found to produce microvesicles that entered cartilage and protected the joint in inflammatory arthritis.[20, 21] Moreover, neutrophils are also responsible for initiating and perpetuating RA progression.[22] In RA, various chemoattractants have been identified that promote neutrophil migration into the joints.[23] Subsequent neutrophil activation stimulates synovial cells to produce chemokines that amplify neutrophil recruitment.[24] Neutrophil activation and granular content release contribute directly to cartilage destruction and bone resorption.[25] Importantly, remission and subsequent reversion of RA have been linked with a decrease in neutrophil recruitment to the synovial fluid.[26]

2.2 Results and discussion

2.2.1 Preparation and characterization

Based on the active roles played by neutrophils in RA, herein, we developed neutrophil-like nanoparticles (denoted 'neutrophil-NPs') by fusing neutrophil membrane onto polymeric cores and investigated their use as a broad-spectrum anti-inflammatory agent for RA management. By displaying neutrophil plasma membrane on their surface, the neutrophil-NPs were anticipated to mimic the source cells and thus to bind with immunoregulatory molecules that would otherwise target endogenous neutrophils (Figure 2.1a).

To synthesize neutrophil-NPs, plasma membrane derived from purified and activated human peripheral blood neutrophils was coated onto poly(lactic-*co*-glycolic acid) (PLGA) polymeric cores. The completeness of membrane coating was verified, which provided neutrophil-NPs with superior colloidal stability. Dynamic light scattering measurements revealed that the hydrodynamic diameter of the neutrophil-NPs increased approximately 18 nm from the uncoated PLGA cores; the surface zeta potential was less negative than the cores but comparable to neutrophil membrane-derived vesicles (Figure 2.1b). The neutrophil-NPs were visualized by transmission electron microscopy after uranyl acetate staining and showed a spherical core–shell structure (Figure 2.1c), consistent with a unilamellar membrane coating around the polymeric core.[14, 27] Furthermore, immunoblotting confirmed the presence and enrichment of key surface antigens, including TNF-α receptor (TNF-αR), IL-1 receptor (IL-1R), and lymphocyte function-associated antigen 1 (LFA-1) on neutrophil-NPs, further confirming the translocation of neutrophil membrane onto the polymeric cores (Figure 2.1d). A right-side-out protein orientation was verified by immunostaining and quantifying LFA-1 antigen on neutrophil-NPs as compared to that on neutrophil cells with equal amount of membrane proteins (Figure 2.1e). Overall, a series of quality assurance specifications for the production of neutrophil-NPs were established to ensure physicochemical and biological reproducibility of the nanoparticles.
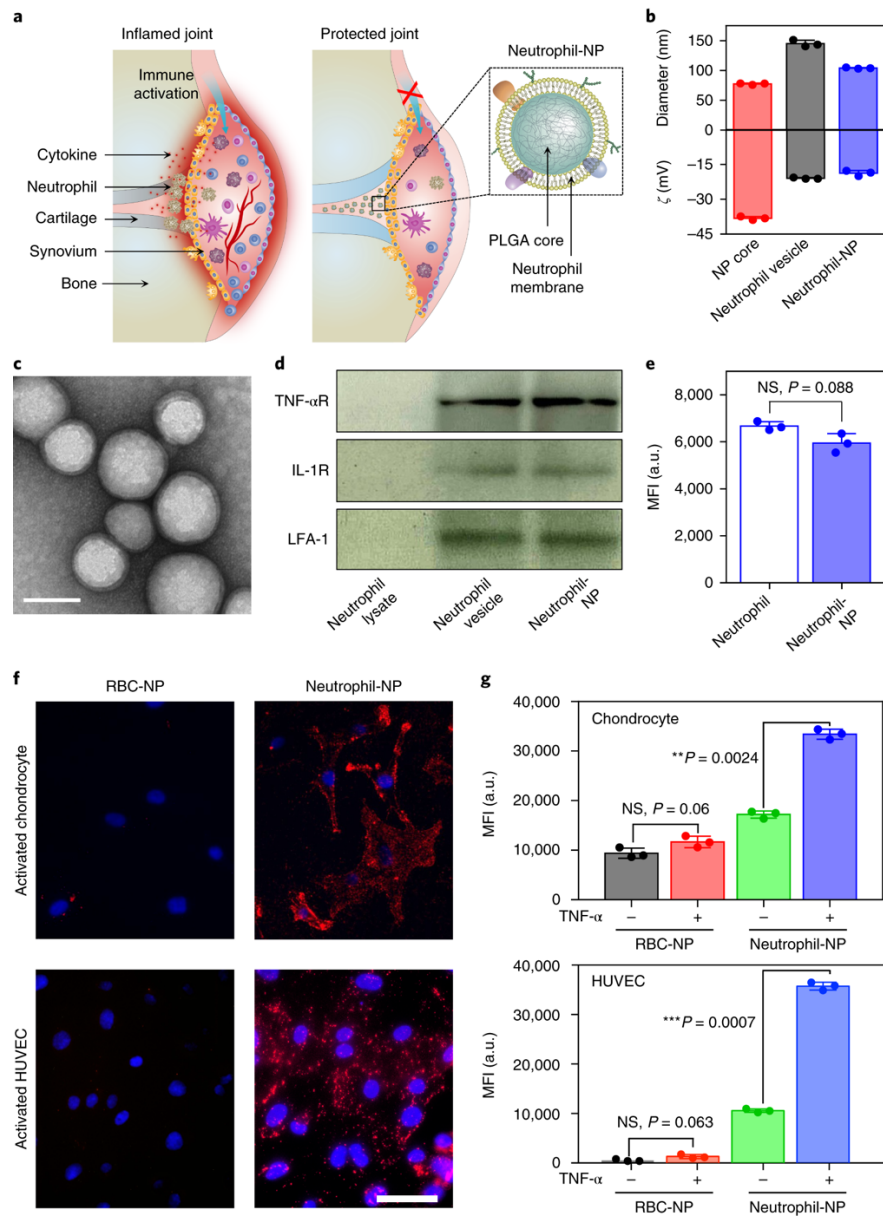
Figure 2.1 Preparation and characterization of neutrophil-NPs. a, Schematic representation of neutrophil-NPs designed for suppressing synovial inflammation and ameliorating joint destruction in inflammatory arthritis. Neutrophil-NPs are constructed by wrapping polymeric cores with natural human neutrophil membranes, which mimic source cells to bind with immunoregulatory molecules without potentiating the immune cascades for disease progression. **b,** Dynamic light scattering measurements of neutrophil-NP hydrodynamic size (diameter) and zeta potential (ζ). **c,** Representative images of neutrophil-NPs examined with transmission electron microscopy. Samples were stained with uranyl acetate (scale bar, 100 nm). **d,** Characteristic protein bands of neutrophil cell lysates, neutrophil membrane-derived vesicles, and neutrophil-NPs resolved by using western blotting. **e,** Comparison of the fluorescence intensity measured from neutrophils (approximately 2.5×10^6 cells) and neutrophil-NPs (100 μL of suspensions, 0.2 mg/mL protein content) stained with APC anti-mouse LFA antibodies. (*n.s.* = not significant). **f,** Fluorescent images of chondrocytes and human umbilical vein endothelial cells (HUVECs) after incubation with neutrophil-NPs or RBC-NPs. Red colour represents nanoparticles and blue represents nuclei. Cells were activated with TNF-α prior to nanoparticle incubation (scale bar, 50 μm). **g,** Flow cytometric analysis of nanoparticle binding to human chondrocytes or HUVECs (n = 3). Statistical analysis was performed using paired two-tailed t-test. All bars represent means ± s.d.. In all datasets, n = 3 independent experiments but using the same batch of human neutrophil membrane.

31

2.2.2 Inhibition of pro-arthritogenic factors

In RA, neutrophils are known to engage in receptor-mediated adhesion with cytokine-activated chondrocytes.[28] Herein, human neutrophil-NPs were fluorescently labeled and added to monolayers of chondrocytes activated with TNF-α and human umbilical vein endothelial cells (HUVECs). RBC-NPs were tested as a control because they had similar particulate structures as neutrophil-NPs but RBCs are less plastic in promoting and resolving inflammations compared to neutrophils.[29] After incubation and washing, significant fluorescence was observed on cells incubated with neutrophil-NPs, but not with RBC-NPs (Figure 2.1f). Flow cytometry measurements confirmed that activated chondrocytes and HUVECs, when incubated with neutrophil-NPs, showed a significant increase in mean fluorescence intensity (MFI) compared to naïve cells (without TNF-α activation) (Figure 2.1g). These results demonstrate the ability of neutrophil-NPs to target inflamed cells conferred by their neutrophil membrane coating. The binding is likely attributed to specific interactions between LFA-1 on the neutrophil membrane and the intercellular activation molecule 1 (ICAM-1) overexpressed on activated chondrocytes and HUVECs.[22, 23]

We next investigated the ability of human neutrophil-NPs to inhibit pro-arthritogenic factors, with a focus on IL-1β and TNF-α due to their prominent roles in initiating RA and promoting disease progression.[6, 8] We first tested the binding capability of neutrophil-NPs to IL-1β and TNF-α. Based upon the measured binding kinetic profiles, it was determined using Hill equation that neutrophil-NPs had an IC50 (half maximal inhibitory concentration) value of 188 μg mL^{-1} for IL-1β binding and 1327 μg mL^{-1} for TNF-α binding (Figure 2.2a). We then evaluated the inhibition of chondrocyte activation induced by IL-1β and TNF-α. In the study, 10 ng mL^{-1} IL-1β or 100 ng mL^{-1} TNF-α was added to the culture medium. After 6 h of incubation, significant chondrocyte activation was observed, indicated by an increased level of ICAM-1 expression.

However, expression levels decreased with the increase of neutrophil-NPs added to the medium, suggesting a dose-dependent inhibition effect (Figure 2.2b). An IC50 value of 0.88 mg mL^{-1} for inhibiting IL-1β and 0.44 mg mL^{-1} for TNF-α were obtained by fitting the data. We also evaluated the capability of neutrophil-NPs in inhibiting chondrocyte apoptosis caused by the cytokines. In the study, 48 h incubation of IL-1β or TNF-α with chondrocytes resulted in 80% of apoptotic cells. However, the fraction of apoptotic cells decreased with the increase of neutrophil-NPs (Figure 2.2c). An IC50 value of 1.58 mg mL^{-1} for inhibiting IL-1β and 0.98 mg mL^{-1} for inhibiting TNF-α were observed. Neutrophil-NPs also inhibited HUVEC activation in a similar dose-dependent manner. In contrast, the control group RBC-NPs did not show any detectable cytokine neutralization effects.

The ability of human neutrophil-NPs to inhibit pro-arthritogenic factors was further tested with human synovial fluid (hSF) samples obtained from three RA patients. Chondrocytes showed enhanced activation after 6 h of incubation with all three hSF samples, with 2.0, 2.4, and 2.2-fold increases, respectively. In contrast, when the hSF samples were pre-treated with neutrophil-NPs at a concentration of 2 mg mL^{-1} for 2 h, they showed significantly reduced activation of chondrocytes with 1.5, 1.5, and 1.4-fold increase, respectively (Figure 2.2d). Meanwhile, prolonged incubation with hSF samples caused 53.5, 67.3, and 53.6% chondrocyte apoptosis, while pre-treatment with neutrophil-NPs reduced these values to 5.3, 15.4, and 27.2%, respectively (Figure 2.2e). Neutrophil-NPs also inhibited HUVEC activation by all three hSF samples. Moreover, the presence of neutrophil-NPs induced near 2-fold decrease of matrix metalloproteinase-3 (MMP-3) plateau concentration in the culture medium for all three samples (Figure 2.2f). Neutrophil-NPs also significantly increased the production of aggrecan from hSF-activated chondrocytes (Figure 2.2g). Quantitatively, the three hSF-activated chondrocyte samples

had aggrecan production of 65.8%, 55.4%, and 61.1%, respectively, compared to naïve chondrocytes, which were increased to 85.9%, 82.8%, and 98.6%, respectively, in the presence of neutrophil-NPs (Figure 2.2h). Neutrophil-NPs reduced aggrecanolysis caused by either aggrecanase or MMP, attributable to their neutralization of pro-arthritic cytokines. It should be noted that different hSF samples caused different levels of cell activation, apoptosis, and catabolic status, likely due to the variation of pro-arthritogenic profiles of different individuals.[30] Nevertheless, neutrophil-NPs showed varying but significant neutralization efficacy across all samples without pre-existing knowledge of the hSF composition. Further study found that the catabolic status of chondrocytes remained unaltered when neutrophil-NPs alone were used without hSF, suggesting that the observed effects of neutrophil-NPs on chondrocytes were indeed related to their neutralization of pro-arthritogenic factors.
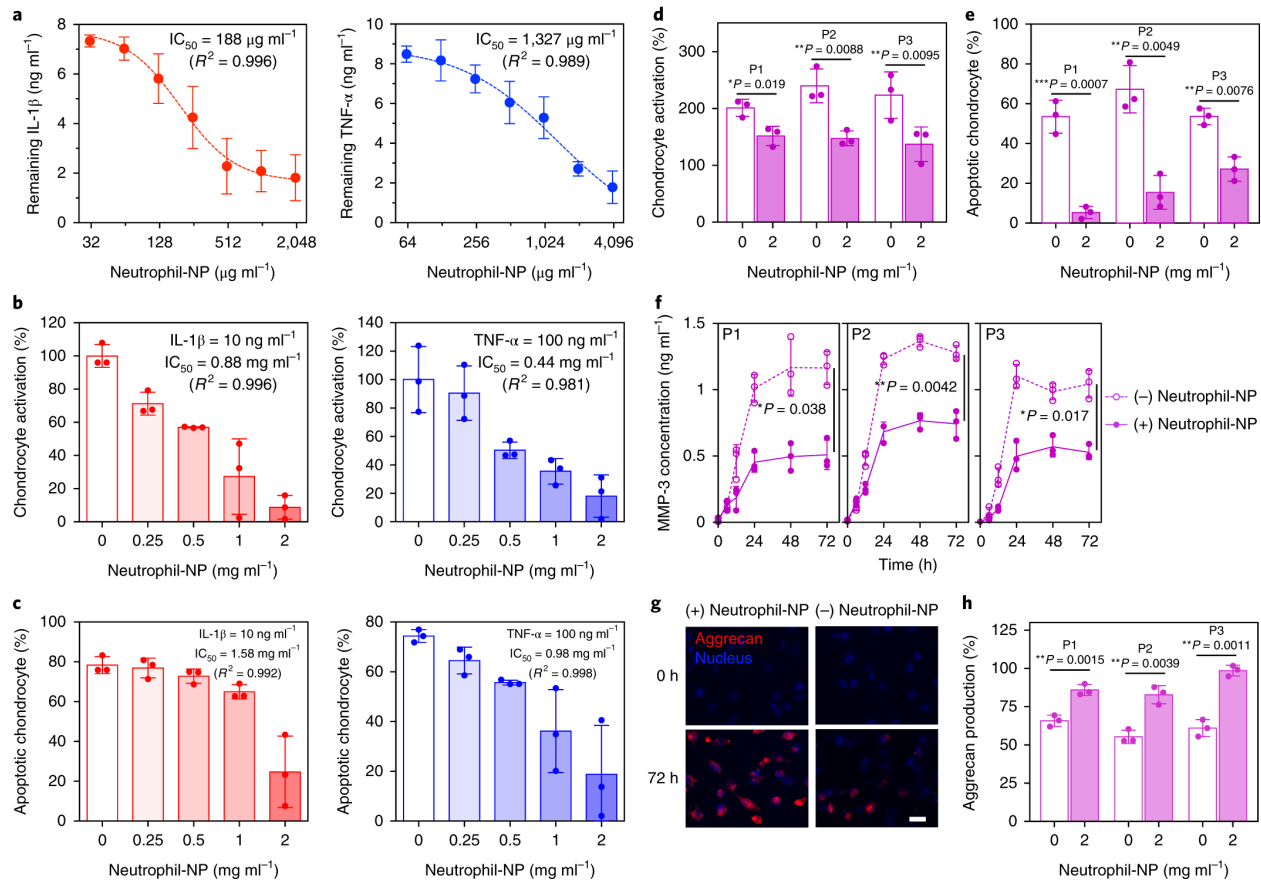
Figure 2.2 Neutrophil-NPs inhibit pro-arthritogenic factors *in vitro*. a, Binding capacity of human neutrophil-NP with IL-1β and TNF-α, respectively. **b-c,** Dose-response inhibition of chondrocyte activation (**b**) and chondrocyte apoptosis (**c**), induced by IL-1β or TNF-α. Concentration of IL-1β was maintained at 10 ng mL^{-1} and that of TNF-α at 100 ng mL^{-1}; neutrophil-NP concentrations were varied from 0 to 2 mg mL^{-1}. Values measured from chondrocytes treated with cytokines only (without neutrophil-NPs) served as 100%. **d-f,** Effects of neutrophil-NPs on chondrocyte activation (**d**), apoptosis (**e**), and matrix metalloproteinase-3 (MMP-3) secretion (**f**), elicited by human synovial fluid (hSF) samples collected from three rheumatoid arthritis patients. In the study, chondrocyte activation was quantified by measuring the level of ICAM-1 expression. Chondrocyte apoptosis was measured by examining mitochondrial activity through cell staining with 3,3'-dihexyloxacarbocyanine iodide (DiOC$_6$) dye. Neutrophil-NPs were removed following incubation with the cytokine solutions or hSF samples. **g-h**, Effects of neutrophil-NPs on aggrecan production from synovial fluid-activated chondrocytes. Representative fluorescence images (**g,** scale bar, 20 μm) and quantification of aggrecan based on fluorescence staining (**h**) from hSF-activated chondrocytes with or without neutrophil-NPs. Values measured from naïve chondrocytes without addition of hSF nor neutrophil-NPs served as 100%. Statistical analysis for hSF-induced chondrocyte activation, apoptosis, and aggrecan production was performed using paired t-test. Analysis for chondrocyte MMP-3 secretion was performed using repeated measure one-way ANOVA. All bars represent means ± s.d.. *$P \leq 0.05$, **$P \leq 0.01$, ***$P \leq 0.001$. In all datasets, n = 3 independent experiments but using the same batch of human neutrophil membrane. IC50 values were derived from the variable slope model by using Graphpad Prism 7.

2.2.3 Protection against inflammation-induced cartilage damage

To study the ability of neutrophil-NPs to penetrate injured cartilage in a mouse model, the nanoparticles were fabricated using mouse neutrophil membrane, which showed comparable

35

properties with human neutrophil-NPs. Mouse femoral head explants were collected and cultured in media supplemented with IL-1β to mimic inflammatory arthritis.[21] Fluorescently labeled mouse neutrophil-NPs or RBC-NPs were then added to the explants, followed by 18 h of incubation before sectioning. Using fluorescence microscopy, we observed the accumulation of neutrophil-NPs on the distal region of the femoral heads with clear penetration into the tissue (Figure 2.3a). Dual fluorescence labeling demonstrated colocalization of the polymeric cores and the neutrophil membranes during cartilage penetration. Below the surface zone, nanoparticles distributed throughout the cartilage matrix. Strong nanoparticle signal in close proximity to the stained nuclei implied an intracellular uptake by stimulated chondrocytes. RBC-NPs also showed accumulation in the distal surface region, but with much weaker fluorescence intensity (Figure 2.3b). Below the distal surface, RBC-NPs accumulated primarily around the chondrocytes, and the pericellular matrix was essentially free of nanoparticles. Fluorescence intensity at different penetration depths was quantified by sampling image stacks with a width of 5 μm and normalized to the outmost section of tissue treated with neutrophil-NPs. The signal from neutrophil-NPs decayed with increasing penetration depth, which dropped to approximately 1% at a penetration depth of 140 μm (Figure 2.3c). In contrast, the signal of RBC-NPs was about 60% at the distal surface compared to that from neutrophil-NPs, which decayed rapidly to 1% at a penetration depth of 30 μm. The enhanced cartilage penetration of neutrophil-NPs is likely attributable to the adhesion interactions between neutrophils and chondrocytes. Besides LFA-1 and ICAM-1, neutrophils may exploit other ligands for adhesion.[31, 32] Despite the complexity of cell ligands, the top-down fabrication of neutrophil-NPs can bypass the need for ligand identification and conjugation.[14, 15]

We further examined whether neutrophil-NPs, with their combined ability to neutralize cytokines and penetrate deep into cartilage, would provide chondroprotection in inflammation-

induced cartilage damage. We extracted the femoral heads from mice and maintained them in culture media under various conditions, followed by safranin-O staining for cartilage histopathology analysis.[21] The control femoral head sample without additional manipulation showed cartilage with an intact surface and perichondrium with homogenous cartilage matrix (Figure 2.3d). When the culture medium was supplemented with 10 ng mL^{-1} IL-1β, the femoral head showed obvious cartilage loss with matrix fibrillation that extended vertically downward into the mid zone. The sample also showed significant cartilage matrix loss in both superficial zones and fissured domains (Figure 2.3e). When RBC-NPs were added, the stained section showed similar pathology as the sample treated with IL-1β alone (Figure 2.3f). However, when neutrophil-NPs were added to the tissue culture, cartilage damage induced by IL-1β was halted. The sample showed a mostly intact surface with a large area of continuous cartilage matrix preserved below the superficial zone with reduced areas of disorganization, increased number of chondrocytes, and absence of fissures (Figure 2.3g). The cartilage content of the samples represented by areas with Safranin-O staining (dark red) was further quantified (Figure 2.3h). In tissues cultured with IL-1β alone or with supplemented RBC-NPs, only about 40% of the cartilage remained when compared to the unmanipulated control. In contrast, the tissue cultured with IL-1β and neutrophil-NPs was able to maintain more than 80% of its cartilage, suggesting a strong chondroproection effect conferred by neutrophil-NPs. Notably, without adding cytokines, neutrophil-NPs or RBC-NPs alone did not alter the cartilage content, implying that the observed chondroprotective effect was mediated by neutralization of arthritic factors.
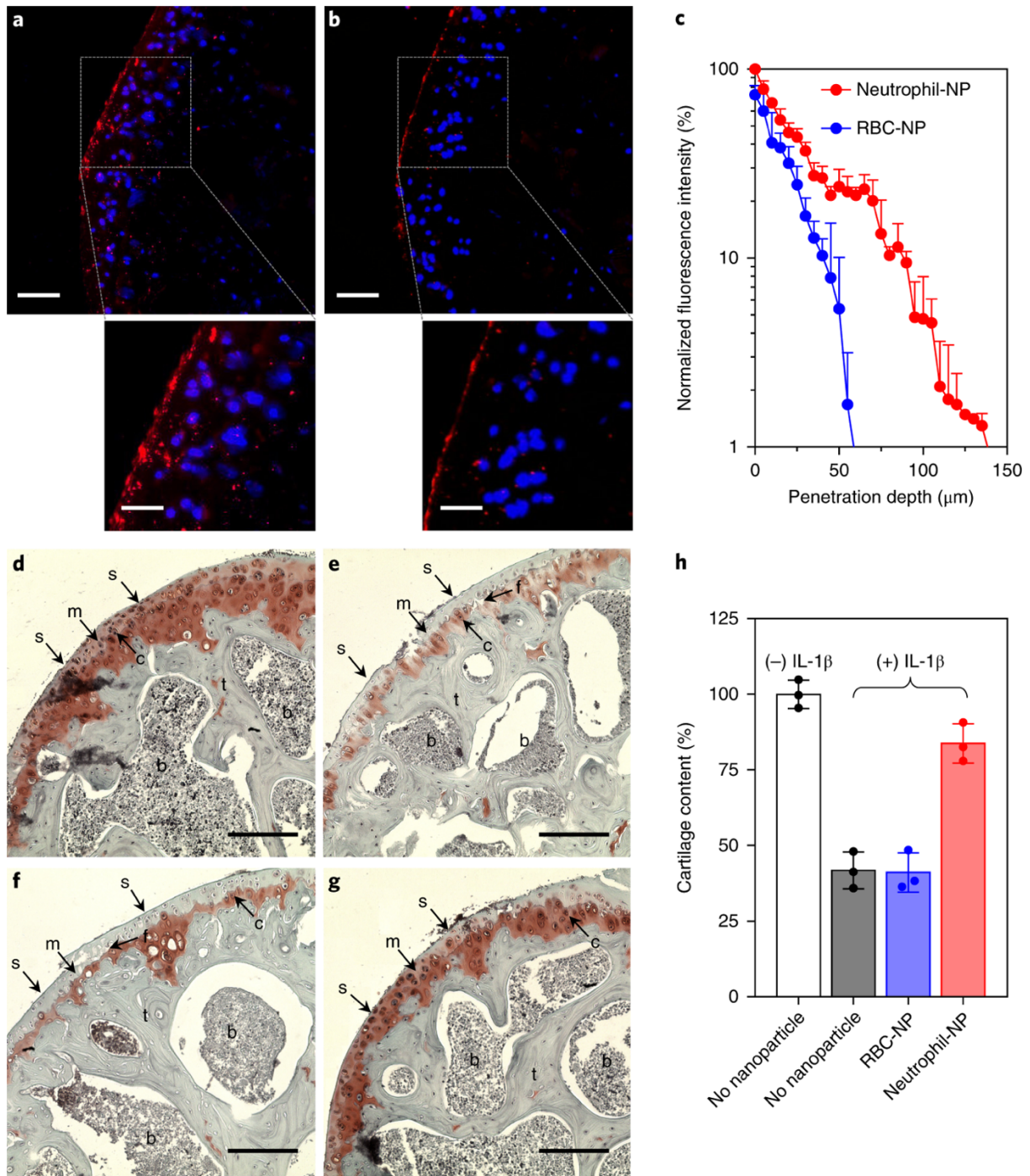
Figure 2.3 Neutrophil-NPs enhance cartilage penetration and confer chondroprotection. a-b, Representative fluorescence images of the cross-section of mouse femoral heads stimulated with recombinant mouse IL-1β and incubated with fluorescence-labeled mouse neutrophil-NPs **(a)** or RBC-NPs **(b)** (scale bar, 100 μm). **c,** Quantitative analysis of nanoparticle penetration depth into IL-1β-stimulated mouse femoral heads. **d-g,** Representative safranin-O stained cross-sections of mouse femoral head explants under various treatment conditions, including without either IL-1β stimulation or nanoparticle treatment **(d)**, stimulated but without nanoparticle treatment **(e)**, stimulated and treated with RBC-NPs **(f)**, and stimulated and treated with neutrophil-NPs **(g)**. On the images, s: superficial zone, m: mid zone, c: chondrocytes, f: fissure, b: bone marrow, t: bone trabeculae. Scale bar = 100 μm. **(h)** Quantitative analysis of safranin-O positive area among the above groups. All bars represent means ± s.d.. In all datasets, n = 3 femoral heads from different mice.

2.2.4 Efficacy in animal models of rheumatoid arthritis

The efficacy of neutrophil-NPs to ameliorate joint destruction was first evaluated using a murine model of collagen-induced arthritis (CIA).[33] Following arthritis induction, CIA mice developed mild swelling of the knee joints, where mouse neutrophil-NPs were injected (Figure 2.4a). Mice injected with PBS, anti-IL-1β, or anti-TNF-α served as controls.[34, 35] At the study endpoint, the transverse knee diameter of mice injected with neutrophil-NPs was comparable to that of mice treated with anti-IL-1β or anti-TNF-α, but significantly smaller than the PBS control group, indicating a reduction in cellular influx and oedema formation (Figure 2.4b). Knee joints of the mice were also sectioned for histological analysis. Haemotoxylin and Eosin (H&E)-stained sections from neutrophil-NP group showed an even distribution of chondrocytes within the articulate cartilage without obvious degeneration. In contrast, chondrocytes in PBS group were largely absent and an intense neutrophil infiltration was observable in the joints and synovium. Anti-cytokines treated groups showed less neutrophil infiltration but slight enlargement and depletion of chondrocytes (Figure 2.4c). Sections stained with Safranin-O showed a higher level of sulfated glycosaminoglycans (sGAGs) in the cartilage of neutrophil-NP group than PBS group, but similar to anti-IL-1β and anti-TNF-α groups (Figure 2.4d, e). The phenotype of fibroblast-like synoviocytes (FLS) in the synovial intimal lining was also examined. Specifically, we stained FLS for the expression of CD248 and fibronectin known to upregulate with IL-1β and TNF-α.[36, 37] Elevated expression of these markers indicates an aggressive phenotype that invades the extracellular matrix and exacerbates joint damage in RA.[38] As shown in Figure 2.4f, neutrophil-NP group showed weak staining of CD248 with few positively stained cells in synovium. In contrast, a large number of CD248-postive cells were found in sections of PBS group. Similarly, fibronectin-positive cells were largely present in PBS control joints, but not within the synovium of neutrophil-NP and anti-

cytokine groups. Collectively, these results demonstrate an effective protective role of neutrophil-NPs against joint destruction in the CIA mouse model.

We further examined the cartilage protection efficacy of neutrophil-NPs using a human transgenic mouse model of inflammatory arthritis, where mice express a human TNF-α transgene and spontaneously develop arthritis.[39] In the study, mouse neutrophil-NPs or controls including PBS and anti-TNF-α were injected into the knee of transgenic mice after 6 weeks of arthritis development (Figure 2.4g).[40] Similar as observed in the CIA model, at the study endpoint, the knee diameter of neutrophil-NP group was smaller than that of the PBS group, but comparable with the anti-TNF-α group (Figure 2.4h). H&E-stained sections from neutrophil-NP group showed the preservation of chondrocytes in the articular cartilage, contrasting with the chondrocyte depletion and matrix deformation in sections of PBS group, but consistent with features in sections of anti-TNF-α group (Figure 2.4i). In addition, neutrophil-NP group maintained a higher level of sGAGs in the cartilage than PBS group, but comparable to anti-TNF-α group (Figure 2.4j,k). Moreover, most FLS in neutrophil-NP and anti-TNF-α groups remained CD248-negative and fibronectin-negative, contrasting with the positive ones in PBS group (Figure 2.4l).
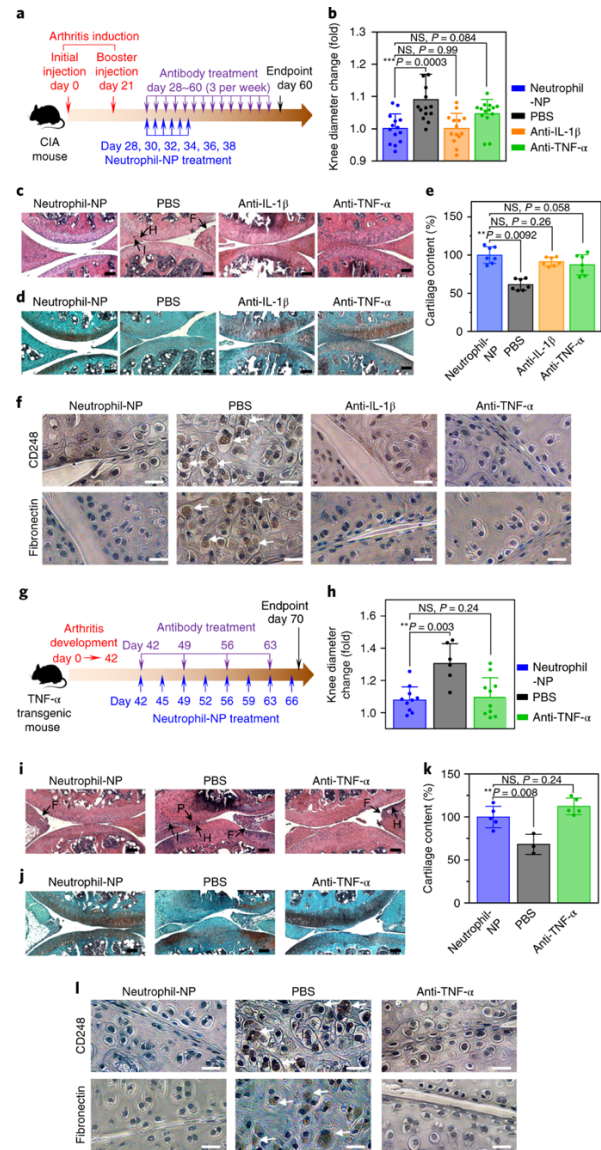
Figure 2.4 Neutrophil-NPs ameliorate joint destruction in a mouse model of collagen-induced arthritis and a human transgenic mouse model of inflammatory arthritis. a, The study protocol of a therapeutic regimen with a collagen-induced arthritis (CIA) mouse model. **b,** Change of hind knee diameter on day 60 after CIA induction compared to that on day 0. **c-d,** Representative images of H&E staining (**c**) and safranin-O staining (**d**) on knee sections from mice treated with neutrophil-NPs, PBS, anti-IL-1β antibody, or anti-TNF-α antibody (scale bar, 100 μm). On the images, F: synovial membrane fibrillation, H: synovium hyperplasia, I: immune cell infiltration. **e,** Cartilage content was quantified from safranin-O stained sections of mice treated with different groups. **f,** Representative images of immunohistochemical staining for CD248 (top row) and fibronectin (bottom row) on knee sections from mice treated with different groups (scale bar, 10 μm). **g,** The study protocol of a therapeutic regimen with a human TNF-α transgenic mouse model of inflammatory arthritis. **h,** Change of hind knee diameter on day 70 compared to that on day 0. **i-j,** Representative images of H&E staining (**i**) and safranin-O staining (**j**) on knee sections from mice treated with neutrophil-NPs, PBS, or anti-TNF-α antibody (scale bar, 100 μm). On the images, F: synovial membrane fibrillation, H: synovium hyperplasia, I: immune cell infiltration. P: pannus formation. **k,** Cartilage content was quantified from safranin-O stained sections of mice treated with different groups. **l,** Representative images immunohistochemical staining for CD248 (top row) and fibronectin (bottom row) on knee sections from mice treated with different groups (scale bar, 10 μm). Statistical analysis was performed using one-way ANOVA with Dunnett's post hoc analysis. All bars represent means ± s.d. In CIA mouse study, n = 7 mice for all groups. In transgenic mouse study, n = 5 mice for neutrophil-NP and anti-TNF-α antibody groups, n = 3 mice for PBS group. *P ≤ 0.05, **P ≤ 0.01, and ***P ≤ 0.001.

41

Finally, to evaluate the broad applicability of the neutrophil-NPs, we tested their anti-arthritis effectiveness using CIA mice with early stage arthritis following a prophylactic regimen (Figure 2.5a). We first observed chondral protection at the knee joints where the mouse neutrophil-NPs were injected. Specifically, at the study endpoint the knee diameter measured from mice in neutrophil-NP group is significantly smaller than that in PBS group, but comparable with values in anti-IL-1β and anti-TNF-α groups (Figure 2.5b). Histological analysis also confirmed reduction of immune infiltration and preservation of cartilage in mice received neutrophil-NPs (Figure 2.5c-e). In addition, most FLS in PBS group showed CD248-postive and fibronectin-positive phenotypes as opposed to negative ones in neutrophil-NP and anti-cytokines groups (Figure 2.5f). Notably, similar inhibition of CD248 and fibronectin expression with neutrophil-NPs was also observed in synovium tissues further away from cartilage. While the neutrophil-NPs were injected locally and retained primarily at the knee joints, they might still be able to neutralize diffusive arthritic factors and thus elicit a systemic therapeutic response, thereby alleviating overall disease progression and severity. To examine the potential systemic response, we monitored the serum levels of TNF-α and IL-1β in CIA mice, which are known to increase with the onset of arthritis and correlate strongly with disease severity. Surprisingly, alleviated concentrations of these cytokines were observed for the neutrophil-NP and anti-cytokines treated groups as compared to PBS group, indicating effective reduction of arthritis at systemic level (Figure 2.5g). In addition, neutrophil-NP group showed the smallest diameter of ankle below the knee (Figure 2.5h). Meanwhile, paws of the mice receiving PBS developed erythema and severe swelling; this effect was significantly lessened for mice treated with neutrophil-NPs or anti-cytokines, quantified by measuring paw volume (Figure 2.5i) and paw cartilage loss. Moreover, blinded scoring of the swelling and redness of the mouse paws was conducted to evaluate the severity of arthritis of the experimental mice.[41] The results showed that

neutrophil-NP treated mice had significantly lower arthritis score as compared to the PBS group (Figure 2.5j). These results clearly demonstrate promising efficacy of neutrophil-NPs in suppressing systemic inflammation and overall arthritis severity.
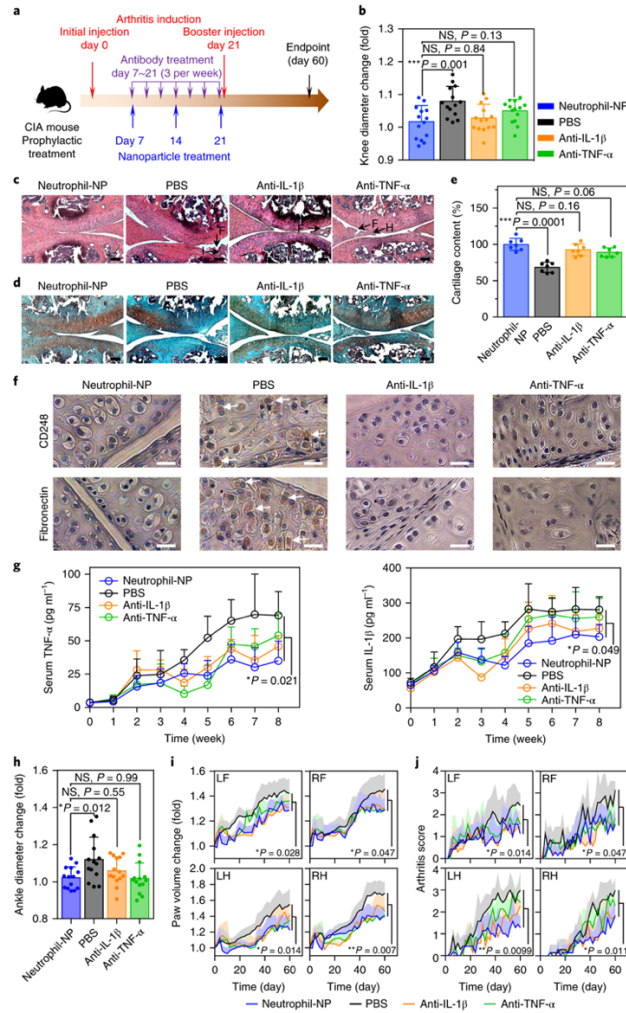
Figure 2.5 Neutrophil-NPs ameliorate joint destruction and elicit systemic therapeutic response following a prophylactic regimen. a, The study protocol of a prophylactic regimen with a collagen-induced arthritis (CIA) mouse model. **b,** Change of hind knee diameter on day 60 after arthritis induction compared to that on day 0. On day 60, mice were euthanized and the hind knees were sectioned for histological analysis. **c-d,** Representative images of H&E staining (**c**) and safranin-O staining (**d**) on knee sections from mice treated with neutrophil-NPs, PBS, anti-IL-1β antibody, or anti-TNF-α antibody (scale bar, 100 μm). On the images, F: synovial membrane fibrillation, H: synovium hyperplasia, I: immune cell infiltration. **e,** cartilage content was quantified from safranin-O stained sections of mice treated with neutrophil-NPs, PBS, anti-IL-1β antibody, or anti-TNF-α. **f,** Representative images of CD248 and fibronectin immunohistochemical staining on knee sections (scale bar, 10 μm). **g,** Concentration profiles of TNF-α and IL-1β in the serum of CIA mice treated with different groups. **h,** Change of hind ankle diameter on day 60 after arthritis induction compared to that on day 0. **i-j,** Values of paw volume (**i**) and arthritis score (**j**) were recorded every other day for a total of 60 days. Statistical analysis was performed using one-way ANOVA with Dunnett's post hoc analysis. Arthritis score was analyzed by Kruskal-Wallis non-parametric test with Dunnett's post hoc analysis. All data points represent means ± s.d. (n = 7 CIA mice). *$P \le 0.05$, **$P \le 0.01$, and ***$P \le 0.001$.

43

2.3 Methods

Animal care. Mice were housed in an animal facility at the University of California San Diego (UCSD) under federal, state, local, and National Institutes of Health (NIH) guidelines. All animal experiments were performed in accordance with NIH guidelines and approved by the Institutional Animal Care and Use Committee (IACUC) of UCSD.

Neutrophil collection. Fresh human peripheral blood neutrophils were purchased from ZenBio Inc. and activated within 16 h after the blood collection from human donors. Neutrophils were purified by the manufacturer with OptiPrep^{TM} density gradient centrifugation to a purity of approximately 95%.[48] Briefly, leukocyte-rich plasma was layered over a 1.077/1.090 g mL^{-1} OptiPrep gradient and centrifuged at 800 ×*g* for 25 min. Neutrophil fraction was collected between 1.077 and 1.090 g mL^{-1} interface. Cells received were washed with 1× PBS and then suspended in serum-free RPMI media (Thermo Fisher Scientific) at a density of 2×10^7 cells mL^{-1}. Neutrophils were then stimulated with 50 ng mL^{-1} recombinant human TNF-α (Thermo Fisher Scientific) for 2 h at 37 °C. Stimulated cells were then washed with 1X PBS, resuspended in 1:1 mixture of serum-free RPMI and HyCryo 2× cryopreservation medium (GE Healthcare), and stored at -80 °C for subsequent membrane derivation. Mouse neutrophils were collected from whole blood of ICR mice (six-week-old, male, Harlan Laboratories) using a modified Percoll® gradient method. Specifically, prior to the blood collection, 1.5 mg kg^{-1} lipopolysaccharide from *Escherichia coli* K12 (LPS, 1 mg mL^{-1} in 1X PBS, InvivoGen) was injected intraperitoneally into the mice to activate neutrophils *in vivo*. After 6 h, blood was collected by submandibular bleeding. Pooled blood was centrifuged (3220 ×*g*, 5 min, 4 °C) and the buffy coat on the top was aspirated and placed over a three-layer Percoll® gradient of 78%, 69% and 52%. Samples were centrifuged (1500 ×*g*, 30 min, 4° C) and cell contents from the interface of the 69% and 78% gradient layers and the upper part of 78% layer were collected.

Then RBCs were lysed (Thermo Fisher Scientific). Neutrophils were purified by washing with 1X PBS three times, suspended, and stored at -80 °C for subsequent membrane derivation.

Process of isolating mouse neutrophils was optimized to ensure high yield. Mouse neutrophils were co-stained with FITC anti-mouse Gr-1 antibody for identification and PE anti-mouse LFA-1 antibody (Biolegend) for confirming the activation. In the collection time optimization experiment, mice were injected with 1.5 mg kg^{-1} LPS and whole blood was collected at the designated time points. In the LPS dosage optimization experiment, mice were injected with the designated dosage of LPS, and whole blood was collected at 6 h post-injection. Washed mouse neutrophils were resuspended in PBS at 1×10^6 cells mL^{-1} and analyzed by a Becton Dickinson FACSCanto-II flow cytometer. Results were analyzed using FlowJo software.

Neutrophil membrane derivation. Plasma membrane of neutrophils was harvested by following a previously published protocol[49]. Briefly, frozen cells were thawed and washed with 1X PBS three times (centrifugation at 800 $\times g$). Cells were then suspended in a hypotonic lysing buffer containing 30 mM Tris-HCl (pH = 7.5), 225 mM D-mannitol, 75 mM sucrose, 0.2 mM EGTA (all Sigma), and protease and phosphatase inhibitor cocktail (Thermo Fisher Scientific). Cells were then disrupted using a dounce homogenizer with a tight-fitting pestle (20 passes). The homogenized solution was centrifuged at 20,000 $\times g$ for 25 min at 4 °C. The pellet was discarded and the supernatant was centrifuged again at 100,000 $\times g$ for 35 min at 4 °C. Following the centrifugation, membranes were collected as the pellet and washed twice with 0.2 mM EDTA in water. Membrane content was quantified by using a BCA kit (Pierce) in reference with a bovine serum albumin (BSA) standard. Approximately 125 million human neutrophils or 200 million mouse neutrophils were able to yield 1 mg membrane material (protein weight). Membrane was

suspended with 0.2 mM EDTA to a protein concentration of 4 mg mL^{-1} and stored at -80 °C for subsequent studies.

RBC membrane derivation. RBC membrane was derived based on a previously published protocol[18]. Briefly, washed RBCs were resuspended in 0.25X PBS on ice for 20 minutes, then centrifuged at 800 ×*g* for 5 min. The hemoglobin was removed, and the pink pellet was resuspended in 0.25X PBS on ice for 20 min. The process was repeated until hemoglobin was completely removed. The RBC membrane was resuspended in water at a protein concentration of 4 mg mL^{-1} and stored at -80 °C for subsequent studies.

Synthesis of neutrophil membrane-coated nanoparticles (neutrophil-NPs). Neutrophil-NPs were synthesized by using a sonication method. Briefly, to synthesize nanoparticle cores, 0.2 mL poly(dl-lactic-*co*-glycolic acid) (50:50 PLGA, 0.67 dL g^{-1}, Lactel Absorbable Polymers) in acetone (20 mg mL^{-1}) was added dropwise into 1 mL water. The solution was placed under a vacuum aspirator until acetone evaporated completely. For fluorescence imaging experiments, 1,1′-dioctadecyl-3,3,3′,3′-tetramethylindodicarbocyanine perchlorate (DiD, excitation = 644 nm/emission = 665 nm, Thermo Fisher Scientific) was encapsulated into PLGA cores (0.1 wt%). For membrane coating, neutrophil membrane was mixed with PLGA cores at a polymer-to-membrane protein weight ratio of 2:1. The mixture was then sonicated with a bath sonicator for 2 min (Fisher Scientific FS30D). RBC membrane-coated nanoparticles (RBC-NPs) used in control groups were synthesized by following the same procedure. Coating completeness was confirmed by studying nanoparticle stability in 1X PBS.[50]

Nanoparticle characterization. Neutrophil-NPs were measured for hydrodynamic size and surface zeta potential with dynamic light scattering (DLS, ZEN 3600 Zetasizer, Malvern). To examine the morphology, nanoparticles were stained with uranyl acetate (0.2 wt%) and visualized

using transmission electron spectroscopy (FEI 200 kV Sphera). Neutrophil-specific surface markers on neutrophils, neutrophil membranes and neutrophil-NPs were examined by western blotting. In the study, all samples were prepared in lithium dodecyl sulfate (LDS) loading buffer and ran at equivalent protein concentrations on NuPAGE Novex 4%-12% Bis-Tris minigels in MOPS running buffer. The gel was transferred onto a nitrocellulose membrane and probed with antibodies specific for human or mouse CD120b, IL-1R, LFA-1, along with HRP-conjugated secondaries against mouse IgG or rat IgG (Biolegend).

Cell culture. Primary human chondrocytes between passages 2 and 6 were cultured in human chondrocyte growth medium (both from Cell Applications) at 37 °C in a 5% CO_2 environment. Human umbilical vein endothelial cells (HUVECs, ATCC) were maintained in human endothelial cell growth medium (Cell Applications) at 37 °C in a 5% CO_2 environment. Cell lines were purchased with certification of authentication and free from *mycoplasma*.

Neutrophil-NP adhesion assay. HUVECs or human chondrocytes were seeded in 12-well tissue culture plates at 50% confluency and cultured overnight. Cell culture media was changed and recombinant human TNF-α or IL-1β (Thermo Fisher Scientific) was added to desired concentrations. After 6 h of stimulation, cells were washed with 1× PBS and fixed with 10% phosphate buffered formalin (Fisher Scientific) for 10 min and blocked with 1% BSA for 1 h. The cells were then incubated with 0.2 mg mL^{-1} DiD-labeled neutrophil-NPs or RBC-NPs in PBS at 4 °C for 60 s. After the incubation, cells were washed five times with ice-cold PBS, mounted with Vectashield Antifade Mounting Medium with DAPI (Vector Laboratories), and imaged with an EVOS® inverted fluorescence microscope (Thermo Fisher Scientific). For flow cytometric analysis, cells were scraped and collected after PBS wash, then analyzed with a Becton Dickinson FACSCanto-II flow cytometer. Results were analyzed using FlowJo software.

Quantification of cytokine binding by neutrophil-NPs. Recombinant human TNF-α (Thermo Fisher Scientific, final concentration 8.82 ± 0.80 ng mL^{-1}) or human IL-1β (Thermo Fisher Scientific, final concentration 7.92 ± 1.28 ng mL^{-1}) was mixed with neutrophil-NPs at final concentrations ranging from 0 to 4 mg mL^{-1}. The mixtures were incubated for 2 h at 37 °C and then centrifuged at 16,100 ×g for 10 min to remove the nanoparticles. Nanoparticle removal was confirmed by comparing fluorescence signal from DiD-labeled neutrophil-NP suspension and supernatant after nanoparticles were centrifuged at 16,100 ×g for 10 min. Cytokine concentration in the supernatant was quantified by human TNF-α or human IL-1β ELISA kits (Biolegend). Non-linear fitting of the curves was performed in GraphPad Prism 7.

Chondrocyte apoptosis assay. Human chondrocytes were seeded in 12-well tissue culture plates at a density of 1×10^6 cells per well and cultured overnight. TNF-α or IL-1β were incubated with neutrophil-NPs or RBC-NPs in chondrocyte culture medium at the desired concentrations at 37 °C for 2 h. Human synovial fluid (hSF) samples from rheumatoid arthritis (RA) patients (BioIVT) were filtered with sterile 0.22 μm syringe filter (Spectrum Laboratories) and incubated with neutrophil-NPs or RBC-NPs in chondrocyte culture medium at 37 °C for 2 h. The mixture was then centrifuged at 16,100 ×g for 10 min to remove the nanoparticles. The supernatant was used to stimulate chondrocytes for 48 h. The cells were detached with 0.25% trypsin-EDTA (Thermo Fisher Scientific) and washed with sterile PBS. To determine mitochondrial activity, cells were stained with DiOC$_6$ (100 nM final concentration from 10 mM stock in 100% ethanol, Life Technologies) for 30 min at 37 °C. The cells were washed with PBS and analyzed using a Becton Dickinson FACSCanto-II flow cytometer. Results were analyzed using FlowJo software. For fluorescent imaging experiments, a chondrocyte monolayer was cultured, stimulated, and imaged with an EVOS® inverted fluorescence microscope. Apoptotic cells are FITC^{dim} while non-apoptotic cells

are FITC^{bright}. In hSF experiments, hSF samples (BioIVT) were incubated with neutrophil-NPs or RBC-NPs in the same condition. Supernatant was used to stimulate the cells as described above. Statistical analysis was performed using paired t-test (n $\geq$ 3).

Chondrocyte activation assay. Chondrocytes were prepared as described above. Cytokines were incubated with nanoparticles in culture media at 37 °C for 2 h. Filtered hSF samples from RA patients were incubated with neutrophil-NPs or RBC-NPs in chondrocyte culture medium at 37 °C for 2 h. The mixture was then centrifuged at 16,100 ×g for 10 min to remove the nanoparticles. The supernatant was used to stimulate chondrocytes for 6 h. Cells were then washed, fixed, and blocked. Cells were stained with anti-human CD54 (Biolegend) for 30 min at room temperature, then stained with FITC-anti-mouse IgG (Biolegend). Washed cells were scraped and analyzed by a Becton Dickinson FACSCanto-II flow cytometer. Results were analyzed using FlowJo software. For fluorescent imaging experiments, chondrocyte and HUVEC monolayers were cultured and stimulated in tissue culture plates. ICAM-1 expression was probed with anti-human CD54 antibody as described above, then detected with Alexa647-anti-mouse IgG (for HUVECs, Biolegend) and FITC-anti-mouse IgG (for chondrocytes). Cells were then mounted with Vectashield Antifade Mounting Medium with DAPI. An EVOS® inverted fluorescence microscope was used to image the cells. To study activation with hSF, hSF samples were incubated with neutrophil-NPs or RBC-NPs in the same condition. Supernatant was used to stimulate the cells as described above. Statistical analysis was performed using paired t-test (n $\geq$ 3).

Chondrocyte MMP-3 secretion assay. Chondrocytes were seeded onto 96-well tissue culture plates (1 × 10^5 cells/well) and cultured overnight. Filtered hSF samples were diluted 4 × with chondrocyte culture medium and added to chondrocytes. Neutrophil-NPs or RBC-NPs were added to chondrocytes to achieve a final concentration of 2 mg mL^{-1}. At designated timepoints,

MMP-3 concentration from undiluted culture medium was quantified with human MMP-3 PicoKine™ ELISA kit (Boster Biological Technology). Statistical analysis was performed using repeated-measure one-way ANOVA (n ≥ 3).

Chondrocyte aggrecan production assay. Cells were prepared in the same way as described above. Filtered hSF samples were diluted 4 × with chondrocyte culture medium and added to the chondrocytes. Neutrophil-NPs or RBC-NPs were added to chondrocytes to achieve a final concentration of 2 mg mL^{-1}. Cells were cultured at 37 °C for 24 h. Then, the culture medium was replaced with fresh medium, and fresh hSF samples and nanoparticles were added. This treatment was repeated three times. Then chondrocytes were washed and stained with anti-human aggrecan (Biolegend) at room temperature for 2 h, and further probed with FITC-anti-mouse IgG at room temperature for 30 min. Washed cells were analyzed by a Becton Dickinson FACSCanto-II flow cytometer. Results were analyzed using FlowJo software. For fluorescence imaging experiment, cells were mounted with Vectashield Antifade Mounting Medium with DAPI and imaged with an EVOS® inverted fluorescence microscope. Statistical analysis was performed using paired t-test (n ≥ 3).

Neutrophil-NP penetration study. Mouse femoral heads were collected from 12-week-old ICR mice and cultured for 48 h in high glucose serum-free DMEM medium (4.5 g L^{-1} glucose, Hyclone). Following the culture, 10 ng mL^{-1} of recombinant mouse IL-1β (ThermoFisher Scientific) was added to the culture on days 0, 1, and 2. Culture medium was changed each time before IL-1β was added. On day 3, 0.2 mg mL^{-1} of DiD-labeled mouse neutrophil-NPs were incubated with the femoral heads at 37 °C for 24 h. After incubation, femoral heads were washed with PBS and embedded in Tissue-Tek® O.C.T. Compound (Sakura® Finetek) for frozen sectioning. Frozen sections were mounted (Vectashield Antifade Mounting Medium with DAPI)

and imaged with an EVOS® inverted fluorescence microscope. Images were analyzed with ImageJ to quantify nanoparticle penetration into the cartilage. Specifically, images were divided into 5 μm thick sections, starting from the distal femoral head surface. Fluorescence within each image section was measured with ImageJ and normalized to the fluorescence of the outermost tissue of the neutrophil-NP-treated femoral head. Mouse RBC-NPs were used as the control.

Mouse femoral head degradation assay. Mouse femoral heads were collected using the same procedure as described above. To study degradation, 10 ng mL^{-1} of IL-1β was mixed with 2 mg mL^{-1} neutrophil-NPs in medium and added to femoral head cultures to stimulate cartilage degradation for 48 h. The medium was then changed, and the same amount of cytokine-nanoparticle mixture was added to the femoral heads. A total of 3 treatments, 48 h each, was used. The samples were then fixed and processed for safranin-O staining. Proportions of safranin-O positive area were quantified with ImageJ. PBS and mouse RBC-NP-treated samples were used as control groups.

Mouse models of inflammatory arthritis. A collagen-induced arthritis (CIA) mouse model was established by following a previously published protocol with immunizations on day 1 and day 21.[33] Human TNF-α transgenic mice (5-week-old male) were obtained from Taconic Biosciences. Mice were randomized before the experiment.

Study protocols for evaluating anti-arthritis efficacy of neutrophil-NPs in vivo. To study therapeutic efficacy with CIA mice, 20 μL of mouse neutrophil-NPs (2 mg mL^{-1}) was injected into each knee joint of the hind legs on days 28 (first day of obvious clinical signs of arthritis), 30, 32, 34, 36, and 38. Sterile PBS as negative control was injected intra-articularly to mice on the same days. Anti-mouse IL-1β (3 mg kg^{-1}) or an anti-mouse TNF-α (3 mg kg^{-1}) were used as positive controls and injected intra-articularly to mice three times a week from day 28 to 60. To study

therapeutic efficacy with human TNF-α transgenic mice, 20 μL of mouse neutrophil-NPs (2 mg mL^{-1}) was injected into each knee joint of the hind legs on days 42, 45, 49, 52, 56, 59, 63, and 66. Sterile PBS (negative control) was injected intra-articularly on the same days. Anti-human TNF-α (positive control, 10 mg kg^{-1}, Biolegend) was administered intraperitoneally on days 42, 49, 56, and 63. To study prophylactic efficacy with CIA mice, 20 μL of mouse neutrophil-NPs (2 mg mL^{-1}) was injected into each knee joint of the hind legs on days 7, 14, and 21. Sterile PBS was injected to control mice intra-articularly on the same days. Positive control mice were injected intraperitoneally with an anti-mouse IL-1β (3 mg kg^{-1}) or an anti-mouse TNF-α (3 mg kg^{-1}) three times a week from day 7 to 21.

Histological analysis of mouse knee joints. At study endpoints, mice were sacrificed and hind knee joints were collected for hematoxylin and eosin (H&E) staining or safranin-O staining. To analyze fibroblast-like synoviocyte activation, knee joint sections were stained with a rabbit anti-CD248 (Bioss Antibodies) or a rabbit anti-fibronectin (Novus Biologicals). Biotinylated anti-rabbit IgG was used as the secondary antibody for chromagen development. Sections were counter-stained with hematoxylin to visualize cell nuclei. Images were taken with a Micromaster^{TM} II Microscope (Fisher Scientific). Proportions of safranin-O positive area were quantified by using ImageJ.

Quantification of serum cytokines. CIA mouse serum samples were collected on days 8, 15, 22, 29, 36, 43, 50, 57 and concentrations of IL-1β and TNF-α were quantified with ELISA. Specifically, the whole blood of CIA mice was collected with submandibular bleeding into microtubes and allowed to clot at room temperature for 30 min. Samples were then centrifuged at 2,000 ×g for 6 min to collect serum from the supernatant. Serum samples were immediately frozen

at -20 °C until analysis by using mouse IL-1β and mouse TNF-α ELISA kits (Biolegend) within 3 days after collection.

Joint swelling assessment and arthritis scoring. Mouse hind knee joint diameters were measured with a digital caliber at study endpoints. Images of mouse paws were taken every 2 days from day 0 to day 60 and paw volumes were calculated by analyzing images with ImageJ. Specifically, the length, width, and thickness of mouse paws were measured from the top- and side-view images of each paw. The volume was approximated as the product of these three parameters assuming equivalent importance of each in reflecting the extent of inflammation in the paw. Paw scorings (score = 0~4) were given by a blinded researcher based on the following criteria: 0—normal; 1—mild redness of ankle or tarsal joints; 2—mild redness and swelling extending from ankle to the tarsals; 3—moderate redness and swelling from ankle to metatarsal joints; 4—severe redness and swelling encompassing the ankle, foot and digits. Hind ankle joint diameters were measured with a digital caliber at day 60.

Statistical analysis was performed using one-way ANOVA. Paw scoring data was analyzed by using Kruskal-Wallis test. Replicates represent different mice subjected to the same treatment. In CIA studies, n = 7 for all groups. In human TNF-α transgenic mouse study, n = 5 for neutrophil-NP group and anti-TNF-α group, n = 3 for PBS group.

2.4 Conclusions

In summary, we have developed neutrophil-NPs and demonstrated their potential as an anti-inflammatory strategy for RA management. Neutrophil-NPs inherit the antigenic exterior of their source cells and act as decoys capable of engaging in the interfacing roles of neutrophils without potentiating inflammatory processes that can promote RA. Unlike existing anti-cytokine

agents that inhibit specific and limited targets, neutrophil-NPs provide a function-driven, broad-spectrum, and disease-relevant blockade that dampens the inflammation cascade in the disease process. In addition, the direct use of membrane from the effector cells of the disease allows neutrophil-NPs to neutralize highly relevant inflammatory factors without the need to identify them. Even if the target is known, the top down fabrication of neutrophil-NPs can avoid the necessity to engineer binding motifs that are often difficult to identify, synthesize, and conjugate.

In this work we chose to mimic neutrophils for nanoparticle fabrication and anti-inflammatory efficacy. Notably, the rheumatoid synovium contains a mixture of cells with origins of monocytes, macrophages, dendritic cells, and T cells, which together orchestrate RA process.[6, 42] Membrane of these cells can be also derived for coating and combined with other nanotherapeutic agents for targeted and synergistic therapy for RA.[43][44] Similarly to RA, various infections, traumatic injuries, and chronic diseases are marked by inflammatory responses that can damage host tissue and cause organ dysfunction.[45] The neutrophil-NPs developed here can likely be adopted to address some of these diseases, promising to eventually improve the clinical outcomes of the patients. In this study, neutrophils were collected from human or mouse whole blood for membrane derivation. Regarding future clinical translation of neutrophil-NPs, it is critical to consider scale-up and manufacturing issues because of the use of naturel cell membranes. In terms of the source materials, bioprocesses for *ex vivo* production of neutrophils at a clinical scale can supply large quantity of neutrophil membranes.[46] Meanwhile, significant progress has been made in producing human cells with universal immune compatibility, which would also enable cell supply for clinical studies.[47] These technological advances together offer a promising prospect to the translation of neutrophil-NPs and cell membrane-coating technology in general.

Chapter 2, in full, is a reprint of the material as it appears in *Nature Nanotechnology*, 2018, Qiangzhe Zhang, Diana Dehaini, Yue Zhang, Julia Zhou, Xiangyu Chen, Lifen Zhang, Ronnie H. Fang, Weiwei Gao, and Liangfang Zhang. The dissertation author was the primary author of this paper.

2.5 References

1. Smolen, J.S. and Aletaha, D., *Rheumatoid arthritis therapy reappraisal: strategies, opportunities and challenges.* Nature Reviews Rheumatology, 2015. **11**(5): p. 276-289.

2. Firestein, G.S., *Evolving concepts of rheumatoid arthritis.* Nature, 2003. **423**(6937): p. 356-361.

3. Firestein, G.S. and McInnes, I.B., *Immunopathogenesis of Rheumatoid Arthritis.* Immunity, 2017. **46**(2): p. 183-196.

4. Burmester, G.R., Feist, E., and Doerner, T., *Emerging cell and cytokine targets in rheumatoid arthritis.* Nature Reviews Rheumatology, 2014. **10**(2): p. 77-88.

5. Goulielmos, G.N., Zervou, M.I., Myrthianou, E., Burska, A., Niewold, T.B., and Ponchel, F., *Genetic data: The new challenge of personalized medicine, insights for rheumatoid arthritis patients.* Gene, 2016. **583**(2): p. 90-101.

6. McInnes, I.B. and Schett, G., *Cytokines in the pathogenesis of rheumatoid arthritis.* Nature Reviews Immunology, 2007. **7**(6): p. 429-442.

7. Noack, M. and Miossec, P., *Selected cytokine pathways in rheumatoid arthritis.* Seminars in Immunopathology, 2017. **39**(4): p. 365-383.

8. Choy, E.H.S. and Panayi, G.S., *Mechanisms of disease: Cytokine pathways and joint inflammation in rheumatoid arthritis.* New England Journal of Medicine, 2001. **344**(12): p. 907-916.

9. Smolen, J.S., Aletaha, D., Koeller, M., Weisman, M.H., and Emery, P., *New therapies for treatment of rheumatoid arthritis.* Lancet, 2007. **370**(9602): p. 1861-1874.

10. Bykerk, V., *Unmet Needs in Rheumatoid Arthritis.* Journal of Rheumatology, 2009. **36**: p. 42-46.

11.   Taylor, P.C., Moore, A., Vasilescu, R., Alvir, J., and Tarallo, M., *A structured literature review of the burden of illness and unmet needs in patients with rheumatoid arthritis: a current perspective.* Rheumatology International, 2016. **36**(5): p. 685-695.

12.   Iwata, S. and Tanaka, Y., *Progress in understanding the safety and efficacy of Janus kinase inhibitors for treatment of rheumatoid arthritis.* Expert Review of Clinical Immunology, 2016. **12**(10): p. 1047-1057.

13.   Smolen, J.S., Breedveld, F.C., Burmester, G.R., Bykerk, V., Dougados, M., Emery, P., Kvien, T.K., Navarro-Compan, M.V., Oliver, S., Schoels, M., Scholte-Voshaar, M., Stamm, T., Stoffer, M., Takeuchi, T., Aletaha, D., Andreu, J.L., Aringer, M., Bergman, M., Betteridge, N., Bijlsma, H., Burkhardt, H., Cardiel, M., Combe, B., Durez, P., Fonseca, J.E., Gibofsky, A., Gomez-Reino, J.J., Graninger, W., Hannonen, P., Haraoui, B., Kouloumas, M., Landewe, R., Martin-Mola, E., Nash, P., Ostergaard, M., Ostor, A., Richards, P., Sokka-Isler, T., Thorne, C., Tzioufas, A.G., van Vollenhoven, R., de Wit, M., and van der Heijde, D., *Treating rheumatoid arthritis to target: 2014 update of the recommendations of an international task force.* Annals of the Rheumatic Diseases, 2016. **75**(1): p. 3-15.

14.   Hu, C.M.J., Fang, R.H., Copp, J., Luk, B.T., and Zhang, L., *A biomimetic nanosponge that absorbs pore-forming toxins.* Nature Nanotechnology, 2013. **8**(5): p. 336-340.

15.   Hu, C.M.J., Fang, R.H., Wang, K.C., Luk, B.T., Thamphiwatana, S., Dehaini, D., Nguyen, P., Angsantikul, P., Wen, C.H., Kroll, A.V., Carpenter, C., Ramesh, M., Qu, V., Patel, S.H., Zhu, J., Shi, W., Hofman, F.M., Chen, T.C., Gao, W., Zhang, K., Chien, S., and Zhang, L., *Nanoparticle biointerfacing by platelet membrane cloaking.* Nature, 2015. **526**(7571): p. 118-121.

16.   Copp, J.A., Fang, R.H., Luk, B.T., Hu, C.M.J., Gao, W., Zhang, K., and Zhang, L., *Clearance of pathological antibodies using biomimetic nanoparticles.* Proceedings of the National Academy of Sciences of the United States of America, 2014. **111**(37): p. 13481-13486.

17.   Thamphiwatana, S., Angsantikul, P., Escajadillo, T., Zhang, Q., Olson, J., Luk, B.T., Zhang, S., Fang, R.H., Gao, W., Nizet, V., and Zhang, L., *Macrophage-like nanoparticles concurrently absorbing endotoxins and proinflammatory cytokines for sepsis management.* Proceedings of the National Academy of Sciences of the United States of America, 2017. **114**: p. 11488-11493.

18.   Tak, P.P., Smeets, T.J.M., Daha, M.R., Kluin, P.M., Meijers, K.A.E., Brand, R., Meinders, A.E., and Breedveld, F.C., *Analysis of the synovial cell infiltrate in early rheumatoid synovial tissue in relation to local disease activity.* Arthritis and Rheumatism, 1997. **40**(2): p. 217-225.

19.   Horckmans, M., Ring, L., Duchene, J., Santovito, D., Schloss, M.J., Drechsler, M., Weber, C., Soehnlein, O., and Steffens, S., *Neutrophils orchestrate post-myocardial infarction*

healing by polarizing macrophages towards a reparative phenotype. European Heart Journal, 2017. **38**(3): p. 187-197.

20. Dalli, J., Montero-Melendez, T., Norling, L.V., Yin, X.K., Hinds, C., Haskard, D., Mayr, M., and Perretti, M., *Heterogeneity in Neutrophil Microparticles Reveals Distinct Proteome and Functional Properties.* Molecular & Cellular Proteomics, 2013. **12**(8): p. 2205-2219.

21. Headland, S.E., Jones, H.R., Norling, L.V., Kim, A., Souza, P.R., Corsiero, E., Gil, C.D., Nerviani, A., Dell'Accio, F., Pitzalis, C., Oliani, S.M., Jan, L.Y., and Perretti, M., *Neutrophil-derived microvesicles enter cartilage and protect the joint in inflammatory arthritis.* Science Translational Medicine, 2015. **7**(315): p. article number 315ra190.

22. Wright, H.L., Moots, R.J., and Edwards, S.W., *The multifactorial role of neutrophils in rheumatoid arthritis.* Nature Reviews Rheumatology, 2014. **10**(10): p. 593-601.

23. Wipke, B.T. and Allen, P.M., *Essential role of neutrophils in the initiation and progression of a murine model of rheumatoid arthritis.* Journal of Immunology, 2001. **167**(3): p. 1601-1608.

24. Cedergren, J., Forslund, T., Sundqvist, T., and Skogh, T., *Intracellular oxidative activation in synovial fluid neutrophils from patients with rheumatoid arthritis but not from other arthritis patients.* Journal of Rheumatology, 2007. **34**(11): p. 2162-2170.

25. Chakravarti, A., Raquil, M.A., Tessier, P., and Poubelle, P.E., *Surface RANKL of Toll-like receptor 4-stimulated human neutrophils activates osteoclastic bone resorption.* Blood, 2009. **114**(8): p. 1633-1644.

26. Wright, H.L., Cox, T., Moots, R.J., and Edwards, S.W., *Neutrophil biomarkers predict response to therapy with tumor necrosis factor inhibitors in rheumatoid arthritis.* Journal of Leukocyte Biology, 2017. **101**(3): p. 785-795.

27. Hu, C.-M.J., Zhang, L., Aryal, S., Cheung, C., Fang, R.H., and Zhang, L., *Erythrocyte membrane-camouflaged polymeric nanoparticles as a biomimetic delivery platform.* Proceedings of the National Academy of Sciences of the United States of America, 2011. **108**(27): p. 10980-10985.

28. Declerck, L.S., Degendt, C.M., Bridts, C.H., Vanosselaer, N., and Stevens, W.J., *Expression of neutrophil activation markers and neutrophil adhesion to chondrocytes in rheumatoid-arthritis patients - relationship with disease-activity.* Research in Immunology, 1995. **146**(2): p. 81-87.

29. Karsten, E., Breen, E., and Herbert, B.R., *Red blood cells are dynamic reservoirs of cytokines.* Scientific Reports, 2018. **8**: p. article number 3101.

30. Brzustewicz, E., Bzoma, I., Daca, A., Szarecka, M., Bykowska, M.S., Witkowski, J.M., and Bryl, E., *Heterogeneity of the cytokinome in undifferentiated arthritis progressing to rheumatoid arthritis and its change in the course of therapy. Move toward personalized medicine.* Cytokine, 2017. **97**: p. 1-13.

31. Ley, K., Laudanna, C., Cybulsky, M.I., and Nourshargh, S., *Getting to the site of inflammation: the leukocyte adhesion cascade updated.* Nature Reviews Immunology, 2007. **7**(9): p. 678-689.

32. Schmidt, E.P., Yang, Y.M., Janssen, W.J., Gandjeva, A., Perez, M.J., Barthel, L., Zemans, R.L., Bowman, J.C., Koyanagi, D.E., Yunt, Z.X., Smith, L.P., Cheng, S.S., Overdier, K.H., Thompson, K.R., Geraci, M.W., Douglas, I.S., Pearse, D.B., and Tuder, R.M., *The pulmonary endothelial glycocalyx regulates neutrophil adhesion and lung injury during experimental sepsis.* Nature Medicine, 2012. **18**(8): p. 1217-1223.

33. Brand, D.D., Latham, K.A., and Rosloniec, E.F., *Collagen-induced arthritis.* Nature Protocols, 2007. **2**(5): p. 1269-1275.

34. Williams, R.O., Marinova-Mutafchieva, L., Feldmann, M., and Maini, R.N., *Evaluation of TNF-alpha and IL-1 blockade in collagen-induced arthritis and comparison with combined anti-TNF-alpha/anti-CD4 therapy.* Journal of Immunology, 2000. **165**(12): p. 7240-7245.

35. Joosten, L.A.B., Helsen, M.M.A., Saxne, T., van de Loo, F.A.J., Heinegard, D., and van den Berg, W.B., *IL-1 alpha beta blockade prevents cartilage and bone destruction in murine type II collagen-induced arthritis, whereas TNF-alpha blockade only ameliorates joint inflammation.* Journal of Immunology, 1999. **163**(9): p. 5049-5055.

36. Maia, M., de Vriese, A., Janssens, T., Moons, M., Van Landuyt, K., Tavernier, J., Lories, R.J., and Conway, E.M., *CD248 and Its Cytoplasmic Domain A Therapeutic Target for Arthritis.* Arthritis and Rheumatism, 2010. **62**(12): p. 3595-3606.

37. Pascual, V., Allantaz, F., Arce, E., Punaro, M., and Banchereau, J., *Role of interleukin-1 (IL-1) in the pathogenesis of systemic onset juvenile idiopathic arthritis and clinical response to IL-1 blockade.* Journal of Experimental Medicine, 2005. **201**(9): p. 1479-1486.

38. Bartok, B. and Firestein, G.S., *Fibroblast-like synoviocytes: key effector cells in rheumatoid arthritis.* Immunological Reviews, 2010. **233**: p. 233-255.

39. Li, P. and Schwarz, E.M., *The TNF-alpha transgenic mouse model of inflammatory arthritis.* Springer Seminars in Immunopathology, 2003. **25**(1): p. 19-33.

40. Shealy, D.J., Wooley, P.H., Emmell, E., Volk, A., Rosenberg, A., Treacy, G., Wagner, C.L., Mayton, L., Griswold, D.E., and Song, X.Y.R., *Anti-TNF-alpha antibody allows healing of joint damage in polyarthritic transgenic mice.* Arthritis Research, 2002. **4**(5): p. article number R7.

41.   Seeuws, S., Jacques, P., Van Praet, J., Drennan, M., Coudenys, J., Decruy, T., Deschepper, E., Lepescheux, L., Pujuguet, P., Oste, L., Vandeghinste, N., Brys, R., Verbruggen, G., and Elewaut, D., *A multiparameter approach to monitor disease activity in collagen-induced arthritis.* Arthritis Research & Therapy, 2010. **12**(4): p. article number R160.

42.   Graham, J.M., *Isolation of human polymorphonuclear leukocytes (granulocytes) from a leukocyte-rich fraction.* Scientific World Journal, 2002. **2**: p. 1393-1396.

43.   Fang, R., Hu, C.-M., Luk, B., Gao, W., Copp, J., Tai, Y., O'Connor, D., and Zhang, L., *Cancer cell membrane-coated nanoparticles for anticancer vaccination and drug delivery.* Nano Letters, 2014. **14**: p. 2181-2188.

44.   Luk, B.T., Hu, C.M.J., Fang, R.N.H., Dehaini, D., Carpenter, C., Gao, W., and Zhang, L., *Interfacial interactions between natural RBC membranes and synthetic polymeric nanoparticles.* Nanoscale, 2014. **6**(5): p. 2730-2737.

45.   Kremer, J.M., Westhovens, R., Leon, M., Di Giorgio, E., Alten, R., Steinfeld, S., Russell, A., Dougados, M., Emery, P., Nuamah, I.F., Williams, G.R., Becker, J.C., Hagerty, D.T., and Moreland, L.W., *Treatment of rheumatoid arthritis by selective inhibition of T-cell activation with fusion protein CTLA4Ig.* New England Journal of Medicine, 2003. **349**(20): p. 1907-1915.

46.   Kang, T., Zhu, Q.Q., Wei, D., Feng, J.X., Yao, J.H., Jiang, T.Z., Song, Q.X., Wei, X.B., Chen, H.Z., Gao, X.L., and Chen, J., *Nanoparticles Coated with Neutrophil Membranes Can Effectively Treat Cancer Metastasis.* ACS Nano, 2017. **11**(2): p. 1397-1411.

47.   Dolati, S., Sadreddini, S., Rostamzadeh, D., Ahmadi, M., Jadidi-Niaragh, F., and Yousefi, M., *Utilization of nanoparticle technology in rheumatoid arthritis treatment.* Biomedicine & Pharmacotherapy, 2016. **80**: p. 30-41.

48.   Tabas, I. and Glass, C.K., *Anti-Inflammatory Therapy in Chronic Disease: Challenges and Opportunities.* Science, 2013. **339**(6116): p. 166-172.

49.   Jie, Z., Zhang, Y., Wang, C., Shen, B., Guan, X., Ren, Z., Ding, X., Dai, W., and Jiang, Y., *Large-scale ex vivo generation of human neutrophils from cord blood CD34(+) cells.* Plos One, 2017. **12**(7): p. article number e0180832.

50.   Feng, Q., Shabrani, N., Thon, J.N., Huo, H., Thiel, A., Machlus, K.R., Kim, K., Brooks, J., Li, F., Luo, C., Kimbrel, E.A., Wang, J., Kim, K.-S., Italiano, J., Cho, J., Lu, S.-J., and Lanza, R., *Scalable Generation of Universal Platelets from Human Induced Pluripotent Stem Cells.* Stem Cell Reports, 2014. **3**(5): p. 817-831.

Chapter 3

Macrophage-like nanoparticles concurrently absorbing endotoxins and proinflammatory cytokine for sepsis management

3.1 Introduction

Sepsis is a life-threatening complication characterized by systemic inflammatory response caused by bacterial infections.[1] Uncontrolled inflammatory responses in sepsis result in the collapse of cardiovascular function, leading to multiple organ dysfunction syndrome and death.[2, 3] Despite many efforts devoted to finding an effective treatment, sepsis continues to cause a high mortality rate, and the number of hospitalizations resulting from the condition continues to rise.[4, 5] Endotoxin, an important pathogenic trigger of sepsis, induces a systemic inflammatory response characterized by production of proinflammatory cytokines and nitric oxide, fever, hypotension, and intravascular coagulation, which ultimately lead to septic shock.[6] Endotoxin enters the bloodstream via infection sites or by the systemic spread of the bacteria. Emerging evidence suggests that the systemic spread of endotoxin, rather than bacteremia itself, is crucial in the pathogenesis of this dramatic immune dysregulation.[7, 8] It has been found that a higher level of endotoxin correlates with worsened clinical outcomes.[9, 10] Clearly, effective endotoxin removal is critical for successful sepsis management.

Endotoxin neutralization and removal face various challenges. While all endotoxins share a common architecture, they vary greatly in their structural motifs, which are dependent on bacterial genus, species, and strain.[11, 12] Accordingly, their interactions with ligands can differ substantially, which poses challenges for structure-based neutralization strategies. Antibiotics effective in neutralizing endotoxin such as polymyxins only have limited clinical use due to their strong nephrotoxicity and neurotoxicity.[13, 14] Attaching these molecules to solid-phase carriers for hemoperfusion can retain their endotoxin-binding properties while minimizing the toxic effects, but clinical evidence of therapeutic efficacy has yet to be established.[15, 16] In addition, such solid-phase perfusion strategies are impractical in resource-limited environments.[17]

Recently, cell membrane-coated nanoparticles have emerged as a new biomimetic nanomedicine platform, enabling a broad range of biodetoxification applications.[18, 19] In particular, nanoparticles coated with membranes derived from red blood cells (RBC nanosponges) have taken advantage of functional similarities shared by various pore-forming toxins to neutralize their hemolytic activity regardless of molecular structure.[20] This unique core-shell nanoparticle exhibits prolonged systemic circulation, preventing further bioactivity of the toxins that it absorbs and diverting them away from their intended cellular targets. RBC nanosponges have also been developed as therapeutic detoxification agents to neutralize pathological antibodies in autoimmune diseases [21] as well as organophosphate nerve agents.[22]

The therapeutic potential of membrane-coated nanoparticles for broad-spectrum detoxification inspired us to develop biomimetic nanoparticles for endotoxin removal, potentially enabling effective sepsis management. In sepsis, endotoxin, also referred to as lipopolysaccharide (LPS), is released from the bacteria during cell division, cell death, or under antibiotic treatment, and it is subsequently recognized by monocytes and macrophages.[23, 24] In the blood, LPS-binding protein (LBP) binds with high affinity to LPS via lipid A, and the LPS-LBP complex subsequently engages CD14 present on the surface of macrophages.[25, 26] Following the binding interaction, LPS can induce various changes in cellular activity. For example, LPS is cytotoxic to the cells, attributable to the excessive production of nitric oxide; LPS-treated macrophages demonstrate dose-dependent production of nitric oxide in culture.[10] In addition, LPS-macrophage binding activates toll-like receptor 4 (TLR4) and subsequently enhances phagocytosis.[27] TLR4 activation has been considered to play a significant role in the regulation of bacterial uptake, translocation, and cell death.[28, 29] Furthermore, LPS-induced engagement of TLR4 also activates the nuclear factor-κB (NF-κB) transcription factor, which results in the production and secretion of

proinflammatory cytokines such as tumor necrosis factor- α (TNF-α), interleukin 6 (IL-6), and interleukin 8 (IL-8).[30, 31]

Compelled by the critical roles played by macrophages in endotoxin signaling, herein, we develop biomimetic nanoparticles consisting of a biodegradable polymeric nanoparticle core coated with cell membrane derived from macrophages (denoted MΦ-NPs, Figure 3.1A). MΦ-NPs possess an antigenic exterior the same as the source macrophage cells, thus inheriting their capability to bind with endotoxins. In addition, MΦ-NPs also act as decoys to bind with cytokines, inhibiting their ability to potentiate downstream inflammation cascades. These two steps together enable effective intervention during uncontrollable immune activation, providing a therapeutic strategy with significant potential for the management of sepsis.

3.2 Results and discussion

The preparation of MΦ-NPs was divided into two steps. In the first step, cell membranes from J774 mouse macrophages were derived and purified using a process involving hypotonic lysis, mechanical disruption, and differential centrifugation. In the second step, we used a sonication method to form membrane vesicles and subsequently fused them onto poly(lactic-*co*-glycolic acid) (PLGA) cores to form MΦ-NPs. Following membrane fusion, the diameter of the nanoparticles measured with dynamic light scattering (DLS) increased from 84.5 ± 1.9 nm to 102.0 ± 1.5 nm, corresponding to the addition of a bilayered cell membrane onto the polymeric cores (Figure 3.1B). Meanwhile, the surface zeta potential changed from -41.3 ± 3.6 mV to -26.7 ± 3.1 mV, which was likely due to charge screening by the membrane. The resulting MΦ-NPs were then stained with uranyl acetate and visualized by transmission electron microscopy (TEM). Under the microscope, nanoparticles showed a spherical core-shell structure, in which the PLGA core was

wrapped with a thin shell (Figure 3.1C). Following the formulation, MΦ-NPs were suspended in 1× PBS and 50% serum, respectively. Within 72 h, their sizes were monitored with DLS and showed negligible changes, suggesting an excellent stability conferred by membrane coating (Figure 3.1D). Improved colloidal stability is attributable to the stabilizing effect by the macrophage membrane's hydrophilic surface glycans. Together, these results demonstrate the successful coating of PLGA cores with unilamellar macrophage membranes.

Through membrane coating, MΦ-NPs are expected to inherit biological characteristics of the source cells. By using western blotting analysis, we verified that MΦ-NPs preserved critical membrane proteins responsible for LPS binding, including CD14 and TLR4 (Figure 3.1E). Representative cytokine-binding proteins were also preserved, including CD126 and CD130 for interleukin 6 (IL-6), CD120a and CD120b for tumor necrosis factor (TNF), and CD119 for interferon gamma (IFN-γ). Notably, the membrane derivation process not only preserved these proteins, but also resulted in significant protein enrichment. We also studied the systemic circulation time of MΦ-NPs by labeling the nanoparticles with a hydrophobic DiD fluorophore (Figure 3.1F). At 24 h and 48 h, MΦ-NPs showed 29% and 16% retention in the blood, respectively. Based on a two-compartment model that has been applied in previous studies to fit the circulation results of nanoparticles, the elimination half-life was calculated as 17.2 h. We investigated the in vivo tissue distribution of the MΦ-NPs to further evaluate their potential for systemic applications (Figure 3.1G). When analyzed per organ, MΦ-NPs were distributed mainly in the blood and the liver. Per gram of tissue, MΦ-NPs were mainly contained in the liver and spleen, two primary organs of the reticuloendothelial system (RES). Meanwhile, significant fluorescence was also observed in the blood. As the blood fluorescence decreased, a corresponding increase in signal was observed in the liver, suggesting the uptake of MΦ-NPs by the RES over time.
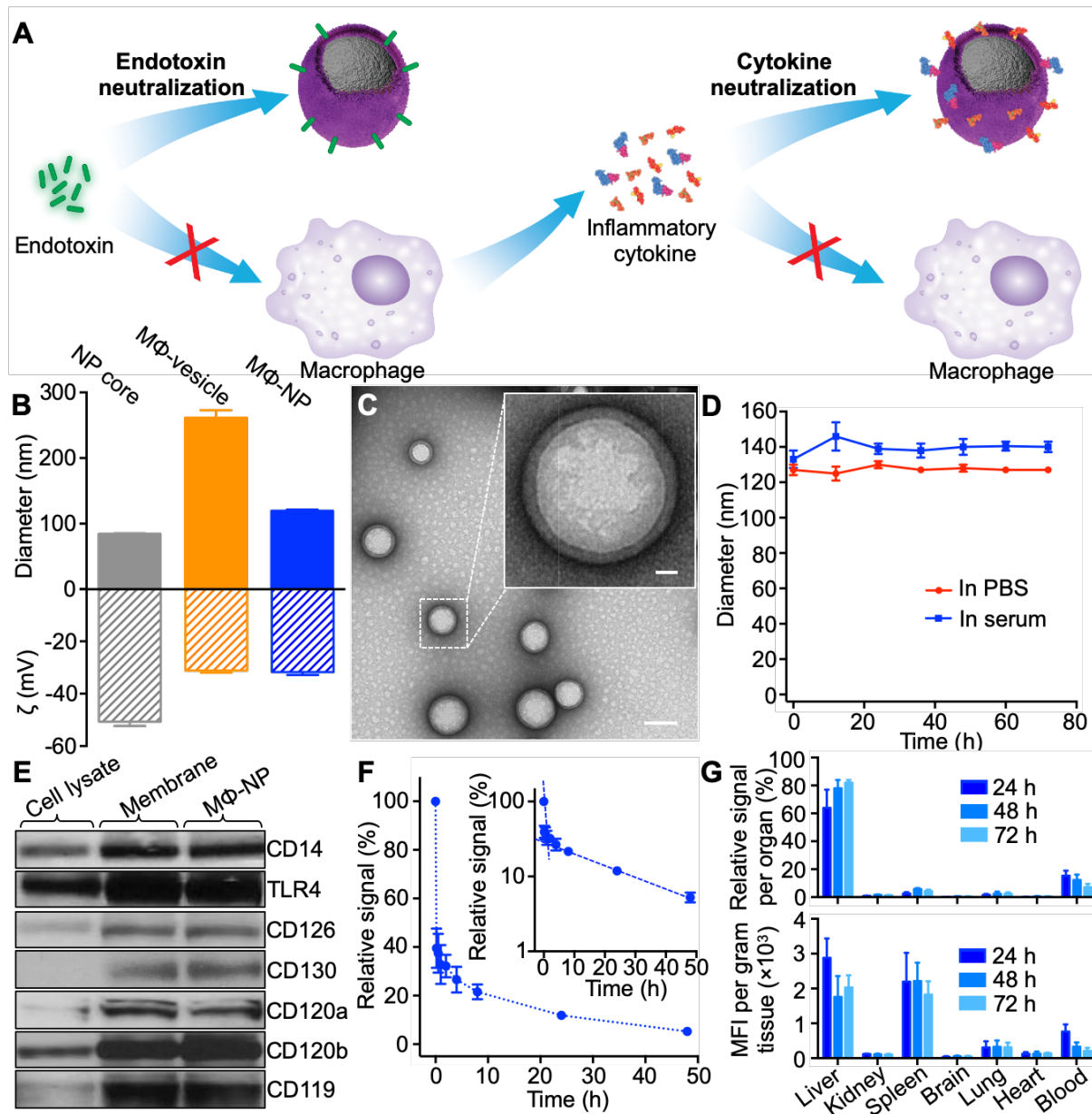
Figure 3.1 Formulation and characterization of macrophage membrane-coated nanoparticles (MΦ-NPs). (A) Schematic representation of using MΦ-NPs to neutralize endotoxin and proinflammatory cytokines as a two-step process for sepsis management. (B) Hydrodynamic size (diameter, nm) and surface zeta potential (ζ, mV) of PLGA polymeric cores before and after coating with macrophage membrane as measured by dynamic light scattering (n = 6). (C) TEM images of MΦ-NPs negatively stained with uranyl acetate. Scale bar = 100 nm. Inset: the roomed-in view of a single MΦ-NP. Scale bare = 10 nm. (D) Stability of MΦ-NPs in 1× PBS or 50% FBS, determined by monitoring particle size (diameter, nm), over a span of 72 h. (E) Representative protein bands of macrophage cell lysate, membrane vesicles, and MΦ-NPs resolved using western blotting. (F) DiD-labeled MΦ-NPs were injected intravenously via the tail vein of mice. At various time points, blood was collected and measured for fluorescence (excitation/emission = 644/670 nm) to evaluate the systemic circulation lifetime of the nanoparticles (n = 6). Inset: the semilog plot of fluorescence signal at various time points. (G) Biodistribution of the MΦ-NPs collected by injecting DiD-labeled MΦ-NPs intravenously into the mice. At each time point (24, 48, and 72 h), the organs from a randomly grouped subset of mice were collected, homogenized, and quantified for fluorescence. Fluorescence intensity per gram of tissue and relative signal per organ were compared (n = 6).

We next examined the ability of MΦ-NPs to bind with LPS, which is known to first form high-affinity complexes with LPS-binding protein (LBP). These complexes then bind to TLR4 through CD14, which are both present on the cell surface of macrophages. We first tested the effect of LBP on LPS binding to MΦ-NPs. In the study, we mixed MΦ-NPs with FITC-LPS conjugate and incubated the mixture at 37°C. Following the incubation, MΦ-NPs were removed with ultracentrifugation and binding was evaluated by comparing FITC fluorescence intensity from the supernatant. As shown in Figure 3.2A, with the absence of LBP, nearly 80% of LPS remained in the solution. However, when LBP was supplemented, only 10% of LPS was left, suggesting a significant increase of LPS binding with MΦ-NPs. We then examined whether LPS binding with MΦ-NPs was dependent on surface markers known to mediate LPS binding with macrophages including CD14 and TLR4. In the study, we used anti-TLR4 or anti-CD14 to block these surface markers. Following each blockade, the amount of unbound LPS remaining in the supernatant increased compared to samples without added antibodies, indicating the decrease of binding interactions between MΦ-NPs and LPS (Figure 3.2B). The study suggests that LPS binding with MΦ-NPs is indeed mediated by CD14 and TLR4. Overall, compared to macrophages, MΦ-NPs show similar dependence on LBP, TLR4, and CD14 in binding with LPS, suggesting that MΦ-NPs inherit the biological characteristics of the source cells.

Next, we quantified LPS removal capability of MΦ-NPs through two sets of experiments. First, we fixed the total amount of MΦ-NPs at 0.4 mg and incubated it with various amounts of LPS (5, 10, 25, and 50 ng, respectively). After removing nanoparticles with ultracentrifuge, it was found that the added amount of MΦ-NPs was able to neutralize up to 25 ng LPS, translating to a LPS removal capacity of 62.5 ng LPS /mg MΦ-NPs (Figure 3.2C). In the second experiment, we fixed the total amount of LPS at 25 ng and varied the amounts of MΦ-NPs (0, 0.1, 0.2, 0.3, 0.4 mg,

respectively). When MΦ-NP concentration was increased from 0.1 to 0.4 mg, a linear decrease of remaining LPS in the supernatant was observed. The measurement showed that 0.4 mg MΦ-NPs are needed to neutralize 25 ng LPS, corresponding to a removal capacity of 62.5 ng LPS /mg MΦ-NPs (Figure 2D), which was consistent with the results of the first experiment.

The ability of MΦ-NPs to bind with proinflammatory cytokines, including IL-6, TNF-α, and IFN-γ, was also investigated. Solutions with known initial concentrations of the cytokines were added with different concentrations of MΦ-NPs and allowed for incubation at 37°C for 30 min. Following the incubation, nanoparticles were removed with ultracentrifugation and the amount of remaining cytokines in the supernatant was quantified. As shown in Figure 3.2E-G, when 1 mg of MΦ-NPs was added, 105.1 pg of IL-6, 4.3 pg of TNF-α, and 6.5 pg of IFN-γ were removed from the mixture, corresponding to a cytokine removal efficiencies of 52.6%, 11.6%, and 14.8%, respectively. When 4 mg of MΦ-NPs was added, 194.4 pg of IL-6, 6.7 pg of TNF-α, and 13.9 pg of IFN-γ were removed from the mixture, corresponding to a cytokine removal yields of 97.2%, 18.1%, and 31.6%, respectively. These quantification results suggest that the MΦ-NPs can effectively sequester various types of proinflammatory cytokines in a concentration dependent manner.
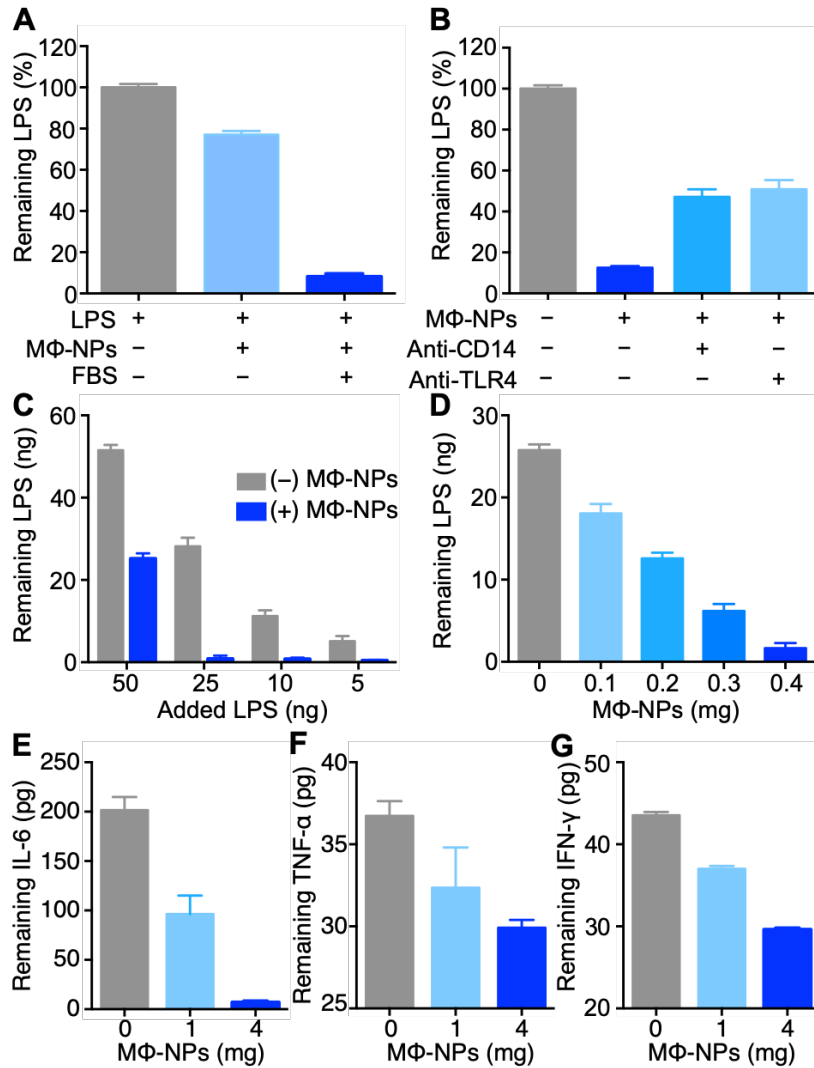
Figure 3.2 In vitro LPS and proinflammatory cytokines removal with MΦ-NPs. (A) LPS removal with MΦ-NPs with and without LPS binding protein (LBP) supplemented from fetal bovine serum (FBS). (B) LPS removal with MΦ-NPs with and without antibodies blocking CD14 and TLR4, respectively. (C) Quantification of LPS removal with a fixed amount of MΦ-NPs (0.4 mg) while varying the amount of added LPS. (D) Quantification of LPS removal with a fixed amount of LPS (25 ng) while varying the amount of added MΦ-NPs. (E-G) Removal of proinflammatory cytokines, including (E) IL-6, (F) TNF-α, and (G) IFN-γ, with MΦ-NPs. In all studies, three samples were used in each group.

Following the LPS and proinflammatory cytokine removal studies, we investigated the ability of MΦ-NPs to neutralize the function of LPS in vitro. Among various cell receptors, TLR4 receptor is well known to interact with LPS and induce an inflammatory response.[27-29] To evaluate the neutralization, we used engineered HEK293 TLR4 reporter cells that produce secreted

embryonic alkaline phosphatase (SEAP) in response to TLR4 activation (Figure 3.3A). When free LPS was added into the cell culture, within 5 h, pronounced TLR4 activation was observed. However, when LPS was incubated with MΦ-NPs prior to their addition to the culture, TLR4 activation was abrogated. To confirm that the neutralization was specific to MΦ-NPs, we also used RBC-NPs and PLGA nanoparticles functionalized with synthetic polyethylene glycol (PEG-NPs). Incubation of LPS with these two control nanoparticle formulations was ineffective in inhibiting TLR4 activation. LPS is also known to induce the overproduction of intracellular nitric oxide (iNO) by inducible NO synthase in various cell types, including macrophages.[10] As a recognized marker of proinflammatory responses, the strong release of iNO may trigger inflammatory cascades in activated cells. We investigated LPS neutralization by examining the attenuation of LPS-induced iNO production by MΦ-NPs (Figure 3.3B). Macrophages incubated with free LPS showed a continual increase of iNO, whereas LPS incubated with MΦ-NPs was unable to enhance iNO production, revealing a clear inhibitory effect; control RBC-NPs or PEG-NPs had no such activity.

Endothelial cells are known to rapidly respond to a minute amount of LPS exposure, which rapidly induces the expression of the cell adhesion molecule E-selectin.[32] As such, we used LPS-mediated induction of E-selectin on human umbilical vein endothelial cells (HUVECs) to further investigate LPS neutralization by MΦ-NPs. In the study, cultured cells were incubated with LPS, and the levels of E-selectin expression were quantified by an enzyme immunoassay. As shown in Figure 3.3C, the addition of LPS at a concentration of 10 ng/mL caused a continuous increase of E-selectin expression. However, when the LPS was added together with 1 mg/mL of MΦ-NPs, E-selectin expression remained at a level comparable to untreated cells. The addition of control nanoparticle groups, including RBC-NPs and PEG-NPs, was unable to inhibit the overexpression

of E-selectin, confirming the specificity of MΦ-NPs in LPS neutralization. Three hours after adding LPS, cells were also stained with antibodies to fluorescently label E-selectin. Under the microscope, cells incubated with LPS alone, LPS with RBC-NPs, and LPS with PEG-NPs showed strong green fluorescence in the cytoplasmic and nuclear peripheral regions (Figure 3.3D). In contrast, little expression was observed on HUVECs incubated with LPS together with MΦ-NPs. These results further confirm the capability of MΦ-NPs in neutralizing LPS.

The LPS neutralization by MΦ-NPs was further evaluated in mice by examining the inhibition of acute inflammatory responses to endotoxin. In the study, LPS at a dosage of 5 μg/kg was injected intravenously via the tail vein of the mice (Figure 3.3E). Following the injection, blood was collected at various time points and the levels of inflammatory cytokines, including TNF-α and IL-6, were quantified by ELISA. Cytokine levels increased and reached maximums at 3 h following injection of LPS alone. By 6 h, they returned to baseline levels. Remarkably, in the study group, where MΦ-NPs at a dosage of 80 mg/kg were injected immediately after the LPS, no increase in cytokine levels was observed. Both TNF-α and IL-6 remained at background levels during the course of the study, demonstrating potent LPS neutralization by the MΦ-NPs. Meanwhile, when MΦ-NPs were replaced with RBC-NPs or PEG-NPs for injection, the cytokine levels followed similar kinetics compared with the LPS only group.

Treatment of mice with D-galactosamine is known to dramatically increase their sensitivity to the lethal effects of LPS. By monitoring the survival rate of LPS-challenged sensitized mice, we further validated MΦ-NPs for their LPS neutralization capability in vivo. As shown in Figure 3.3F, a single intravenous injection of LPS at a dose of 5 μg/kg showed 100% mortality by 32 h after the injection. Mice in the treatment groups received an intravenous injection of MΦ-NPs, RBC-NPs, or PEG-NPs at a dose of 200 mg/kg. In the group treated with MΦ-NPs, 60% of mice survived the

lethal LPS challenge (n = 10). In contrast, RBC-NPs and PEG-NPs failed to improve the survival

rate of the LPS-challenged mice, and there was no significant difference in survival between these

groups and the LPS only group. These results together validated the potential of MΦ-NPs as a novel

endotoxin bioscavenger.
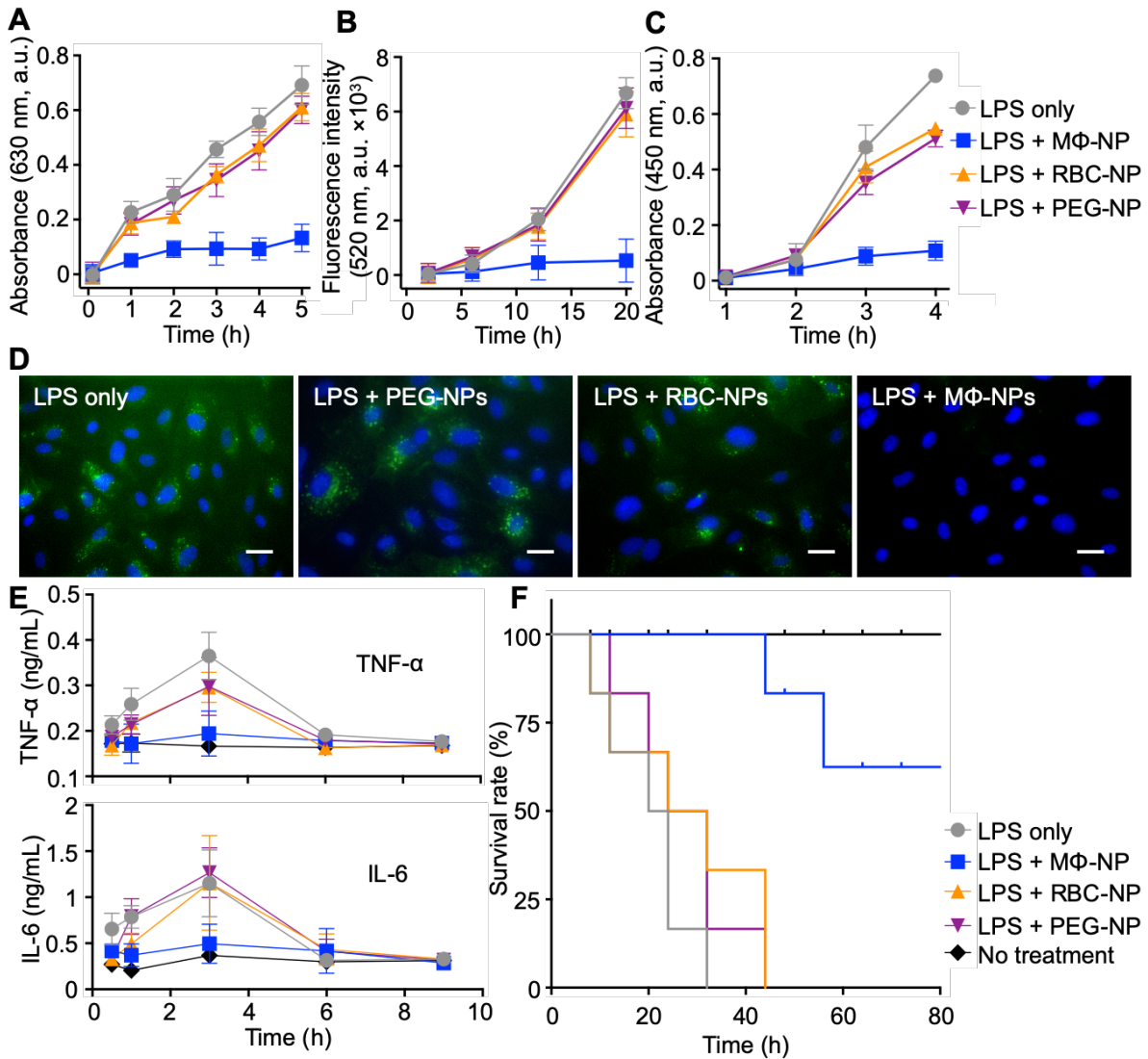
Figure 3.3 In vitro and in vivo LPS neutralization with MΦ-NPs. (A-C) LPS-inducible cell functions, including (A) TLR4 activation on HEK293 cells, (B) intracellular nitric oxide (iNO) production from J774 macrophages, and (C) E-selectin expression of HUVECs, were studied by stimulating corresponding cells with LPS alone or LPS mixed with MΦ-NPs, RBC-NPs, or PEG-NPs, respectively. (D) Fluorescent images collected from samples in (C) after 4 h of incubation. Cells were stained with mouse anti-human E-selectin, followed by staining with anti-mouse IgG Alexa 488-conjugates (green) and DAPI (blue). Scale bars = 5 μm. Three samples were used in each group. (E-F) For in vivo evaluation, (E) levels of inflammatory cytokines, including TNF-α and IL-6, in plasma (n=6) and (F) survival (n=10) were studied after injecting mice with LPS alone or LPS mixed with MΦ-NPs, RBC-NPs, or PEG-NPs. Untreated mice were also included as a control group.

71

Finally, the therapeutic potential of MΦ-NPs in vivo was examined in a mouse model of bacteria-induced systemic inflammation. Mice were challenged intraperitoneally with a lethal dose of *Escherichia coli* (1×10^7 CFU) and treated with either MΦ-NPs (300 mg/kg) or 10% sucrose solution as the control 30 min after bacterial challenge. In this lethal model, all animals in the control group treated with sucrose solution died, whereas four of ten animals treated with MΦ-NPs reached the experimental endpoint of 60 h, demonstrating a significant survival benefit ($p < 0.05$, Figure 3.4A). We then examined the bacterial colonization in key organs, including the blood, spleen, kidney, and liver, 4 h after bacterial injection. In the blood and spleen of the mice treated with MΦ-NPs, the bacterial counts were found to be significantly lower compared to those of the control group. Notably, the kidney and liver from the mice of both groups showed comparable levels of bacterial counts (Figure 3.4B). Furthermore, the reduction of bacterial colonization in the blood and spleen conferred by MΦ-NPs corresponded with a significant reduction of pro-inflammatory cytokines, including IL-6, TNF-α, and IFN-γ, in these organs (Figure 3.4C).
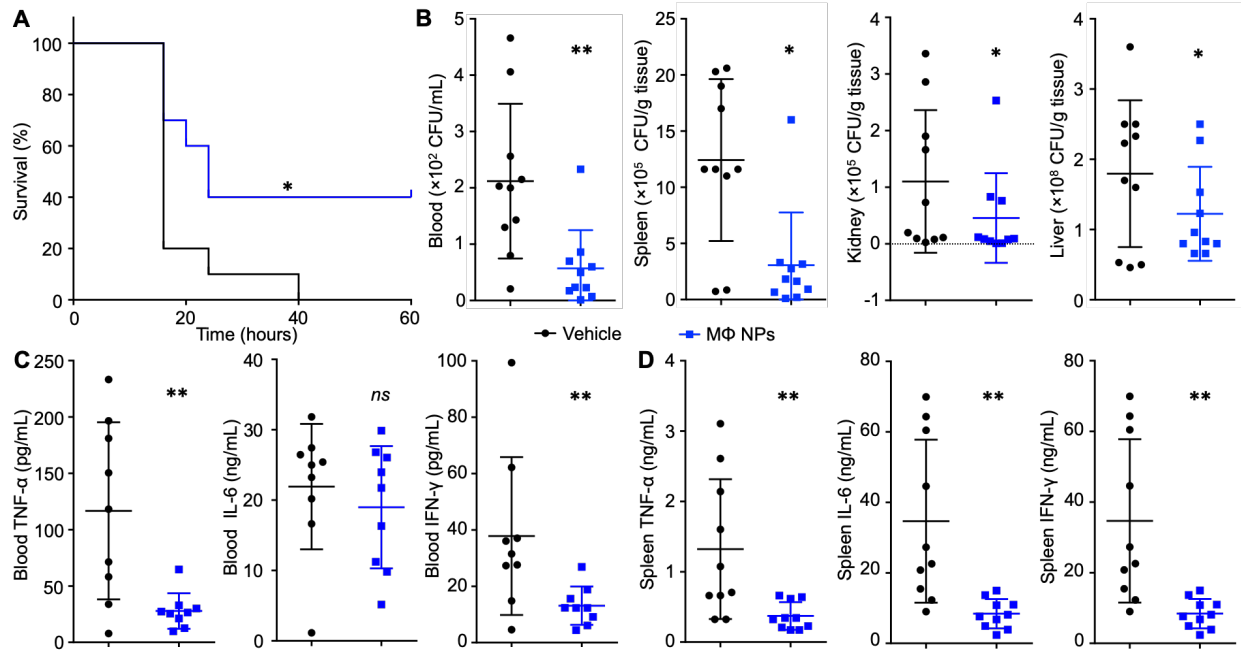
Figure 3.4 In vivo therapeutic efficacy of MΦ-NPs evaluated with a mouse bacteremia model. (A) Survival curve of mice with bacteremia after treatment with MΦ-NPs (n = 10). (B) Bacteria enumeration in blood, spleen, kidney, and liver at 4 h after MΦ-NPs were intraperitoneally injected. (C-D) Pro-inflammatory cytokines, including IL-6, TNF-α, and IFN-γ, from the blood and spleen were quantified with a cytometric bead array. (ns = not significant, *$p < 0.05$, **$p < 0.01$).

3.3 Methods

Macrophage membrane derivation. The murine J774 cell line was purchased from the American Type Culture Collection (ATCC) and maintained in Dulbecco's Modified Eagle Medium (DMEM, Invitrogen) supplemented with 10% fetal bovine serum (FBS, Hyclone) and 1% penicillin-streptomycin (Invitrogen). Plasma membrane was collected according to a previously published centrifugation method.[33] Specifically, cells were grown in T-175 culture flasks to full confluency and detached with 2 mM ethylenediaminetetraacetic acid (EDTA, USB Corporation) in phosphate buffered saline (PBS, Invitrogen). The cells were washed with PBS three times (500 × g for 10 min each) and the cell pellet was suspended in homogenization buffer containing 75 mM sucrose, 20 mM Tris-HCl (pH = 7.5, Mediatech), 2 mM MgCl$_2$ (Sigma Aldrich), 10 mM KCl (Sigma Aldrich), and 1 tablet of protease/phosphatase inhibitors (Pierce ThermoFisher). The

73

suspension was loaded into a dounce homogenizer and the cells were disrupted with 20 passes. Then the suspension was spun down at 3,200 × g for 5 min to remove large debris. The supernatant was collected and centrifuged at 20,000 × g for 25 min, after which the pellet was discarded and the supernatant was centrifuged at 100,000 × g for 35 min. After the centrifugation, the supernatant was discarded and the plasma membrane was collected as an off-white pellet for subsequent experiments. Membrane protein content was quantified with a Pierce BCA assay (Life Technology).

MΦ-NP preparation and characterization. MΦ-NPs were formulated in two steps. In the first step, approximately 80 nm polymeric cores were prepared using 0.67 dL/g carboxyl-terminated 50:50 poly(lactic-*co*-glycolic acid) (PLGA, LACTEL Absorbable Polymers) through a nanoprecipitation method. The PLGA polymer was first dissolved in acetone at a concentration of 10 mg/mL. Then 1 mL of the solution was added rapidly to 3 mL of water. For fluorescently labeled PLGA cores, 1,1'-dioctadecyl-3,3,3',3'-tetramethylindodicarbocyanine perchlorate (DiD, excitation/emission = 644 nm/665 nm, Life Technologies) was loaded into the polymeric cores at 0.1 wt%. The nanoparticle solution was then stirred in open air for 4 h to remove the organic solvent. In the second step, the collected macrophage membranes were mixed with nanoparticle cores at a membrane protein-to-polymer weight ratio of 1:1. The mixture was sonicated with a Fisher Scientific FS30D bath sonicator at a frequency of 42 kHz and a power of 100 W for 2 min. Nanoparticles were measured for size and size distribution with dynamic light scattering (DLS, ZEN 3600 Zetasizer, Malvern). All measurements were done in triplicate at room temperature. Serum and PBS stabilities were examined by mixing 1 mg/mL of MΦ-NPs in water with 100% FBS and 2× PBS, respectively, at a 1:1 volume ratio. Membrane coating was confirmed with transmission electron microscopy (TEM). Briefly, 3 μL of nanoparticle suspension (1 mg/mL) was

deposited onto a glow-discharged carbon-coated copper grid. Five minutes after the sample was deposited, the grid was rinsed with 10 drops of distilled water, followed by staining with a drop of 1 wt% uranyl acetate. The grid was subsequently dried and visualized using an FEI 200 kV Sphera microscope.

Membrane protein characterization. MΦ-NPs were purified from free vesicles, membrane fragments, or unbound proteins by centrifugation at 16,000 × g. Macrophage cell lysates, membrane vesicles, and MΦ-NPs were mixed with lithium dodecyl sulfate (LDS) loading buffer to the same total protein concentration of 1 mg/mL as determined with a Pierce BCA assay (Life Technology). Electrophoresis was carried out with NuPAGE Novex 4-12% Bis-Tris 10-well minigels in MOPS running buffer with an XCell SureLock Electrophoresis System (Invitrogen). Western blot analysis was performed by using primary antibodies including rat anti-mouse CD14, rat anti-mouse CD126, rat anti-mouse CD130, rat anti-mouse CD284, armenian hamster anti-mouse CD120a, armenian hamster anti-mouse CD120b, and armenian hamster anti-mouse CD119 (Biolegend). Corresponding IgG-horseradish peroxidase (HRP) conjugates were used for the secondary staining. Films were developed with ECL western blotting substrate (Pierce) on a Mini-Medical/90 Developer (ImageWorks).

Lipopolysaccharides (LPS) and cytokines binding studies. To study whether LPS binding with MΦ-NPs was dependent on LBP, CD14, or TLR4, the mixture of MΦ-NPs (1 mg/mL) and FITC-LPS (from *E. coli* O111:B4, Sigma, 125 ng/mL) in 1X PBS was added with FBS (10% as the source of LBP), anti-CD14 (Biolegend, 10 μg/mL), or anti-TLR4 (Invivogen, 10 μg/mL), respectively. The solution was incubated at 37°C for 30 min. Following the incubation, MΦ-NPs were spun down with ultracentrifugation (16,000 ×g). The fluorescence intensity from FITC-LPS remaining in the supernatant was measured. The fluorescence intensity from a FITC-LPS solution

of 125 ng/mL served as 100%. The mixtures without adding FBS or antibodies were used as the controls. All experiments were performed in triplicate.

To quantify LPS removal with MΦ-NPs, MΦ-NPs (0.4 mg, 4 mg/mL) were mixed with LPS from *E. coli* K12 (Invivogen) with varying amount of 5, 10, 25, and 50 ng (50, 100, 250, and 500 ng/mL), respectively, in 1X PBS containing 10% FBS. In a parallel experiment, the removal was studied by fixing LPS amount at 50 ng (250 ng/mL) but varying the amount of MΦ-NPs at 0.1, 0.2, 0.3, and 0.4 mg (0.5, 1, 1.5, and 2 mg/mL), respectively. In both cases, the mixtures were incubated for 30 min and then spun down at 16,000 × g for 15 min to pellet the nanoparticles. The free LPS content in the supernatant was quantified by using LAL assay (Thermo Fisher Scientific) per manufacture's instruction. All experiments were performed in triplicate.

To determine MΦ-NP binding with cytokines, including IL-6, TNF-α, and IFN-γ, 100 μL of MΦ-NP samples at concentrations of 1 and 4 mg/mL was incubated with IL-6 (250 pg/mL), TNF-α (50 pg/mL), or IFN-γ (50 pg/mL) in PBS containing 10% FBS at 37 °C for 30 min. Following the incubation, the samples were centrifuged at 16,000 × g for 15 min to pellet the nanoparticles. Cytokine concentrations in the supernatant were quantified by using enzyme-linked immunosorbent assay (ELISA, Biolegend). All experiments were performed in triplicate.

LPS neutralization in vitro. Murine toll-like receptor 4 (TLR4) reporter cells (HEK-Blue™ mTLR4 cells, Invivogen) were first used to determine LPS neutralization by MΦ-NPs. Cells were cultured in DMEM supplemented with 10% FBS, 1% pen-strep, 100 μg/mL Normocin™, 2 mM L-glutamine, and 1× HEK-Blue™ selection (Invivogen). In the study, 2.5×10^4 cells were seeded in each well of a 96-well plate with 160 μL HEK-Blue™ detection medium, followed by adding 20 μL of 100 ng/mL LPS in PBS. Then 20 μL of nanoparticle solution of MΦ-NPs, RBC-NPs, or PEG-NPs (all at a concentration of 10 mg/mL), was added into each well. Control wells were

added with 20 µL PBS. Cells without any treatment served as the background. The mixture was incubated for 12 h. Secreted embryonic alkaline phosphatase (SEAP) was quantified by measuring the absorbance at 630 nm with an Infinite M200 multiplate reader (Tecan). All experiments were performed in triplicate.

Production of intracellular nitric oxide (iNO) was also used to evaluate LPS neutralization with MΦ-NPs. Briefly, 2×10^4 J774 cells were seeded in each well of a 96-well plate. The cells were incubated with 10 µM of 2', 7'-dichlorofluorescin-diacetate (DCFH-DA, Sigma) in culture medium for 1 h, and then washed 3 times with the culture medium. Then the wells were added with 180 µL of medium containing 10 ng/mL of LPS. Then 20 µL of nanoparticle solution of MΦ-NPs, RBC-NPs, or PEG-NPs (all at a concentration of 10 mg/mL), was added into each well. Control wells were added with 20 µL PBS. Cells without any treatment served as the background. The plate was incubated at 37°C for 5 h. The production of iNO was quantified by measuring the fluorescence intensity at 520 nm using an excitation wavelength of 485 nm (Infinite M200 multiplate reader, Tecan). All experiments were performed in triplicate.

LPS neutralization with MΦ-NPs was further evaluated by examining E-selectin expression on human umbilical vein endothelial cells (HUVECs). Specifically, HUVECs were cultured to confluence in a 96-well plate. Then 200 µL of LPS (250 ng/mL) mixed with MΦ-NPs, RBC-NPs, or PEG-NPs (4 mg/mL) in culture medium was added to the cells and the plate was incubated at 37°C. Cells added with LPS and PBS were used as controls. Three wells were used per sample. After 1, 2, 3, and 4 h of incubation at 37°C, medium was removed and cells were washed with PBS. Then the cells were fixed with 4% paraformaldehyde (Sigma) at room temperature for 15 min. Following the fixation, cells were washed twice with PBS and blocked with 1% bovine serum albumin (BSA, Sigma). Subsequently, the reagent was decanted and 50 µL

of primary antibody (mouse anti-human E-selectin, Biolegend, 1:10 dilution in 1% BSA) was added to each well and incubated at 37°C for 45 min. Wells were then rinsed three times with 1X PBS prior to the addition of 50 μl of secondary antibody (HRP-conjugated anti-mouse IgG, Biolegend, 1:10 dilution in 1% BSA) followed by an incubation for 45 min at 37°C. After this, wells were again rinsed three times with 1X PBS and after the final rinse, 100 μl of TMB (3,3',5,5'-tetramethylbenzidine) substrate solution was added to each well. The plate was incubated at 37°C followed by measuring the absorbance at 450 nm.

To visually examine E-selectin expression, cells following the same treatment as above experiment were incubated at 37°C for 4 h and rinsed twice with PBS, fixed with 4% paraformaldehyde for 15 min, permeabilized in 0.2% Triton X-100 (Sigma) in buffer for 10 min, and then incubated with 1% BSA in PBS for 30 min. Cells were then stained with mouse anti-human E-selectin for 1 h, washed 3 times with 1× PBS and then incubated with anti-mouse IgG Alexa 488-conjugates in 1% BSA in PBS for 1 h. Cell nuclei were stained with DAPI (1 mg/mL stock solution, Thermo Fisher Scientific). Fluorescence images were taken with an EVOS fluorescence microscope (Thermo Fisher Scientific).

Animal care and injections. All animal studies were approved under the guidelines of the University of California San Diego (UCSD) Institutional Animal Care and Use Committee (IACUC). Mice were housed in an animal facility at UCSD under federal, state, local, and National Institutes of Health guidelines for animal care. In the study, no inflammation was observed at the sites of injection.

Pharmacokinetics and biodistribution studies. The experiments were performed on 6-week old male ICR mice (Harlan Laboratories). To determine the circulation half-life, 150 μL of DiD-labeled MΦ-NPs (3 mg/mL) were injected intravenously through the tail vein. At 1, 15, 30 min,

and 1, 2, 4, 8, 24, 48, 72 h post-injection, one drop of blood (~30 μL) was collected from each mouse via submandibular puncture. Then 20 μL of blood was mixed with 180 μL PBS in a 96-well plate for fluorescence measurement. Pharmacokinetic parameters were calculated to fit a two-compartment model. For biodistribution study, 150 μL of DiD-labeled MΦ-NPs (3 mg/mL) were injected intravenously through the tail vein. At 24, 48, and 72 h post-injection, organs including the liver, kidneys, spleen, brain, lungs, heart, and blood were collected from six randomly selected mice. The collected organs were weighed and then homogenized in PBS for fluorescence measurement. All fluorescence measurements were carried out with an Infinite M200 multiplate reader (Tecan).

LPS neutralization in vivo. The efficacy of MΦ-NPs in neutralizing LPS was first evaluated with a mouse endotoxemia model with 6-week old male BALB/c mice (Harlan). To evaluate the efficacy through cytokine production, mice were injected with 5 μg/kg LPS through the tail vein. After 15 min, MΦ-NPs, RBC-NPs, or PEG-NPs were injected at 200 mg/kg. Following the injections, blood samples (<30 μL) were collected at predetermined time points via submandibular puncture. Untreated mice and mice injected with LPS alone were used as controls. Cytokines, including IL-6 and TNF-α, in the plasma were quantified by ELISA as described above. In each group, 6 mice were used. To evaluate efficacy through survival, mice were first sensitized with D-galactosamine hydrochloride (Sigma Aldrich) via intraperitoneal injection at a dosage of 800 mg/kg. After 30 min of sensitization, LPS and nanoparticles were injected with the same dosing method. Ten mice were used in each group.

LPS neutralization efficacy was also evaluated with a mouse bacteremia model. Specifically, 6-week old male BALB/c mice were injected intravenously with 1×10^7 CFU of *Escherichia coli* UPEC suspended in 100 μL of 1× PBS. After 20 min, mice were randomly placed

into two groups (n = 10), and each mouse was injected with 500 μL of MΦ-NPs at a concentration of 10 mg/mL in 10% sucrose solution intraperitoneally. Mice were euthanized 4 h after the injection. Blood and organs were collected and homogenized with a Mini Beadbeater-16 (BioSpec) in 1 mL of PBS. Proinflammatory cytokines in the blood, including IL-6, TNF-α, and IFN-γ, were quantified by a cytometric bead array per manufacturer's instruction (BD Biosciences). For bacterial enumeration, homogenized samples were serially diluted with PBS (from 10 to 107 folds) and plated onto agar plates. After 24 h of culture, bacterial colonies were counted. To evaluate efficacy through survival, mice were sensitized with D-galactosamine hydrochloride via intraperitoneally injection at a dosage of 800 mg/kg, followed by the same experimental procedure (n = 10). Survival after the treatment was recorded.

3.4 Conclusions

In summary, we have demonstrated a therapeutic potential of MΦ-NPs for sepsis control through an apparent two-step neutralization process: LPS neutralization in the first step followed by cytokine sequestration in the second step. MΦ-NPs function as an LPS and cytokine decoy, binding the proinflammatory factors through their cognate PRR and cytokine receptors in a manner decoupled from signal transduction and transcriptional activation of macrophage inflammatory cascades. By thus inhibiting the systemic inflammatory response, MΦ-NPs confer a significant survival benefit during septic shock. Unlike conventional endotoxin neutralization agents that compete with endotoxin binding pathways and may be associated with significant clinical toxicity, MΦ-NPs take advantage of the common functionality of endo- toxin binding to macrophages, allowing for a "universal" neutralization approach across different Gram-negative bacterial genus, species, and strains. The top-down fabrication of MΦ-NPs effectively replicates endotoxin-binding

motifs on the target cells that are otherwise difficult to identify, purify, and conjugate. Coating macrophage membranes onto nanoparticle surfaces significantly increases the surface-to-volume ratio of given membrane materials, which is critical for efficient endotoxin neutralization.

In theory, similar first-step benefits as an adjunctive therapeutic agent could be afforded by MΦ-NPs against Gram-positive bacterial sepsis pathogens, by scavenging lipoteichoic acids and peptidoglycans via cognate PRRs TLR2/6, or fungal sepsis pathogen, by scavenging cell wall β-glucans with cognate PRR Dectin-1; although these indications remain to be studied in the manner undertaken with LPS/E. coli in the current paper. Moreover, in septic shock caused by any pathogen, second-step cytokine sequestration properties could be seen to mitigate the pathologic damage of cytokine storm. Given a likely i.v. route of administration, however, the pharmacodynamics efficacy of MΦ-NPs against tissue foci of infection such as pneumonia, peritonitis, or bone/soft tissue infections would have to be validated. Meanwhile, novel LPS-binding ligands have been engineered and applied for endotoxin neutralization and detoxification in sepsis.[34] With a lipid-like structure, they can be introduced onto MΦ-NPs through methods such as lipid insertion[35] or membrane hybridization.[36] both of which have been validated for functionalizing nanoparticles coated with different cell membranes. Overall, MΦ-NPs represent a promising biomimetic detoxification strategy that may ultimately improve the clinical outcome of sepsis patients, potentially shifting the current paradigm of clinical detoxification therapy.

Chapter 3, in full, is a reprint of the material as it appears in *Proceedings of National Academy of Sciences*, 2017, Soracha Thamphiwatana, Pavimol Angsantikul, Tamara Escajadillo, Qiangzhe Zhang, Joshua Olson, Brian T. Luk, Sophia Zhang, Ronnie H. Fang, Weiwei Gao, Victor Nizet, and Liangfang Zhang. The dissertation author was major contributor and co-author of this paper.

3.5 References

1. Angus, D.C. and van der Poll, T., *Severe Sepsis and Septic Shock.* New England Journal of Medicine, 2013. **369**(9): p. 840-851.

2. Cohen, J., *The immunopathogenesis of sepsis.* Nature, 2002. **420**(6917): p. 885-891.

3. Rittirsch, D., Flierl, M.A., and Ward, P.A., *Harmful molecular mechanisms in sepsis.* Nature Reviews: Immunology, 2008. **8**(10): p. 776-787.

4. Ranieri, V.M., Thompson, B.T., Barie, P.S., Dhainaut, J.F., Douglas, I.S., Finfer, S., Gardlund, B., Marshall, J.C., Rhodes, A., Artigas, A., Payen, D., Tenhunen, J., Al-Khalidi, H.R., Thompson, V., Janes, J., Macias, W.L., Vangerow, B., Williams, M.D., and Grp, P.-S.S., *Drotrecogin Alfa (Activated) in Adults with Septic Shock.* New England Journal of Medicine, 2012. **366**(22): p. 2055-2064.

5. Gaieski, D.F., Edwards, J.M., Kallan, M.J., and Carr, B.G., *Benchmarking the Incidence and Mortality of Severe Sepsis in the United States.* Critical Care Medicine, 2013. **41**(5): p. 1167-1174.

6. Yaroustovsky, M., Plyushch, M., Popov, D., Samsonova, N., Abramyan, M., Popok, Z., and Krotenko, N., *Prognostic value of endotoxin activity assay in patients with severe sepsis after cardiac surgery.* Journal of Inflammation, 2013. **10**: p. article number e0129450.

7. Grandel, U. and Grimminger, F., *Endothelial responses to bacterial toxins in sepsis.* Critical Reviews in Immunology, 2003. **23**(4): p. 267-299.

8. Peters, K., Unger, R.E., Brunner, J., and Kirkpatrick, C.J., *Molecular basis of endothelial dysfunction in sepsis.* Cardiovascular Research, 2003. **60**(1): p. 49-57.

9. Wang, Y., *Attenuation of berberine on lipopolysaccharide-induced inflammatory and apoptosis responses in beta-cells via TLR4-independent JNK/NF-kappa B pathway.* Pharmaceutical Biology, 2014. **52**(4): p. 532-538.

10. Nishio, K., Horie, M., Akazawa, Y., Shichiri, M., Iwahashi, H., Hagihara, Y., Yoshida, Y., and Niki, E., *Attenuation of lipopolysaccharide (LPS)-induced cytotoxicity by tocopherols and tocotrienols.* Redox Biology, 2013. **1**(1): p. 97-103.

11. Brandenburg, K. and Wiese, A., *Endotoxins: Relationships between structure, function, and activity.* Current Topics in Medicinal Chemistry, 2004. **4**(11): p. 1127-1146.

12. Gabrielli, L., Capitoli, A., Bini, D., Taraballi, F., Lupo, C., Russo, L., and Cipolla, L., *Recent Approaches to Novel Antibacterials Designed After LPS Structure and Biochemistry.* Current Drug Targets, 2012. **13**(11): p. 1458-1471.

13. Kelesidis, T. and Falagas, M.E., *The safety of polymyxin antibiotics.* Expert Opinion on Drug Safety, 2015. **14**(11): p. 1687-1701.

14. Justo, J.A. and Bosso, J.A., *Adverse Reactions Associated with Systemic Polymyxin Therapy.* Pharmacotherapy, 2015. **35**(1): p. 28-33.

15. Cavaillon, J.M., *Polymyxin B for endotoxin removal in sepsis.* Lancet Infectious Diseases, 2011. **11**(6): p. 426-427.

16. Fujii, T., Ganeko, R., Kataoka, Y., Featherstone, R., Bagshaw, S.M., and Furukawa, T.A., *Polymyxin B-immobilised haemoperfusion and mortality in critically ill patients with sepsis/septic shock: a protocol for a systematic review and meta-analysis.* Bmj Open, 2016. **6**(11): p. article number e012908.

17. Raghavan, R., *When Access to Chronic Dialysis is Limited: One Center's Approach to Emergent Hemodialysis.* Seminars in Dialysis, 2012. **25**(3): p. 267-271.

18. Zhang, L. and Leroux, J.C., *Current and forthcoming approaches for systemic detoxification Preface.* Advanced Drug Delivery Reviews, 2015. **90**: p. 1-2.

19. Hu, C.M.J., Fang, R.H., Wang, K.C., Luk, B.T., Thamphiwatana, S., Dehaini, D., Nguyen, P., Angsantikul, P., Wen, C.H., Kroll, A.V., Carpenter, C., Ramesh, M., Qu, V., Patel, S.H., Zhu, J., Shi, W., Hofman, F.M., Chen, T.C., Gao, W., Zhang, K., Chien, S., and Zhang, L., *Nanoparticle biointerfacing by platelet membrane cloaking.* Nature, 2015. **526**(7571): p. 118-121.

20. Hu, C.M.J., Fang, R.H., Copp, J., Luk, B.T., and Zhang, L., *A biomimetic nanosponge that absorbs pore-forming toxins.* Nature Nanotechnology, 2013. **8**(5): p. 336-340.

21. Copp, J.A., Fang, R.H., Luk, B.T., Hu, C.M.J., Gao, W., Zhang, K., and Zhang, L., *Clearance of pathological antibodies using biomimetic nanoparticles.* Proceedings of the National Academy of Sciences of the United States of America, 2014. **111**(37): p. 13481-13486.

22. Pang, Z.Q., Hu, C.M.J., Fang, R.H., Luk, B.T., Gao, W., Wang, F., Chuluun, E., Angsantikul, P., Thamphiwatana, S., Lu, W.Y., Jiang, X.G., and Zhang, L., *Detoxification of Organophosphate Poisoning Using Nanoparticle Bioscavengers.* ACS Nano, 2015. **9**(6): p. 6450-6458.

23. Akira, S., Takeda, K., and Kaisho, T., *Toll-like receptors: critical proteins linking innate and acquired immunity.* Nature Immunology, 2001. **2**(8): p. 675-680.

24. Medzhitov, R., *Toll-like receptors and innate immunity.* Nature Reviews: Immunology, 2001. **1**(2): p. 135-145.

25. Schutt, C., *Fighting infection: The role of lipopolysaccharide binding proteins CD14 and LBP.* Pathobiology, 1999. **67**(5-6): p. 227-229.

26. Triantafilou, M. and Triantafilou, K., *Lipopolysaccharide recognition: CD14, TLRs and the LPS-activation cluster.* Trends in Immunology, 2002. **23**(6): p. 301-304.

27. Zanoni, I., Ostuni, R., Marek, L.R., Barresi, S., Barbalat, R., Barton, G.M., Granucci, F., and Kagan, J.C., *CD14 Controls the LPS-Induced Endocytosis of Toll-like Receptor 4.* Cell, 2011. **147**(4): p. 868-880.

28. Schilling, J.D., Machkovech, H.M., He, L., Diwan, A., and Schaffer, J.E., *TLR4 Activation Under Lipotoxic Conditions Leads to Synergistic Macrophage Cell Death through a TRIF-Dependent Pathway.* Journal of Immunology, 2013. **190**(3): p. 1285-1296.

29. Hagar, J.A., Powell, D.A., Aachoui, Y., Ernst, R.K., and Miao, E.A., *Cytoplasmic LPS Activates Caspase-11: Implications in TLR4-Independent Endotoxic Shock.* Science, 2013. **341**(6151): p. 1250-1253.

30. Martinon, F., Chen, X., Lee, A.-H., and Glimcher, L.H., *TLR activation of the transcription factor XBP1 regulates innate immune responses in macrophages.* Nature Immunology, 2010. **11**(5): p. 411-418.

31. Spence, S., Greene, M.K., Fay, F., Hams, E., Saunders, S.P., Hamid, U., Fitzgerald, M., Beck, J., Bains, B.K., Smyth, P., Themistou, E., Small, D.M., Schmid, D., O'Kane, C.M., Fitzgerald, D.C., Abdelghany, S.M., Johnston, J.A., Fallon, P.G., Burrows, J.F., McAuley, D.F., Kissenpfennig, A., and Scott, C.J., *Targeting Siglecs with a sialic acid-decorated nanoparticle abrogates inflammation.* Science Translational Medicine, 2015. **7**(303): p. article number 303ra140.

32. Unger, R.E., Peters, K., Sartoris, A., Freese, C., and Kirkpatrick, C.J., *Human endothelial cell-based assay for endotoxin as sensitive as the conventional Limulus Amebocyte Lysate assay.* Biomaterials, 2014. **35**(10): p. 3180-3187.

33. Fang, R.H., Hu, C.M.J., Luk, B.T., Gao, W., Copp, J.A., Tai, Y.Y., O'Connor, D.E., and Zhang, L., *Cancer Cell Membrane-Coated Nanoparticles for Anticancer Vaccination and Drug Delivery.* Nano Letters, 2014. **14**(4): p. 2181-2188.

34. Kang, J.H., Super, M., Yung, C.W., Cooper, R.M., Domansky, K., Graveline, A.R., Mammoto, T., Berthet, J.B., Tobin, H., Cartwright, M.J., Watters, A.L., Rottman, M., Waterhouse, A., Mammoto, A., Gamini, N., Rodas, M.J., Kole, A., Jiang, A., Valentin, T.M., Diaz, A., Takahashi, K., Ingber, D.E., *An extracorporeal blood-cleansing device for sepsis therapy.* Nature Medicine, 2014, **20**, p. 1211-1216.

35. Fang, R.H., Hu, C.M.J., Chen, K.N.H., Luk, B.T., Carpenter, C.W., Gao, W., Li, S.L., Zhang, D.E., Lu, W.Y., and Zhang, L., *Lipid-insertion enables targeting functionalization of erythrocyte membrane-cloaked nanoparticles*, Nanoscale, 2014, **5**, p. 8884-8888.

36.   Dehaini, D., Wei, X., Fang, R.H., Masson, S., Angsantikul, P., Luk, B.T., Zhang, Y., Ying, M., Jiang, Y., Kroll, A.V., Gao, W., Zhang, L., *Erythrocyte-platelet hybrid membrane coating for enhanced nanoparticle functionalization*, Advanced Materials, 2017, **29**(16), 1606209.

Chapter 4

A biomimetic nanoparticle to 'lure and kill' phospholipase A2

4.1 A biomimetic nanoparticle to 'lure and kill' venomous phospholipase A2

4.1.1 Introduction

Phospholipase A2 (PLA2) enzymes catalyze the cleavage of glycerophospholipids yielding a free fatty acid and a lysophospholipid.[1, 2] They play pivotal roles in regulating cellular functions, including phospholipid digestion, host defense, and signal transduction.[3] However, under pathological conditions, an elevated PLA2 activity is linked to numerous diseases such as animal envenomation, autoimmune disorder, and cancer.[4, 5] Accordingly, inhibition of PLA2 has been sought as a therapeutic strategy to treat these diseases.[6] Many inhibitors, including small molecule compounds and antibodies, have been developed and studied in clinical trials, but none has achieved clinical success.[7, 8] The failure is attributed in part to the lack of subtype and functional selectivity of the inhibitors against PLA2. These inhibitors also face additional limitations such as poor solubility and high off-target toxicity. As a result, novel strategies for the effective and safe inhibition of PLA2 are highly desirable.[9, 10].

Recently, advances in nanotechnology have led to nanoparticle approaches to improve PLA2 inhibition. For example, nanoscale liposomes were formulated to encapsulate poorly soluble PLA2 inhibitors otherwise unsuitable for administration.[11] Similar nanoliposomes were able to reduce the toxicity of small molecule inhibitors while improving their bioavailability.[12] In addition, nanoparticles containing cationic polymers have been made to facilitate the intracellular delivery of small interfering RNAs that specifically silenced the expression of cytosolic PLA2 for precise enzyme inhibition.[13] Meanwhile, affinity nanoparticles have been made by screening a library of functional monomers to selectively inhibit certain classes of PLA2.[14, 15]

While synthetic nanoparticles are increasingly explored to inhibit PLA2 for treatment, using natural cell membranes to coat nanoparticles have recently gained much attention as a broad-

spectrum countermeasure platform against various toxicants.[16] The detoxification mechanism is largely function-driven, in which the cell membrane-coated nanoparticles act as decoys of the source cells to capture toxic agents and subsequently divert them away from their intended cellular targets. By coating with membranes of different cell types, the resulting cell-like nanoparticles have been made to capture chemical agents, bacterial toxins, autoantibodies, inflammatory factors, and viruses.[17-22] In addition, by using oil nanodroplets as substrate for coating, the resulting nanostructures combine the specific binding ability of biological receptors present on the cell membrane with the nonspecific absorption function of the oil droplet, leading to a dual-modal and high capacity detoxification platform.[23] Despite the versatility, however, cell membrane-coated nanoparticles have yet been applied to the inhibition of harmful enzymes, owing largely to the sacrificial rather than inhibitive nature of a decoy in enzymatic reactions. To overcome this limitation, novel chemical designs aimed to extend the cell membrane coating technology toward enzyme inhibition are highly desirable.

Herein, we report a biomimetic nanoparticle design based on cell membrane coating technology toward safe and effective PLA2 inhibition based upon a unique 'lure and kill' action mechanism (denoted 'L&K-NP', Figure 4.1A). To formulate L&K-NP, purified RBC membrane was first derived from packed mouse RBCs through a hypotonic treatment.[24] The membrane was then mixed with oleyl-oxyethyl-phosphorylcholine (OOPC, a PLA2 inhibitor) and sonicated to form OOPC-modified RBC membrane vesicles (RBC-OOPC vesicles). Meanwhile, poly(lactic-co-glycolic acid) (PLGA) cores were prepared through a nanoprecipitation method.[24] Following their preparation, RBC-OOPC vesicles and PLGA cores were mixed at a membrane protein-to-PLGA weight ratio of 0.5:1, followed by sonication for coating. After the removal of the uncoated membrane, the nanoparticle coated with RBC-OOPC vesicles (denoted 'RBC-OOPC-NP')

suspension was added with melittin, which spontaneously inserted into the membrane, leading to the final nanoparticles formulation, L&K-NP.[18]

In the L&K-NP design, cell membrane coating allows the nanoparticle to mimic target cells in order to 'lure' PLA2 and divert it away from host cells. Melittin, a membrane lytic peptide known to attract PLA2, is incorporated into the cell membrane.[25] Instead of a simple sacrificial approach for PLA2 absorption, we also incorporate a PLA2 inhibitor with a lipid-like structure into the cell membrane to 'kill' PLA2 when the enzyme attacks the nanoparticle.[26] In this design, the cell membrane not only hosts melittin and the inhibitor, but also avoids the toxicity associated with the PLA2 attractant and inhibitor that makes them overwise impractical for safe use in their free form. Overall, the L&K-NP design not only serves as a platform for the integration of these components, but also orchestrates the bioactivity of each component, leading to a unique and robust anti-PLA2 approach. In this study, we formulate L&K-NPs and show their effective inhibition against PLA2 from bee venom. We also demonstrate that L&K-NPs protect mice from PLA2-induced lethality without obvious toxicity. Overall, L&K-NPs represent a biomimetic nanoparticle platform for effective and safe PLA2 inhibition.

4.1.2 Results and discussion

To formulate L&K-NPs, OOPC and melittin were added at initial input of 16 wt% and 0.2 wt%, respectively (in relation to RBC membrane protein weight). Following the formulation, we confirmed the incorporation of OOPC by analyzing the presence of free OOPC in L&K-NP with mass spectrometry. The loading yield of OOPC and melittin was found to be 15.8% and 0.19 wt%, respectively (in relation to RBC membrane protein weight). After the formulation, L&K-NPs were examined with dynamic light scattering. As shown in Figure 4.1B, the diameter of L&K-NPs

increased from 95.1 ± 1.2 of uncoated PLGA cores to 111.3 ± 2.0 nm after coating, consistent with

the addition of a bilayered RBC membrane onto the polymeric cores.[24] Meanwhile, the surface

zeta potential of L&K-NPs increased from −42.4 ± 1.7 of the uncoated PLGA core to −12.4 ± 1.0

mV, likely due to the charge screening by the membrane. Notably, RBC-NPs, RBC-OOPC-NPs,

and RBC membrane inserted with melittin without OOPC (denoted 'RBC-melittin-NPs') showed

comparable sizes and surface charge. In addition, when analyzed with transmission electron

microscopy (TEM), L&K-NPs displayed a characteristic core-shell morphology (Figure 4.1C).

When suspended in water and 1X PBS, nanoparticle size remained unchanged over 7 days,

demonstrating high colloidal stability (Figure 4.1D). These results together confirm the successful

formulation of L&K-NPs.
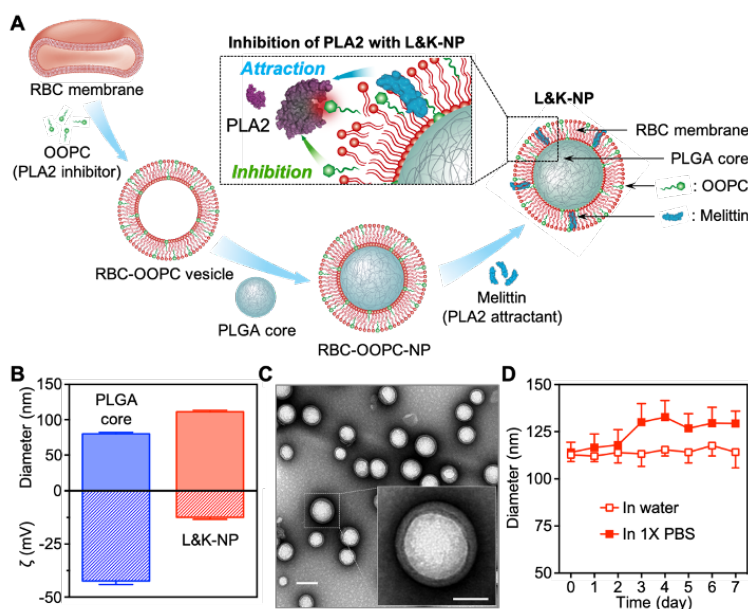
Figure 4.1.1 Formulation and characterization of L&K-NPs. (A) Schematic preparation of L&K-NPs and their use for PLA2 inhibition. To prepare L&K-NPs, oleyl-oxyethyl-phosphorylcholine (OOPC, a PLA2 inhibitor) and melittin (a PLA2 attractant) are incorporated into the RBC membrane in two consecutive steps. The resulting L&K-NPs feature a core-shell structure consisting of OOPC- and melittin-doped RBC membrane shell and a poly(lactic-co-glycolic acid) (PLGA) polymeric core. The incorporated melittin is to entice PLA2 to attack the RBC membrane while the OOPC is to inhibit PLA2 activity when it attacks RBC membrane. **(B)** Dynamic light scattering measurements of hydrodynamic size (diameter, top) and zeta potential (ζ, bottom) of L&K-NPs in comparison with PLGA cores (n = 3). **(C)** Representative images of L&K-NPs examined with transmission electron microscopy. Samples were stained with uranyl acetate (scale bar, 100 nm). Insert: a zoomed-in image of a L&K-NP (scale bar = 50 nm). **(D)** Stability of L&K-NPs in deionized water or 1X PBS, determined by monitoring particle size (diameter), over 7 d (n = 3).

L&K-NPs integrate OOPC and melittin within the cell membrane for bioactivity. We hypothesize that this feature would reduce toxic effects associated with free melittin and OOPC. Melittin and OOPC are known to elicit strong hemolysis on RBCs and cytotoxicity on human umbilical vein endothelial cells (HUVECs).[27, 28] To test the above hypothesis, the hemolytic activity of L&K-NP was first compared with equivalent amounts of free OOPC and melittin. When mixed with RBCs, L&K-NP ranging from 0.0031 to 8 mg/mL appeared non-hemolytic (Figure 4.2A). In contrast, free OOPC induced dose-response hemolysis and a 'hemolytic dosage' needed to lyse 100% of RBCs (denoted 'HD100') was found to be approximately 64 μg/mL (equivalent to the amount of OOPC in 0.4 mg/mL of L&K-NP, Figure 4.2B). Meanwhile, free melittin also induced dose-dependent hemolysis with an HD100 value of 8 μg/mL (equivalent to the amount of melittin in 4 mg/mL of L&K-NP, Figure 4.2C). To further confirm the reduction of toxicity, L&K-NPs and equivalent amounts of free OOPC and melittin were added to HUVECs, respectively. After 48 h, HUVECs incubated with L&K-NP ranging from 0.0031 to 8 mg/mL remained fully viable (Figure 4.2D). In contrast, free OOPC and melittin elicited cell death in a concentration-dependent matter and killed 100% of the cells at 16 and 16 μg/mL, respectively (LD100, equivalent to the amount in 0.1 and 8 mg/mL of L&K-NP, respectively, Figure 4.2E-F). Overall, these results confirm that L&K-NPs abolish the toxic effect of free OOPC and melittin.
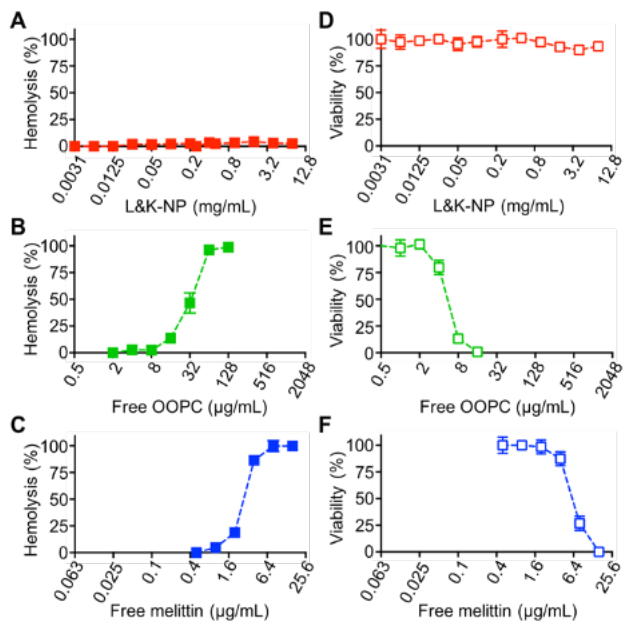
Figure 4.1.2 L&K-NPs abolished the cytotoxicity associated with free OOPC and free melittin. (A–C) Comparison of the hemolytic activity of L&K-NPs (**A**), free OOPC (**B**), and free melittin (**C**). **(D–F)** Comparison of the cytotoxicity on human umbilical vein endothelial cells (HUVECs) of L&K-NPs **(D)**, free OOPC **(E)**, and free melittin **(F)**. In the study, L&K-NP concentrations range from 0.0031 to 8 mg/mL. Equivalent concentrations of free OOPC (0.5–1280 μg/mL) and melittin (0.063–16 μg/mL) were tested in parallel for cytotoxicity.

We next examined the efficacy of L&K-NPs in inhibiting PLA2 from bee venom. We chose the HD100 concentration of PLA2 (4 μg/mL) and evaluated the inhibition efficacy in both preincubation and competitive regimens, respectively. In the preincubation regimen, PLA2 was first incubated with L&K-NPs for 30 min followed by adding to mouse RBCs for hemolysis. Nanoparticle formulations including RBC-OOPC-NPs, RBC-melittin-NPs, and RBC-NPs were used as controls. As shown in Figure 4.3A, RBC-NPs and RBC-melittin-NPs inhibited no more than 30% of PLA2 hemolysis. The inhibition became higher when RBC-OOPC-NPs were added and further increased with L&K-NPs, which showed the lowest hemolysis among all groups (IC50, the concentration needed to inhibit 50% of hemolysis, = 0.44 ± 0.08 μg/mL). The kinetics of PLA2 inhibition was also compared (Figure 4.3B). Groups added with RBC-NPs, RBC-OOPC-NPs, and RBC-melittin-NPs reached 50% ($t_{1/2}$) of hemolysis at 0.67, 0.75, and 1.28 h, respectively. In contrast, the group added with L&K-NPs reached less than 40% of hemolysis after 2 h.

We further evaluated the anti-PLA2 efficacy of L&K-NPs in a competitive regimen, where PLA2, RBCs, and L&K-NPs were mixed simultaneously for hemolysis. Herein, we focused on L&K-NP and RBC-OOPC-NP groups only to emphasize the role played by melittin in promoting PLA2 inhibition. As shown in Figure 4.3C, the inhibition of hemolysis increased as the nanoparticle concentration increased. Compared to RBC-OOPC-NPs, L&K-NPs demonstrated a much higher level of inhibition (IC50 = 2.28 ± 0.44 μg/mL). Similarly, in the kinetics study, 50% of hemolysis was observed with RBC-OOPC-NP group at 1.14 h (Figure 4.3D). In contrast, L&K-NP group had only approximately 40% of hemolysis in 2 h. These results together demonstrate the interplay among the cell membrane, melittin, and OOPC, all working together to inhibit PLA2.
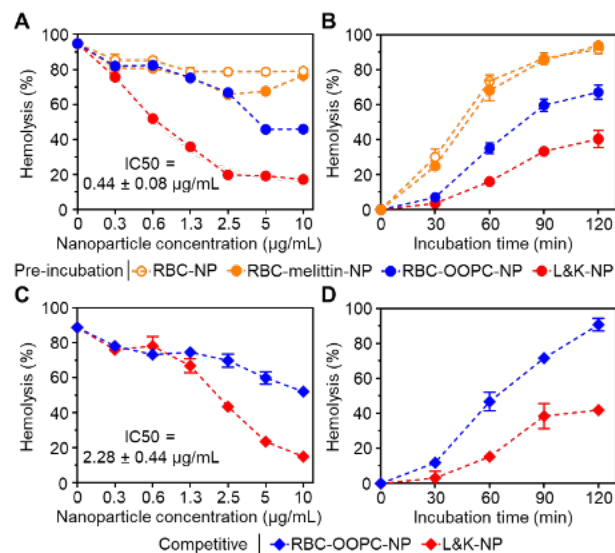
Figure 4.1.3 L&K-NPs inhibited PLA2 activity *in vitro*. (A) Hemolytic activity of PLA2 pre-incubated with RBC-NPs, RBC-melittin-NPs, RBC-OOPC-NPs, or L&K-NPs, at various nanoparticle concentrations. Hemolysis was evaluated at 60 min after mixing PLA2 with RBCs. **(B)** Hemolytic activity of PLA2 pre-incubated with 10 μg/mL of various nanoparticle formulations. Hemolysis was evaluated at various timepoints after mixing PLA2 with RBCs. **(C)** Hemolytic activity of PLA2 mixed simultaneously with RBCs and RBC-OOPC-NPs or L&K-NPs of various concentrations. Hemolysis was evaluated at 60 min after mixing PLA2 with RBCs. **(D)** Hemolytic activity of PLA2 mixed simultaneously with RBCs and 10 μg/mL of RBC-OOPC-NPs or L&K-NPs. Hemolysis was evaluated at various timepoints after mixing PLA2 with RBCs. All data points represent means ± s.d. (n = 3).

L&K-NPs were further evaluated *in vivo* via systemic administration for the anti-PLA2 efficacy. Venomous PLA2 was known to induce severe intravascular hemolysis and lethality *in*

vivo.[14, 29] In the study, a mortality rate of 100% was observed in mice that received 1.0 mg/kg free PLA2 (Figure 4.4A). In contrast, when mice were injected with the same dosage of free PLA2 followed by L&K-NP (2.5 mg/kg, L&K-NP: PLA2 = 2.5:1), 5 out of 6 mice survived, suggesting a strong survival benefit from L&K-NP treatment. The efficacy was further examined by monitoring *in vivo* hemolysis after PLA2 injection. As shown in Figure 4.4B, hemolysis reached a maximum of 66.1% in 5 minutes after intravenous injection of free PLA2. In contrast, a single injection of L&K-NPs following PLA2 administration reduced overall hemolysis with a lower peak value of 43.0%.

Lastly, we evaluated the toxicity of L&K-NPs in mice. In the study, mice were injected with PBS buffer or L&K-NPs once daily for 7 consecutive days. Mice maintained comparable body weights in both groups (Figure 4.4C). During the 7-d period, all the mice showed no obvious weight change. On day 7, mice were sacrificed. Hematoxylin and eosin (H&E) staining of liver sections demonstrated normal tissue architecture with no evidence of hepatic necrosis or hepatocyte apoptosis throughout the parenchyma, indicative of no hepatotoxicity (Figure 4.4D). Overall, the absence of toxicity demonstrates the potential of L&K-NPs as a safe and effective anti-PLA2 nanotherapeutic.
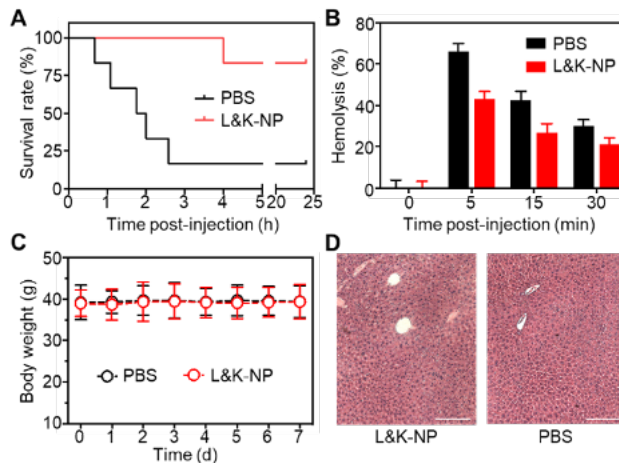
Figure 4.1.4 L&K-NPs conferred anti-PLA2 efficacy *in vivo*. (A) Survival rates of mice over 24 hours following an injection of PLA2 (1.0 mg/kg), followed immediately by an injection of L&K-NPs (2.5 mg/kg). All injections were performed intravenously via tail vein (n = 6). **(B)** *In vivo* hemolysis determined by measuring serum hemoglobin absorbance (540 nm) at various timepoints after PLA2 and L&K-NP injections. The same volume of whole blood from untreated mice was used for positive (RBC fully lysed via sonication, 100%) and negative controls (RBCs intact, 0%), respectively. All data points represent means ± s.d. (n = 6). **(C)** Mice were administered a single injection of L&K-NPs (2.5 mg/kg) or 1X PBS (150 µL) once daily for a consecutive of 7 days and their body weights were monitored. All mice showed no obvious weight changes. Data points represent means ± s.d. (n = 6). **(D)** On day 7, mice were sacrificed, and sections of the liver were stained with hematoxylin and eosin (H&E). L&K-NPs showed the same level of safety as PBS. Each image represents three examined sections (n = 3). Scale bar = 200 µm.

4.1.3 Methods

Animal care. Mice were housed in the Animal Facility at the University of California San Diego (UCSD) under federal, state, local, and National Institutes of Health (NIH) guidelines for animal care. All animal experiments were performed in accordance with NIH guidelines and approved by the Institutional Animal Care and Use Committee (IACUC) of UCSD.

Mouse RBC collection. Mouse whole blood was collected by submandibular bleeding into heparin tubes (approximately 0.4 mL per mouse per blood draw). Pooled blood was centrifuged (at 800 ×*g* and 4°C for 5 min) to collect red blood cells (RBCs). RBCs were repeatedly washed in 1X Dulbecco's phosphate-buffered saline (DPBS) with centrifugation (at 800 ×*g* and 4°C for 5 min) until supernatant appeared colorless and clear.

RBC membrane derivation. RBC membrane was derived based on a previously published protocol. Briefly, washed RBC were resuspended in 0.25X PBS in an ice bath for 20 min for hypotonic treatment, then centrifuged at 20,000 ×*g* for 10 min. The supernatant containing released hemoglobin was removed and the pink pellet was re-suspended in 0.25X PBS in an ice bath again for 20 min. The process was repeated until over 99% hemoglobin was removed. The RBC membrane was resuspended in water at a protein concentration of 4 mg/mL and stored at -80°C for subsequent studies.

RBC-OOPC-NP synthesis. Oleyloxyethyl phosphorylcholine (OOPC, Santa Cruz Biotechnology) in 100% ethanol (10 mg/mL stock) was added to washed RBC membrane (4 mg/mL) at an OOPC-to-membrane protein ratio of 4 – 20 wt% in relation to RBC membrane protein weight. The mixture was sonicated in a bath sonicator for 3 min (Fisher Scientific FS30D) and incubated at 37°C for 10 min. The same sonication-incubation cycle was repeated a total of three times. To synthesize nanoparticle cores, 0.2 mL poly (DL-lactide-*co*-glycolide) acid (PLGA, 50:50 PLGA, 0.67 dL/g, Lactel Absorbable Polymers) in acetone (20 mg/mL) was added dropwise into 1 mL DI water. The solution was placed under a vacuum aspirator to evaporate organic solvent. For membrane coating, RBC-OOPC vesicles were mixed with PLGA cores at a membrane protein-to-polymer weight ratio of 1:2. The mixture was then sonicated with a bath sonicator for 2 min to form RBC-OOPC nanoparticles (RBC-OOPC-NPs). RBC-OOPC-NPs were washed twice with centrifugation. OOPC input into the RBC membrane was optimized by measuring the inhibitory capacity of the resulting RBC-OOPC-NPs against honeybee venom PLA2. Briefly, 4 μg/mL PLA2 was mixed with 10 μg/mL RBC-OOPC-NPs with different OOPC input and incubated at 37 °C for 30 min before the remaining hemolytic activity of PLA2 was measured in a hemolysis assay. To measure the hemolytic activity of PLA2, the total volume of PLA2 and NP mixture was

adjusted to 60 μL with DPBS. Next, 100 μL 5 v/v % RBCs was added to the mixture and incubated

at 37°C for 60 min. Afterwards, the RBC suspension was centrifuged at 16100 ×g for 5 min. Then

20 μL supernatant was added into 80 μL PBS in 96-well plates. Hemoglobin absorption was

measured at 540 nm. Sonicated RBCs were taken as 100% hemolysis, and intact RBCs were taken

as 0% hemolysis. Hemolysis (%) is defined as (A_{sample} - $A_{negative}$) / ($A_{sonicated}$ − $A_{negative}$) × 100 %.

An OOPC input of 16 wt% of NP was chosen when the PLA2 inhibitory capacity plateaued. All

experiments were performed in triplicate.

L&K-NP synthesis. RBC-OOPC-NPs were prepared with an OOPC input of 16 wt% of

NP, as described above. RBC-OOPC-NPs (4 mg/mL in water) were mixed with melittin (2 – 16

μg/mL, corresponding to 0.05 – 0.4% membrane protein weight) in aqueous solution and the

mixture was incubated at 37°C for 30 min to form L&K-NPs. Following the incubation, the

resulting L&K-NPs were washed with centrifugation (16100 ×g for 10 min). The nanoparticle

pellet was suspended in deionized water and washed again at the same setting. Melittin input into

L&K-NPs was optimized by measuring the inhibitory capacity against honey bee venom PLA2.

Briefly, 4 μg/mL PLA2 was mixed with 10 μg/mL L&K-NPs with different melittin input and

incubated at 37 °C for 30 min before the remaining hemolytic activity of PLA2 was measured in

a hemolysis assay as described above. A melittin input of 0.2 wt% of NP was chosen when the

PLA2 inhibitory capacity plateaued.

Confirmation of OOPC incorporation into L&K-NP. Incorporation of OOPC onto

L&K-NPs was confirmed using mass spectrometry analysis. Briefly, 0.625 mg/mL RBC-NPs was

mixed with 0.1 mg/mL OOPC and centrifuged at 16,100 ×g for 10 min. 0.625 mg/mL freshly

prepared, unwashed L&K-NPs was centrifuged at the same setting. The supernatant samples and

a pure OOPC sample (0.1 mg/mL in water) were immediately analyzed by electrospray ionization

mass spectrometry (ESI-MS). Relative abundance of molecular ion peaks was calculated by normalizing peak intensity to that of pure OOPC. Taking the amount of OOPC in sample supernatant as unloaded, the OOPC loading efficiency was calculated to be 98.8%, leading to a loading yield of 15.8 wt% in relation to RBC membrane protein weight.

Confirmation of melittin incorporation into L&K-NP. Incorporation of melittin into L&K-NPs was examined using a hemolysis assay. After mixing 4 mg/mL RBC-OOPC-NPs with 8 µg/mL melittin (Sigma) at 37 °C, supernatant samples were collected at 0 min and 30 min incubation time by centrifuging the mixture at 16,100 ×g for 10 min. Supernatants (60 µL) were added to 100 µL 5 v/v % mouse RBC and hemolysis was measured as described above. Taking the amount of melittin in sample supernatant as unloaded, melittin incorporation efficiency was calculated to be 95.5%, leading to a loading yield of 0.19 wt% in relation to RBC membrane protein weight.

Nanoparticle characterization. Nanoparticles were measured for hydrodynamic size and surface zeta potential with dynamic light scattering (DLS) using a Malvern ZEN 3600 Zetasizer. Nanoparticle morphology was studied with transmission electron microscopy (TEM). In the study, samples were deposited on a glow-discharged, carbon-coated, 400-mesh copper grid (Electron Microscopy Sciences). The grid was then washed with distilled water and negatively stained with uranyl acetate (0.2 wt%). The grid was subsequently dried and visualized using an FEI 200 kV Sphera microscope. For stability test, L&K-NPs were stored at 37°C in deionized water or 1X PBS at a concentration of 0.5 mg/mL. The hydrodynamic size was monitored by DLS over 7 days.

Evaluation of nanoparticle toxicity *in vitro*. Nanoparticle toxicity was evaluated with a hemolysis assay and a cytotoxicity assay, respectively. In the hemolysis assay, various concentrations of free OOPC, free melittin, or L&K-NPs were added to mouse RBCs (100 µL 5

v/v %). The total volume was adjusted to 160 μL with 1X DPBS and hemolysis was measured as described above. In the cytotoxicity assay, human umbilical vein endothelial cells (HUVECs, ATCC) were cultured in endothelial cell growth media (Cell Applications) at 37°C in a 5% CO_2 environment. Prior to the study, cells were seeded at a density of 1×10^4 cells per well on 96-well plates and cultured overnight. Cells were then treated with various concentrations of free OOPC, free melittin, or L&K-NPs for 48 h. Cell viability was then determined by using a CellTiter 96 ® AQ$_{ueous}$ One Solution Cell Proliferation Assay (Promega).

Measurement of phospholipase A2 (PLA2) hemolytic activity. In pre-incubation setting, PLA2 (Sigma, 4 μg/mL) was pre-incubated with various concentrations (0 - 10 μg/mL) of nanoparticles at 37°C for 30 min. The total volume was adjusted to 60 μL with DPBS. Next, 100 μL 5% RBCs was added to the mixture and incubated at 37°C for 60 min. In competitive setting, PLA2 (4 μg/mL) was added to 100 μL 5% RBCs simultaneously with various concentrations (0 - 10 μg/mL) of nanoparticle formulations and incubated in the same condition. Hemolysis was measured as described above. All experiments were performed in triplicate.

***In vivo* survival study.** ICR mice (6-week-old male, Harlan Laboratory) were injected intravenously through the tail vein with 1.0 mg/kg (dose per body weight) of PLA2 followed immediately by 2.5 mg/kg of the nanoparticles or equal volume of sterile PBS. Survival was continuously monitored for 24 hours after injection.

Measurement of hemoglobin concentration in mouse plasma. ICR mice (6-week-old male, Harlan Laboratory) were injected intravenously through the tail vein with 1.0 mg/kg (dose per body weight) of PLA2 followed immediately by 2.5 mg/kg of the nanoformulation or equal volume of sterile PBS. At 0, 5, 15, 30, 60, 120 minutes post-injection, 1-2 drops of mouse whole blood were collected by submandibular bleeding into heparin tubes. The blood was immediately

diluted ten times using sterile PBS and centrifuged at 16100 ×*g* for 5 min. 20 μL supernatant was added into 80 μL PBS in 96-well plates. Hemoglobin absorption was measured at 540 nm. Whole blood from untreated mice was used as positive control (sonicated RBCs) and negative control (intact RBCs).

Evaluation of L&K-NP toxicity. ICR mice (8-week-old male, Harlan Laboratory) were injected everyday intravenously through the tail vein with 2.5 mg/kg of L&K-NPs or equal volume of sterile PBS. Mice body weight was monitored daily for 7 days. Mice were sacrificed on day 7 post-injection and liver tissue was collected, sectioned, and stained with Hematoxylin & Eosin (H&E). Histology slides were imaged with Micromaster™ II Microscope (Fisher Scientific).

4.1.4 Conclusions

In summary, we designed a biomimetic nanoparticle with a 'lure and kill' mechanism for safe and effective inhibition of PLA2 enzyme. In this design, biomimetic nanoparticles were made by wrapping polymeric nanoparticle cores with natural RBC membranes doped with melittin, a PLA2 attractant, and OOPC, a PLA2 inhibitor. The RBC membrane coating, together with melittin, acts as a decoy to lure PLA2 for enzymatic digestion. Upon the attack, PLA2 is exposed to OOPC that effectively kills the enzymatic activity. Such design uses the biomimetic feature of the RBC membrane and further exploits the membrane-binding characteristics of PLA2 attractant and inhibitor. The resulting L&K-NPs eliminate the toxicity associated with the free form of the attractant and inhibitor molecules. As a result, these L&K-NPs were able to inhibit PLA2-induced hemolysis and provide survival benefit to animals with acute PLA2 toxicity. Their administration into mice showed no obvious toxicity. Overall, the L&K-NP design overcomes the sacrificial

nature of cell membrane coating for enzyme inhibition and therefore extends the applications of these nanoparticles for broader detoxification applications.

Current study is mainly focused on inhibiting secreted PLA2s, which are accessible by L&K-NPs through intravenous injections. Notably, PLA2 isoforms show unique origins, tissue distributions, and substrate selectivity.[1, 3, 5] To address such diversity, L&K-NPs can be formulated by coating with membranes from cells sensitive to specific isoforms.[30-32] Meanwhile, besides their stabilization effect, nanoparticle cores can be engineered with additional functionalities.[33-35] In particular, the functionalization of PLGA has been widely explored to facilitate nanoparticle cell entry and cytoplasm delivery.[36-38] These mechanisms are potentially applicable in L&K-NP design to access cytoplasm and inhibit cytosolic PLA2. New compounds are also continually synthesized with unique membrane-binding characteristics and diverse mechanisms that either inhibit or stimulate PLA2.[8, 16, 25] With such abundant selection, L&K-NP design can be fine-tailored to precisely target a specific PLA2. These design features together make L&K-NPs a platform technology as a new path for anti-PLA2 inhibition.

Chapter 4.1, in full, is a reprint of the material as it appears in *Angewandte Chemie International Edition*, 2020, Qiangzhe Zhang, Ronnie H. Fang, Weiwei Gao, and Liangfang Zhang. The dissertation author was the primary author of this paper.

4.1.5 References

1.   Dennis, E.A., Cao, J., Hsu, Y.-H., Magrioti, V., and Kokotos, G., *Phospholipase A(2) Enzymes: Physical Structure, Biological Function, Disease Implication, Chemical Inhibition, and Therapeutic Intervention.* Chemical Reviews, 2011. **111**(10): p. 6130-6185.

2.   Birts, C.N., Barton, C.H., and Wilton, D.C., *Catalytic and non-catalytic functions of human IIA phospholipase A2.* Trends in Biochemical Sciences, 2010. **35**(1): p. 28-35.

3.   Burke, J.E. and Dennis, E.A., *Phospholipase A2 structure/function, mechanism, and signaling.* J Lipid Res, 2009. **50**: p. S237-42.

4.   Murakami, M., Taketomi, Y., Sato, H., and Yamamoto, K., *Secreted phospholipase A(2) revisited.* Journal of Biochemistry, 2011. **150**(3): p. 233-255.

5.   Leslie, C.C., *Thematic Review Series: Phospholipases: Central Role in Lipid Signaling and Disease Cytosolic phospholipase A(2) : physiological function and role in disease.* Journal of Lipid Research, 2015. **56**(8): p. 1386-1402.

6.   Balsinde, J., Balboa, M.A., Insel, P.A., and Dennis, E.A., *Regulation and inhibition of phospholipase A(2).* Annual Review of Pharmacology and Toxicology, 1999. **39**: p. 175-189.

7.   Reid, R.C., *Inhibitors of secretory phospholipase A2 group IIA.* Current Medicinal Chemistry, 2005. **12**(25): p. 3011-3026.

8.   Kokotou, M.G., Limnios, D., Nikolaou, A., Psarra, A., and Kokotos, G., *Inhibitors of phospholipase A(2) and their therapeutic potential: an update on patents (2012-2016).* Expert Opinion on Therapeutic Patents, 2017. **27**(2): p. 217-225.

9.   Magrioti, V. and Kokotos, G., *Phospholipase A(2) inhibitors for the treatment of inflammatory diseases: a patent review (2010-present).* Expert Opinion on Therapeutic Patents, 2013. **23**(3): p. 333-344.

10.   Ong, W.Y., Farooqui, T., Kokotos, G., and Farooqui, A.A., *Synthetic and Natural Inhibitors of Phospholipases A(2): Their Importance for Understanding and Treatment of Neurological Disorders.* Acs Chemical Neuroscience, 2015. **6**(6): p. 814-831.

11.   Gowda, R., Dinavahi, S.S., Iyer, S., Banerjee, S., Neves, R.I., Pameijer, C.R., and Robertson, G.P., *Nanoliposomal delivery of cytosolic phospholipase A(2) inhibitor arachidonyl trimethyl ketone for melanoma treatment.* Nanomedicine, 2018. **14**(3): p. 863-873.

12.   Pardeike, J., Schmidt, C., Volz, I., and Muller, R.H., *Nanostructured lipid carriers as delivery system for the phospholipase A(2) inhibitors PX-18 and PX-13 for dermal application.* Pharmazie, 2011. **66**(5): p. 357-361.

13.   Liu, M.-S., Liu, C.-H., Wu, G., and Zhou, Y., *Antisense inhibition of secretory and cytosolic phospholipase A(2) reduces the mortality in rats with sepsis.* Critical Care Medicine, 2012. **40**(7): p. 2132-2140.

14.   O'Brien, J., Lee, S.H., Onogi, S., and Shea, K.J., *Engineering the Protein Corona of a Synthetic Polymer Nanoparticle for Broad-Spectrum Sequestration and Neutralization of Venomous Biomacromolecules.* Journal of the American Chemical Society, 2016. **138**(51): p. 16604-16607.

15.   O'Brien, J. and Shea, K.J., *Tuning the Protein Corona of Hydrogel Nanoparticles: The Synthesis of Abiotic Protein and Peptide Affinity Reagents.* Accounts of Chemical Research, 2016. **49**(6): p. 1200-1210.

16.   Fang, R.H., Kroll, A.V., Gao, W., and Zhang, L., *Cell Membrane Coating Nanotechnology.* Advanced Materials, 2018. **30**(23): p. 1706759.

17.   Pang, Z.Q., Hu, C.M., Fang, R.H., Luk, B.T., Gao, W., Wang, F., Chuluun, E., Angsantikul, P., Thamphiwatana, S., Lu, W.Y., Jiang, X.G., and Zhang, L., *Detoxification of Organophosphate Poisoning Using Nanoparticle Bioscavengers.* ACS Nano, 2015. **9**(6): p. 6450-6458.

18.   Hu, C.M., Fang, R.H., Copp, J., Luk, B.T., and Zhang, L., *A biomimetic nanosponge that absorbs pore-forming toxins.* Nature Nanotechnology, 2013. **8**(5): p. 336-340.

19.   Copp, J.A., Fang, R.H., Luk, B.T., Hu, C.M., Gao, W., Zhang, K., and Zhang, L., *Clearance of pathological antibodies using biomimetic nanoparticles.* Proceedings of the National Academy of Sciences of the United States of America, 2014. **111**(37): p. 13481-13486.

20.   Wei, X.L., Gao, J., Fang, R.H., Luk, B.T., Kroll, A.V., Dehaini, D., Zhou, J.R., Kim, H.W., Gao, W., Lu, W.Y., and Zhang, L., *Nanoparticles camouflaged in platelet membrane coating as an antibody decoy for the treatment of immune thrombocytopenia.* Biomaterials, 2016. **111**: p. 116-123.

21.   Zhang, Q., Dehaini, D., Zhang, Y., Zhou, J.L., Chen, X.Y., Zhang, L.F., Fang, R.H., Gao, W., and Zhang, L., *Neutrophil membrane-coated nanoparticles inhibit synovial inflammation and alleviate joint damage in inflammatory arthritis.* Nature Nanotechnology, 2018. **13**(12): p. 1182-+.

22.   Zhang, Y., Chen, Y.J., Lo, C., Zhuang, J., Angsantikul, P., Zhang, Q., Wei, X.L., Zhou, Z.D., Obonyo, M., Fang, R.H., Gao, W., and Zhang, L., *Inhibition of Pathogen Adhesion by Bacterial Outer Membrane-Coated Nanoparticles.* Angewandte Chemie International Edition, 2019. **58**(33): p. 11404-11408.

23.   Chen, Y.J., Jia, Z., Zhuang, J., Lee, J.H., Wang, L.C., Fang, R.H., Gao, W., and Zhang, L., *Cell-Membrane-Cloaked Oil Nanosponges Enable Dual-Modal Detoxification.* Acs Nano, 2019. **13**(6): p. 7209-7215.

24.   Hu, C.M., Zhang, L., Aryal, S., Cheung, C., Fang, R.H., and Zhang, L., *Erythrocyte membrane-camouflaged polymeric nanoparticles as a biomimetic delivery platform.* Proc Natl Acad Sci U S A, 2011. **108**(27): p. 10980-5.

25.   Mingarro, I., Perezpaya, E., Pinilla, C., Appel, J.R., Houghten, R.A., and Blondelle, S.E., *Activation of bee venom phospholipase A(2) through a peptide-enzyme complex.* Febs Letters, 1995. **372**(1): p. 131-134.

26.   Gijs, H.L., Willemarck, N., Vanderhoydonc, F., Khan, N.A., Dehairs, J., Derua, R., Waelkens, E., Taketomi, Y., Murakami, M., Agostinis, P., Annaert, W., and Swinnen, J.V., *Primary cilium suppression by SREBP1c involves distortion of vesicular trafficking by PLA2G3.* Molecular Biology of the Cell, 2015. **26**(12): p. 2321-2332.

27.   Miao, J.Y., Kaji, K., Hayashi, H., and Araki, S., *Inhibitors of phospholipase promote apoptosis of human endothelial cells.* Journal of Biochemistry, 1997. **121**(3): p. 612-618.

28.   Chen, Y., Chen, M., Zhang, Y., Lee, J.H., Escajadillo, T., Gong, H., Fang, R., Gao, W., Nizet, V., and Zhang, L., *Broad-spectrum neutralization of pore-forming toxins with human erythrocyte membrane-coated nanosponges.* Advanced Healthcare Materials, 2018. **7**: p. article number 1701366.

29.   Fernandez, M.L., Quartino, P.Y., Arce-Bejarano, R., Fernandez, J., Camacho, L.F., Gutierrez, J.M., Kuemmel, D., Fidelio, G., and Lomonte, B., *Intravascular hemolysis induced by phospholipases A(2) from the venom of the Eastern coral snake, Micrurus fulvius: Functional profiles of hemolytic and non- hemolytic isoforms.* Toxicology Letters, 2018. **286**: p. 39-47.

30.   Zhang, Q., Dehaini, D., Zhang, Y., Zhou, J.L., Chen, X.Y., Zhang, L., Fang, R.H., Gao, W., and Zhang, L., *Neutrophil membrane-coated nanoparticles inhibit synovial inflammation and alleviate joint damage in inflammatory arthritis.* Nature Nanotechnology, 2018. **13**(12): p. 1182-1190.

31.   Thamphiwatana, S., Angsantikul, P., Escajadillo, T., Zhang, Q., Olson, J., Luk, B.T., Zhang, S., Fang, R.H., Gao, W., Nizet, V., and Zhang, L., *Macrophage-like nanoparticles concurrently absorbing endotoxins and proinflammatory cytokines for sepsis management.* Proceedings of the National Academy of Sciences of the United States of America, 2017. **114**(43): p. 11488-11493.

32.   Ren, Z., Li, H., Zhang, M., Zhao, Y., Fang, X., Li, X., Chen, W., Zhang, H., Wang, Y., Pan, L.-L., and Sun, J., *A Novel Derivative of the Natural Product Danshensu Suppresses Inflammatory Responses to Alleviate Caerulein-Induced Acute Pancreatitis.* Frontiers in Immunology, 2018. **9**: p. 2513.

33.   Zhang, Y., Zhang, J.H., Chen, W.S., Angsantikul, P., Spiekermann, K.A., Fang, R.H., Gao, W., and Zhang, L., *Erythrocyte membrane-coated nanogel for combinatorial antivirulence and responsive antimicrobial delivery against Staphylococcus aureus infection.* Journal of Controlled Release, 2017. **263**: p. 185-191.

34.   Zhang, J.H., Gao, W., Fang, R.H., Dong, A.J., and Zhang, L., *Synthesis of Nanogels via Cell Membrane-Templated Polymerization.* Small, 2015. **11**(34): p. 4309-4313.

35. Gao, W., Hu, C.M., Fang, R.H., Luk, B.T., Su, J., and Zhang, L., *Surface Functionalization of Gold Nanoparticles with Red Blood Cell Membranes.* Advanced Materials, 2013. **25**(26): p. 3549-3553.

36. Chou, L.Y.T., Ming, K., and Chan, W.C.W., *Strategies for the intracellular delivery of nanoparticles.* Chemical Society Reviews, 2011. **40**(1): p. 233-245.

37. Radovic-Moreno, A.F., Lu, T.K., Puscasu, V.A., Yoon, C.J., Langer, R., and Farokhzad, O.C., *Surface Charge-Switching Polymeric Nanoparticles for Bacterial Cell Wall-Targeted Delivery of Antibiotics.* ACS Nano, 2012. **6**(5): p. 4279-4287.

38. Kamaly, N., Yameen, B., Wu, J., and Farokhzad, O.C., *Degradable Controlled-Release Polymers and Polymeric Nanoparticles: Mechanisms of Controlling Drug Release.* Chemical Reviews, 2016. **116**(4): p. 2602-2663.

4.2 A biomimetic nanoparticle to 'lure and kill' inflammatory phospholipase A2

4.2.1 Introduction

Acute pancreatitis (AP) is an autoimmune disorder featuring the sudden onset of autogestion in the pancreas.[1, 2] In the U.S. alone, AP causes approximately 270,000 hospital administration annually, and 30% mortality rate in severe cases, making it the most common gastrointestinal disease that requires immediate hospitalization.[3, 4] Clinically approved therapeutic interventions of AP rely on intravenous fluid therapy, which aims to control the levels of circulating inflammatory markers, or, in severe cases of AP, direct drainage of abdominal abscess and necrosectomy.[5, 6] However, effective treatment so far remains unavailable due to the lack of therapeutic target or target specificity.[3, 7] Phospholipase A2 (PLA2), a lipolytic enzyme produced by the pancreatic acinar cells, is a known pathogenic trigger of AP.[8-10] Uncontrolled release of PLA2 from the pancreatic tissue damages the cell membrane of surrounding acinar cells and produces pro-inflammatory signals that recruit leukocytes and exacerbate the inflammation.[11, 12] The spread of PLA2 into systemic circulation could further propagate a system-wide inflammatory response that leads to complications such as acute respiratory distress syndrome (ARDS).[13, 14] Meanwhile, elevated levels of PLA2 activity correlate to aggravated clinical outcome. These findings have motivated the inhibition of PLA2 as a therapeutic strategy for AP management.

Several classes of small molecule inhibitors of PLA2, such as fluoroketones, indole-based, and pyrrolidine-based inhibitors, have been developed and investigated in clinical or pre-clinical settings, but with limited success.[15] For example, varespladib, a specific inhibitor for secreted PLA2, reached Phase II clinical trials for the treatment of sepsis and Phase III for the treatment of cardiovascular diseases, but failed due to lack of efficacy.[16, 17] Several challenges limit the

clinical success of selective inhibition of PLA2.[18, 19] Lack of specificity and functional selectivity greatly limit the therapeutic outcome of PLA2 inhibitors. Furthermore, the inherent toxicity of small molecule PLA2 inhibitors, and their poor pharmacokinetic profile and bioavailability pose serious concerns over systemic administration.[20, 21] To address such challenges, nanoscale liposomes were formulated to encapsulate poorly soluble PLA2 inhibitors otherwise unsuitable for administration.[22] Similar nanoliposomes were able to reduce the toxicity of small molecule inhibitors while improving their bioavailability.[23] In addition, nanoparticles containing cationic polymers have been made to facilitate the intracellular delivery of small interfering RNAs that specifically silenced the expression of cytosolic PLA2 for precise enzyme inhibition.[24] Meanwhile, affinity nanoparticles have been made by screening a library of functional monomers to selectively inhibit certain classes of PLA2.[25, 26] Nanoparticles coated with plasma membrane of neutrophils have also been exploited recently for inflammation-targeted delivery of celastrol, an anti-inflammatory drug inhibiting the interleukin-1 (IL-1) inflammatory signaling pathway, for management of acute pancreatitis.[27]

Recently, a 'lure and kill' nanoparticle (denoted 'L&K-NP) was designed toward effective PLA2 inhibition. This platform features a polymeric nanoparticle core wrapped with natural cell membrane, the natural target of PLA2. The cell membrane was further functionalized with melittin, a PLA2 attractant, and oleyloxyethyl phosphorylcholine (OOPC), a specific inhibitor for PLA2. The cell membrane coating together with melittin attracts PLA2 for attack, during which the PLA2 is inhibited by OOPC, formulating a unique 'lure and kill' action mechanism. These L&K-NPs potently inhibited the activity of venomous PLA2 and protected animals from PLA2-induced lethality without any apparent systemic toxicity. The design of L&K-NP overcomes the sacrificial

rather than inhibitive nature of a decoy approach in enzymatic reactions, making cell membrane-coated nanoparticles attractive for enzyme inhibition.

The initial success in inhibiting venomous PLA2 motivates us to apply the L&K-NP design for the treatment of AP. Herein, we tailor L&K-NP formulation and test their therapeutic efficacy in mouse models of AP. Specifically, we select membrane of macrophages (MΦs) to formulate L&K-NPs, as attack of these cells by PLA2 leads to upregulation of pro-inflammatory responses and potentiation of organ complications during AP progression (Figure 4.2.1*A*).[10] Following the formulation, L&K-NPs are confirmed to eliminate the toxicity associated with free melittin and the inhibitor MJ-33. *In vitro*, we demonstrate that L&K-NPs suppress PLA2 activity in sera of mice and humans of AP. *In vivo* by using mouse models of mild and severe AP, we show that L&K-NPs effectively protect the pancreas and reduce disease severity. Overall, L&K-NPs represent a biomimetic nanoparticle platform for effective and safe PLA2 inhibition with potential for treating PLA2-mediated diseases.

4.2.2 L&K-NP preparation and characterization

To synthesize L&K-NPs, cell membrane was first derived from MΦs.[28] MJ-33, with its lipid-like structure, was then incorporated into the cell membrane through sonication. The membrane was subsequently coated onto poly(lactic-*co*-glycolic acid) (PLGA) cores to form MJ-incorporated MΦ membrane-coated nanoparticles (MΦ-MJ-NPs). Then, the suspension of MΦ-MJ-NPs was added with melittin, which spontaneously inserted into the membrane of the nanoparticles, leading to the final L&K-NP formulation.[29] During the formulation, increasing MJ-33 input caused a higher inhibition of PLA2, but the effect plateaued at an input of 16 wt% (Figure 4.2.1*B*). The incorporation of MJ-33 into MΦ-MJ-NP and L&K-NP was confirmed by

using mass spectrometry (MS). Characteristic molecular ion peak was identified at m/z = 491.3, in agreement with the theoretical molecular weight of MJ-33, indicating successful loading of MJ-33 into the nanoparticle formulations (Figure 4.2.1*C*). Using a calibration curve constructed from MJ-33 standards, an MJ-33 input of 16 wt% was calculated to achieve a loading yield of 9.4 wt%, which was used for all subsequent MΦ-MJ-NP formulation. Similarly, increasing melittin input also led to an increase of PLA2 inhibition (Figure 4.2.1*D*). In this case, a plateau appeared at a 4 wt% input, equivalent to a 3.9 wt% melittin loading yield, calculated by quantifying the remaining melittin after incubation with MΦ-MJ-NP (Figure 4.2.1*E*). This input was used in all subsequent L&K-NP formulation. When examined with dynamic light scattering (DLS), L&K-NPs showed a hydrodynamic diameter larger than that of the uncoated PLGA cores with a less negative surface zeta potential, consistent with the addition of a membrane bilayer structure (Figure 4.2.1*F*). Notably, values of the diameter and zeta potential of L&K-NPs were comparable to those of MΦ-NPs, indicating negligible impacts from membrane incorporation of MJ-33 and melittin. When visualized with transmission electron microscopy (TEM), L&K-NPs showed a core–shell structure that indicated a unilamellar membrane coating around the polymeric core (Figure 4.2.1*G*).[29, 30] The membrane coating bestowed L&K-NPs with extended colloidal stability in both 1× phosphate-buffered saline (PBS) and 0.5× fetal bovine serum (FBS) (Figure 4.2.1*H*). Whereas free MJ-33 was shown to be toxic to MΦs, L&K-NPs with equivalent MJ-33 were non-toxic (Figure 4.2.1*I*), suggesting a strong association of MJ-33 to the nanoparticles that prevented its participation in cell signaling for toxicity. A series of quality assurance specifications was established to ensure the physicochemical and biological reproducibility of fabricating L&K-NPs.
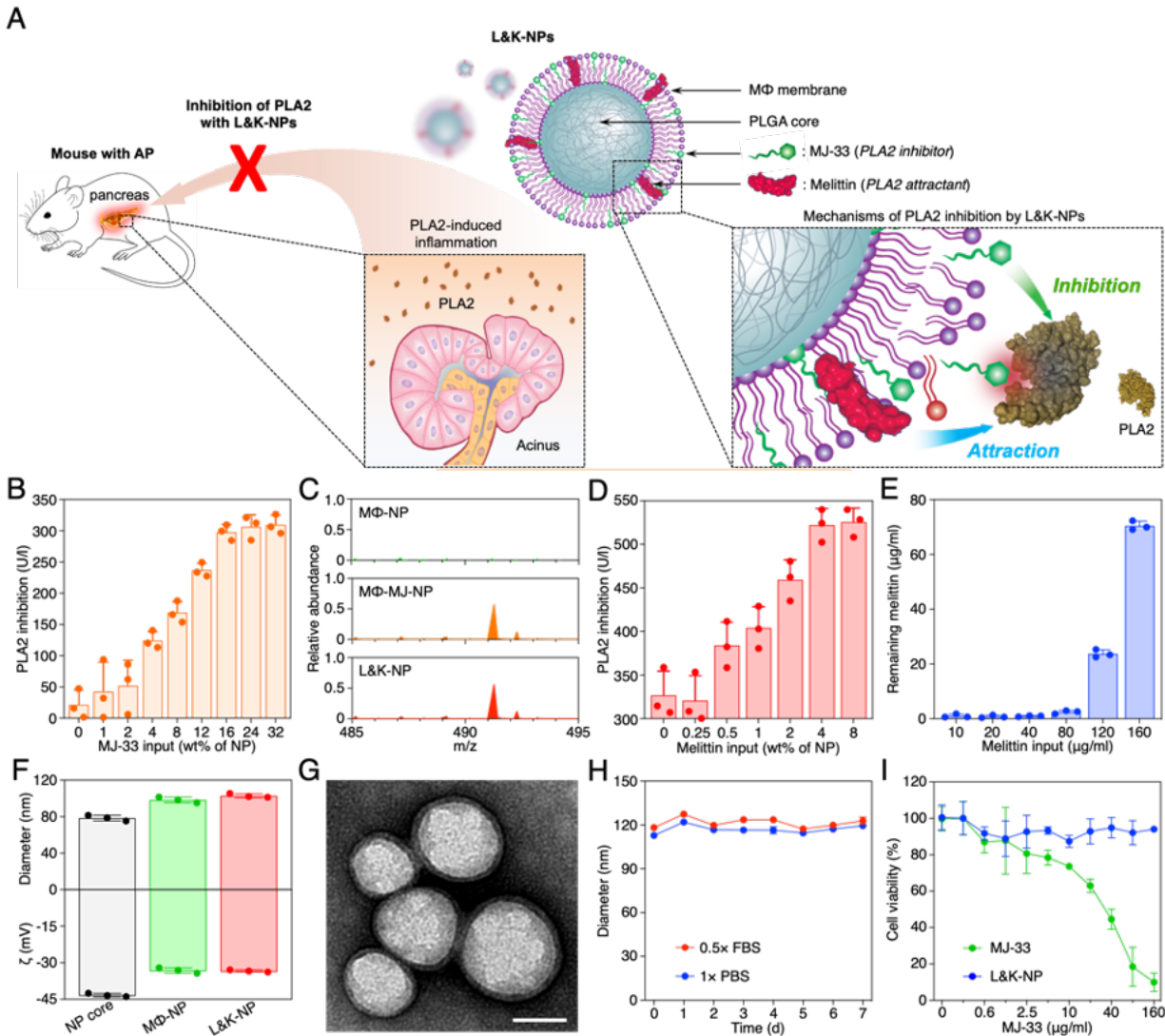
Figure 4.2.1 Fabrication and characterization of L&K-NPs. (*A*) Schematic representation of L&K-NPs designed to inhibit PLA2 during AP progression. (*B*) Optimization of MJ-33 input into MΦ-NPs with a PLA2 inhibition assay. (*C*) Confirmation of MJ-33 loading into MΦ-MJ-NPs using mass spectrometry (MS). (*D*) Optimization of melittin input into MΦ-MJ-NPs with a PLA2 inhibition assay. (*E*) Quantitative analysis of melittin loading into L&K-NPs with a hemolysis assay. (*F*) DLS measurements of L&K-NPs for hydrodynamic size (diameter, nm) and zeta potential (ζ, mV). (*G*) A representative image of L&K-NPs examined with TEM. Samples were stained with uranyl acetate. Scale bar, 100 nm. (*H*) Stability of L&K-NPs 1× PBS or 0.5× FBS, determined by monitoring nanoparticle size (diameter) over 7 d. (*I*) Comparison of the cytotoxicity of free MJ-33 and L&K-NPs loaded with equivalent amounts of MJ-33 on murine J774 MΦs. In all studies, n = 3 using the same batch of nanoparticles.

Next, L&K-NPs were examined for their anti-PLA2 activity *in vitro*. They were added to serum samples collected from mice with caerulein-induced acute pancreatitis (CAE-AP) that contained elevated levels of PLA2 (Figure 4.2.2*A*). L&K-NPs showed a clear inhibitory effect

against PLA2, with an IC_{50} value (half maximal inhibitory concentration) of 72.6 µg/ml. The inhibition capacity measured from MΦ-MJ-NPs was lower ($IC_{50} = 110.2$ µg/ml), attributable to the absence of melittin, which helps to potentiate the inhibition. Meanwhile, MΦ-NPs and MΦ-mel-NPs (melittin-incorporated MΦ-NPs) were unable to inhibit PLA2 in the serum samples. The inhibitory effect of L&K-NPs was also tested on human serum samples from patients with AP. Similarly, L&K-NPs effectively inhibited PLA2 activity in samples from all three patients ($IC_{50} =$ 245, 255, and 188 µg/ml, Figure 4.2.2*B*). In contrast, a weaker inhibition was observed with MΦ-MJ-NPs ($IC_{50} = 630, 673$, and 614 µg/ml, respectively), and no inhibition was observed with MΦ-NPs and MΦ-mel-NPs. Overall, these results demonstrated a 'lure and kill' mechanism through the interplay among lipid membrane, melittin, and MJ-33 that together suppressed PLA2 activity. Toward systemic applications, the circulation time of L&K-NPs was measured with fluorescently labeled nanoparticles after intravenous administration (Figure 4.2.2*C*). At 24 h and 48 h, L&K-NPs showed 17.4% and 8.0% retention in the blood, respectively. Based on a two-compartment model, the elimination half-life was calculated as 18.9 h, comparable to the value measured from MΦ-NPs.[28] The *in vivo* tissue distribution of L&K-NPs was also evaluated (Figure 4.2.2*D*). When analyzed per organ, L&K-NPs distributed mostly in the blood and the liver. When normalized per gram of tissue, the nanoparticles were largely contained in the liver and spleen, two primary organs of the reticuloendothelial system. Meanwhile, significant fluorescence was also observed in the blood. As the blood fluorescence decreased, a corresponding increase in signal was observed in the liver, indicating the uptake of L&K-NPs by the reticuloendothelial system over time. To evaluate the safety of L&K-NPs, a comprehensive metabolic panel was performed 72 h after injecting the nanoparticles into healthy mice (Figure 4.2.2*E*). Compared to mice receiving PBS only, no statistical differences were observed for all parameters that were evaluated.

A blood count and histological analysis of major organs, including the liver, spleen, heart, lungs, and kidneys, showed the absence of toxicity, indicating a high safety profile for the L&K-NPs.
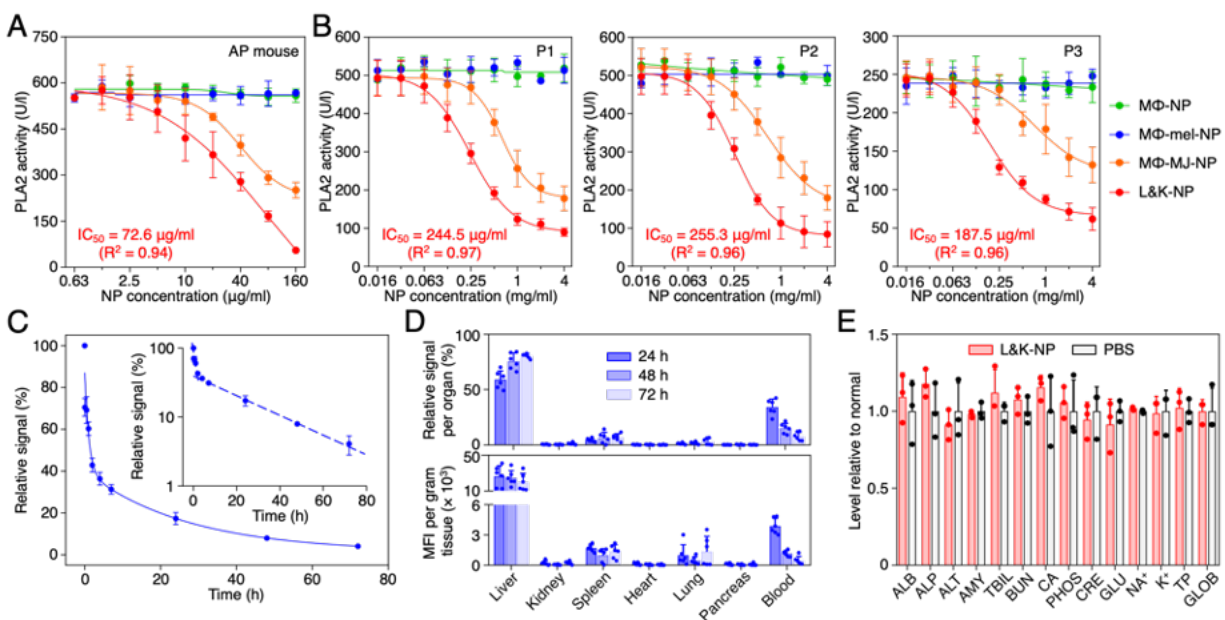
Figure 4.2.2 PLA2 inhibition capacity and in vivo circulation time, biodistribution, and safety of L&K-NPs. (*A-B*) Comparison of the inhibition capacity of MΦ-NP, MΦ-mel-NP, MΦ-MJ-NP, and L&K-NP against PLA2 in serum from mice with acute pancreatitis (*A*) and human patients with acute pancreatitis (*B*). (*C*) Pharmacokinetics of L&K-NPs. DiR-loaded nanoparticles were injected intravenously through the tail vein of mice. At various timepoints, blood was withdrawn intraorbitally and measured for fluorescence at 780 nm to evaluate the systemic circulation lifetime of the nanoparticles (inset, semi-log plot of fluorescence at various timepoints). (*D*) Biodistribution of L&K-NPs. Fluorescently labeled nanoparticles were injected intravenously into the mice. At each timepoint (24, 48, and 72 h), the organs from a randomly grouped subset of mice were collected, homogenized, and quantified for fluorescence (top: relative signal per organ, bottom: fluorescence intensity per gram of tissue). (*E*) Comprehensive blood chemistry panel taken on day 5 after administration of PBS or L&K-NP (80 mg/kg) on days 1-4. ALB, albumin; ALP, alkaline phosphatase; ALT, alanine transaminase; AMY, amylase; TBIL, total bilirubin; BUN, blood urea nitrogen; CA, calcium; PHOS, phosphorus; CRE, creatinine; GLU, glucose; NA+, sodium; K+, potassium; TP, total protein; GLOB, globulin (calculated). Data presented as mean ± s.d. In all *in vitro* studies, n = 3 using the same batch of L&K-NPs. IC$_{50}$ values were derived from the variable slope model with Graphpad Prism 8. In circulation lifetime and biodistribution studies, n = 6 using the same batch of L&K-NPs. In systemic toxicity studies, n = 3 using the same batch of L&K-NPs.

4.2.3 L&K-NPs inhibit pancreatitis-associated inflammation and acinar cell injury

L&K-NPs were examined for their ability to inhibit pancreatitis-associated NF-κB activation in MΦs (Fig. 4.2.3*A*).[31] When naïve MΦs were stained for p65, a subunit of NF-κB, higher fluorescence intensity was observed in the cytoplasm relative to that in the nuclear zone,

corresponding to a low nuclear translocation (1.2%). In contrast, in MΦs exposed to the serum of CAE-AP mice, p65 appeared in both the cytosol and the nuclear zone. In this case, the nuclear translocation increased significantly (58.7%), indicating NF-κB activation. MΦs exposed to the serum mixed with L&K-NPs showed a reduced p65 distribution in the nuclear zone in relation to that in the cytosol. The lower nuclear translocation (17.5%) implied inhibition of NF-κB activation by the L&K-NPs. In comparison, MΦs exposed to the serum mixed with control nanoparticles, including MΦ-NPs, MΦ-mel-NPs, or MΦ-MJ-NPs, all exhibited pronounced NF-κB activation (54.2, 54.6, and 48.8% of the nuclear translocation, respectively). Next, L&K-NPs were examined for their ability to inhibit of pro-inflammatory cytokine production in MΦs (Fig. 4.2.3*B*).[32] MΦs exposed to the serum of CAE-AP mice produced a higher level of IL-6, but the production was inhibited when the serum was also added with L&K-NPs. The inhibition increased as the concentration of L&K-NPs increased. At all concentrations tested, L&K-NPs inhibited IL-6 production more than all control formulations. In addition to IL-6, analysis on additional pro-inflammatory cytokines, including TNF-α and IL-1β, also showed similar inhibition effects.

Acinar cell death is a hallmark of AP,[33] and L&K-NPs were thus examined for their ability to protect pancreatic acinar cells (PACs). Exposure to the serum of CAE-AP mice significantly reduced the viability of PACs (Figure 4.2.3*C*). However, viability increased when L&K-NPs were added to the PACs, indicating a protective effect against cell death. The cell viability increased as the nanoparticle concentration increased, corresponding to an EC_{50} (half-maximal effective concentration) value of 59.9 µg/ml. A dose-dependent increase of PAC viability was also observed when MΦ-MJ-NPs were added, but a lower EC_{50} value was obtained (363 µg/ml). PACs added with MΦ-NPs and MΦ-mel-NPs showed viability no higher than 50%, suggesting that they were ineffective in protecting PACs from the serum. The protection was

further analyzed for APC necrosis and apoptosis (Figure 4.2.3*D*). Exposure to the serum of CAE-AP mice resulted in significant portions of necrotic and apoptotic cells. When L&K-NPs were added to the cells, the percentages of both cell populations were reduced, confirming the nanoparticles were able to protect against cell death. Similarly, MΦ-MJ-NPs showed partial protection of the APCs, whereas MΦ-NPs and MΦ-mel-NPs showed negligible protection.
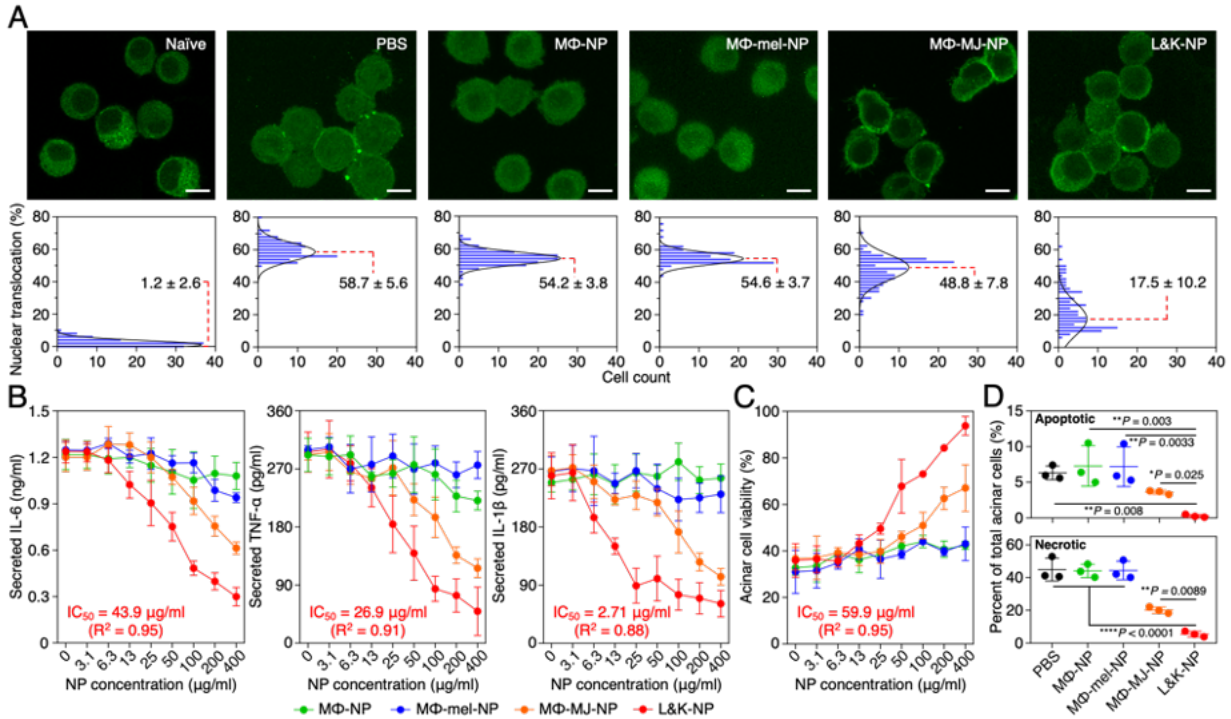
Figure 4.2.3 L&K-NPs suppress PLA2-induced inflammatory response *in vitro*. (*A*) Effects of L&K-NPs and control formulations on NF-κB nuclear translocation of PLA2-stimulated MΦs. Representative fluorescence images (top row, scale bar, 10 μm) and quantification of nuclear translocation (bottom row) based on corresponding fluorescence images. (*B*) Effects of L&K-NPs and control formulations on IL-6, TNF-α, and IL-1β production from PLA2-stimulated MΦs. (*C*) The effect of L&K-NPs and control formulations on cell viability of PLA2-stimulated pancreatic acinar cells. (*D*) Effects of L&K-NPs and control formulations on apoptosis and necrosis analyzed by flow cytometry using annexin V/PI double staining. Data presented as mean ± s.d. In all datasets, n = 4 using the same batch of L&K-NPs. IC$_{50}$ and EC$_{50}$ values were derived from the variable slope model using Graphpad Prism 8.

4.2.4 L&K-NPs protect mice with mild acute pancreatitis

L&K-NPs were further evaluated for their protective effects in a murine model of mild acute pancreatitis (CAE-AP) induced by intraperitoneal injections of caerulein.[34] Following AP induction, L&K-NPs or control formulations, including MΦ-NPs, MΦ-mel-NPs, MΦ-MJ-NPs, and

PBS, were injected intravenously through the mouse tail vein for efficacy evaluation (Figure 4.2.4*A*). First, the treatment efficacy was evaluated at a systemic level by examining serum levels of PLA2 and pro-inflammatory cytokines, including IL-6, TNF-α, and IL-1β, for 24 h during the disease progression (Figure 4.2.4*B-E*). In the study, the injection of caerulein led to a rapid increase of serum PLA2 level, which reached maximum in 2 h and then gradually decreased. Throughout the study, the PLA2 level in mice injected with L&K-NPs (40 mg/kg) remained significantly lower compared to PLA2 levels in all other groups treated with control formulations, indicating an inhibitory effect against AP development. Meanwhile, the injection of caerulein also boosted serum cytokine levels, which reached maximum in 4 h and then started to decrease. The levels of these cytokines in mice injected with L&K-NPs remained significantly lower compared to those in mice injected with control formulations, further confirming the inhibition of AP by L&K-NPs. Notably, L&K-NPs showed a significantly higher inhibition than MΦ-MJ-NPs, suggesting the role of melittin in further potentiating anti-PLA2 effects.

Next, the efficacy of L&K-NPs was evaluated at a tissue level by examining the pathological changes of the pancreas during the treatment. In the study, mice were sacrificed at 24 h after the initial AP induction. The pancreas was harvested for histopathological analysis. As shown in Figure 4.2.4*F*, H&E-stained pancreatic sections from healthy naïve mice showed tight interlobular and intralobular spaces, with the absence of acinar necrosis or immune infiltration. However, tissue sections from CAE-AP mice injected with PBS exhibited diffuse widening of interlobular and intralobular spaces (edema), marked acinar necrosis, and evident cell infiltration into the interlobular spaces. Similar features were also observable in sections from CAE-AP mice injected with MΦ-NPs, MΦ-mel-NPs, or MΦ-MJ-NPs, indicating a lack of efficacy from these formulations. In contrast, the tissue of CAE-AP mice injected with L&K-NPs appeared similar to that of healthy naïve mice

without obvious acinar necrosis or immune infiltration, demonstrating clear protection of the pancreas during AP. Comprehensive histopathological analysis was performed on sections from all animals in the study.[35] Based on such analysis, the degree of pancreatic edema was evaluated by scoring the extent of interlobular and intralobular space widening in the pancreatic sections (Figure 4.2.4*G*). While mice injected with PBS received an edema score of 2.6 ± 0.8, those injected with L&K-NPs had a significantly reduced score of 0.1 ± 0.1, comparable to that of the healthy naïve mice. Scores from mice injected with control nanoparticles remained significantly higher, indicating a lack of protection on the pancreas. Furthermore, counts of necrotic acinar cells were elevated in CAE-AP mice injected with PBS, but remained at the basal levels in those injected with L&K-NPs (Figure 4.2.4*H*). Notably, mice injected with MΦ-MJ-NPs showed a partial reduction of necrotic acinar cell count, likely due to the presence of the inhibitor without melittin. The pancreatic tissues were also examined for PLA2 activity (Figure 4.2.4*I*). At 24 h after the initial AP induction, mice injected with PBS showed a reduced level of PLA2 in the pancreas when compared with the naïve mice, indicating the loss of PLA2 due to acinar injury.[36] In contrast, pancreatic PLA2 levels were comparable between healthy mice and mice injected with L&K-NPs, indicating the protection of normal acinar functions. Furthermore, the immune infiltration into the pancreatic parenchyma was examined by staining the pancreatic sections for CD45, a pan-leukocyte marker (Fig. S14) [37]. As shown in Figure 4.2.4*J*, a higher level of infiltrating leukocytes was found in CAE-AP mice compared to healthy naïve mice. The level was also elevated in mice treated with MΦ-NPs, MΦ-mel-NPs, or MΦ-MJ-NPs. Compared to these groups, counts of CD45$^+$ cells were significantly lower in mice treated with L&K-NPs, indicating a clear reduction of disease severity.
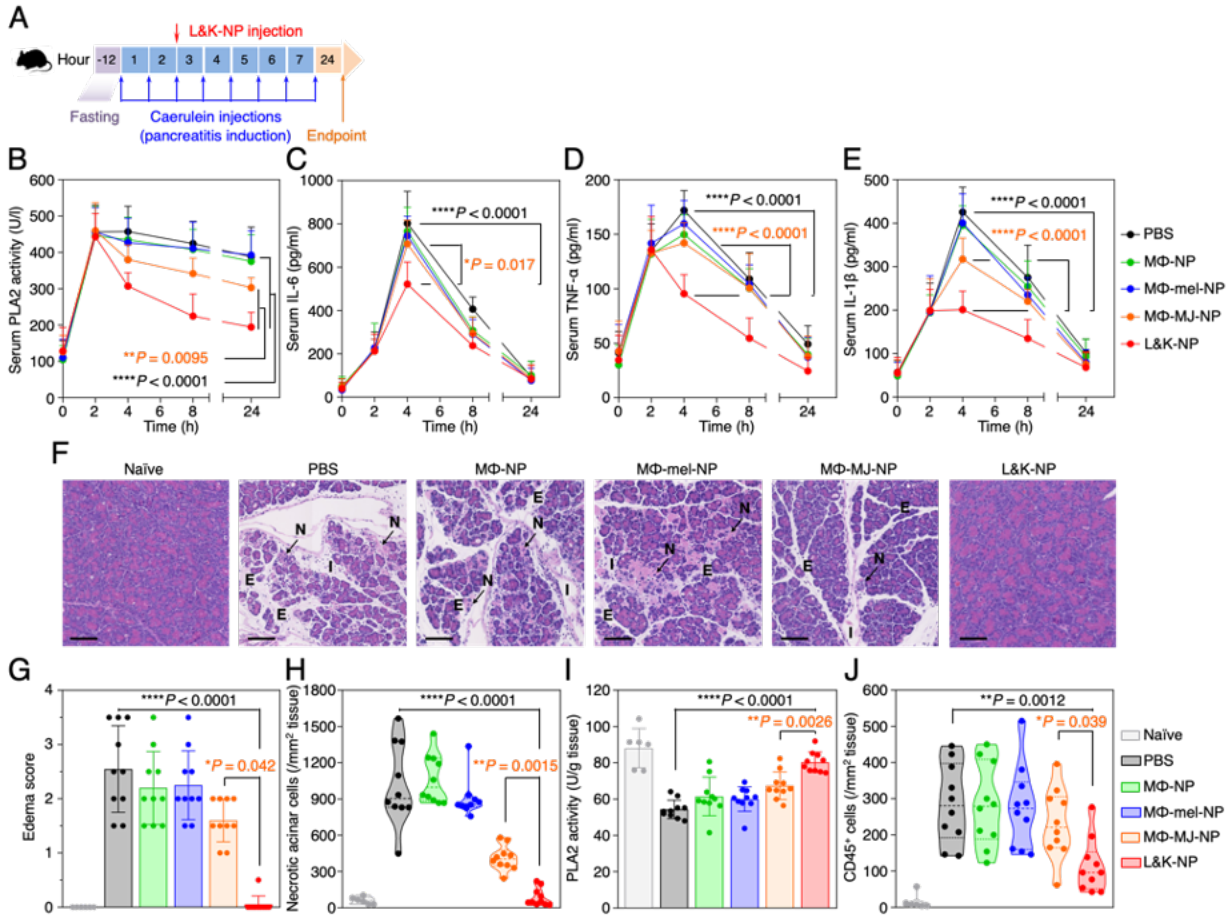
Figure 4.2.4 L&K-NPs alleviate PLA2-induced inflammation and tissue destruction in a mouse model of mild acute pancreatitis. (*A*) The study protocol of pancreatitis induction and treatment with L&K-NPs. (*B*) PLA2 activity profile in serum of CAE-AP mice treated with different nanoparticle formulations. (*C-E*) Concentration profiles of key inflammatory cytokines, including IL-6 (*C*), TNF-α (*D*), and IL-1β (*E*), in the serum of CAE-AP mice treated with different nanoparticle formulations. (*F*) Representative images of H&E staining on pancreas sections from CAE-AP mice collected 24 h after receiving the treatments. Scale bars, 100 μm. N: acinar necrosis, E: edema, I: cell infiltration. (*G*) Edema score of H&E-stained pancreas sections from CAE-AP mice after receiving different nanoparticle treatments. (*H*) Quantification of necrotic cells in the H&E-stained pancreas sections from CAE-AP mice receiving different nanoparticle treatments. (*I*) PLA2 activity in the pancreatic tissue of CAE-AP mice treated with different nanoparticle formulations. (*J*) Quantification of CD45$^+$ cells in the anti-CD45-stained pancreas sections from CAE-AP mice receiving different nanoparticle treatments. For serum PLA2 and cytokine profiles, statistical analysis was performed using repeated-measure one-way ANOVA with Dunnett's post hoc analysis. Statistical difference in edema scores was analyzed by Kruskal-Wallis non-parametric test with Dunnett's post hoc analysis. Necrotic cell counts, tissue PLA2 activity, and CD45$^+$ cell counts were analyzed by using one-way ANOVA with Dunnett's post hoc analysis. Data presented as mean ± s.d. *$P \leq 0.05$, **$P \leq 0.01$, ***$P \leq 0.001$, ****$P \leq 0.0001$. In all datasets, n = 10 mice treated with the same batch of L&K-NPs.

4.2.5 L&K-NPs protect mice with severe acute pancreatitis

The protective effects of L&K-NPs were further evaluated in a murine model of severe AP (CDE-AP) induced by feeding mice with a choline-deficient diet supplemented with DL-ethionine. The diet intake period was positively correlated with the severity of AP.[38] In the study, female CD-1 mice were placed on a CDE-diet for 3 days and each day L&K-NPs were injected along with other control formulations for efficacy evaluation (Figure 4.2.5*A*). A dosage of 80 mg/kg per injection was selected. As shown in Figure 4.2.5*B*, all mice injected with PBS, MΦ-NP, or MΦ-mel-NP died by day 4, indicating a lack of therapeutic efficacy from the control nanoparticles. Meanwhile, the survival rate of those injected with MΦ-MJ-NPs was only 20%, suggesting ineffective protection if only MJ was incorporated into the nanoparticles. In contrast, the survival rate of mice injected with L&K-NPs increased significantly to 60%, demonstrating a clear benefit against AP development. As another evaluation of the efficacy at a systemic level, we monitored serum levels of PLA2, together with pro-inflammatory cytokines, including IL-6, TNF-α, and IL-1β, during days 0 to 3 of the study, a period prior to the occurrence of any death (Fig. 4.2.5*C-F*). Intake of CDE-diet drastically elevated serum PLA2 and cytokine levels in mice injected with PBS, which plateaued after day 2. In day 2 and 3, serum PLA2 and cytokine levels in mice administered with L&K-NPs remained significantly lower than those in all control groups. The results demonstrated the effective suppression of serum PLA2 and cytokines in CDE-AP, indicating a protective effect of L&K-NPs.

L&K-NPs against severe AP was further evaluated by examining the histopathological changes in the pancreatic tissue during disease progression. In the study, mice were euthanized on day 3 of AP induction and the pancreatic tissues were collected for analyses. The pancreatic sections from naïve mice displayed characteristics of a normal healthy pancreas including tight

118

interlobular space and absence of acinar necrosis or immune infiltration (Figure 4.2.5*G*). In contrast, the sections from CDE-AP mice injected with PBS showed marked parenchymal edema, pronounced acinar necrosis, and obvious signs of hemorrhage, which all are characteristic features of severe AP.[38] These features were also clearly observable in mice injected with MΦ-NPs, MΦ-mel-NPs, or MΦ-MJ-NPs, indicating a lack of therapeutic efficacy from these formulations. Comprehensive histopathological analyses revealed a significantly reduced edema score in mice injected with L&K-NPs, compared to mice receiving PBS or control formulations (Figure 4.2.5*H*). In addition, counts of necrotic acinar cells were effectively reduced to basal levels in mice injected with L&K-NPs (Figure 4.2.5*I*), further confirming the protective effect of L&K-NPs against severe AP. The hemorrhagic area in the pancreatic tissue was also measured and found to be reduced in mice treated with L&K-NPs but not in those treated with PBS or control formulations (Figure 4.2.5*J*). Pancreatic sections were also stained for CD45 for analyses of leukocyte infiltration (Figure 4.2.5*K*). When compared to healthy naïve mice, leukocyte infiltration in those injected with control formulations was significantly elevated, but remained significantly lower for L&K-NP-treated mice. These results again confirmed the ability of L&K-NPs in protecting animals against severe AP.
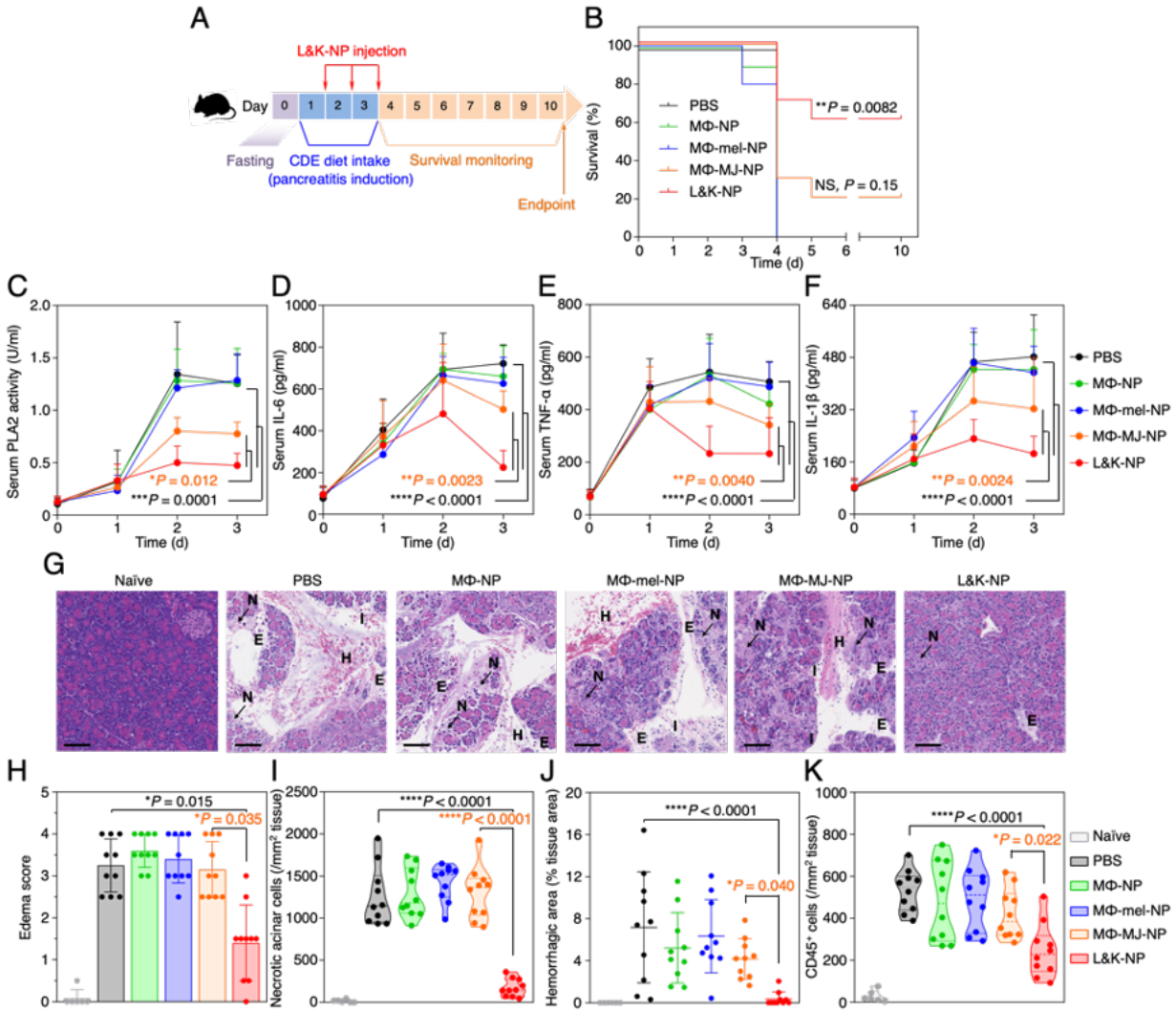
Figure 4.2.5 L&K-NPs attenuate disease severity and confer survival benefits in a mouse model of severe acute pancreatitis. (*A*) The study protocol of lethal pancreatitis induction and treatment with L&K-NPs. (*B*) Survival rates of mice over 10 days after initial diet intake. NS, not significant. (*C*) PLA2 activity profiles in serum of CDE-AP mice treated with different formulations. (*D-F*) Concentration profiles of key inflammatory cytokines, including IL-6 (*D*), TNF-α (*E*), and IL-1β (*F*), of CDE-AP mice treated with different formulations. (*G*) Representative images of H&E staining on pancreas sections from CDE-AP mice collected on day 3 after initial diet intake. Scale bars, 100 μm. N: acinar necrosis, E: edema, I: cell infiltration, H: hemorrhage. (*H*) Edema score of H&E-stained pancreas sections from CDE-AP mice after receiving different nanoparticle treatments. (*I*) Quantification of necrotic cells in the H&E-stained pancreas sections from CDE-AP mice receiving different nanoparticle treatments. (*J*) Quantification of hemorrhagic area in the H&E-stained pancreas sections from of CDE-AP mice receiving different nanoparticle treatments. (*K*) Quantification of CD45^{+} cells in the anti-CD45-stained pancreas sections from CDE-AP mice treated with different formulations. For survival study, statistical analysis was performed on groups treated with MΦ-MJ-NPs or L&K-NPs in comparison with PBS-treated group using log-rank (Mantel-Cox) test. For serum PLA2 and cytokine profiles, statistical analysis was performed using repeated-measure one-way ANOVA with Dunnett's post hoc analysis. Statistical difference in edema scores was analyzed by Kruskal-Wallis non-parametric test with Dunnett's post hoc analysis. Necrotic cell counts, quantification of hemorrhagic area, and CD45^{+} cell counts were analyzed by using one-way ANOVA with Dunnett's post hoc analysis. Data presented as mean ± s.d. *$P \leq 0.05$, **$P \leq 0.01$, ***$P \leq 0.001$, ****$P \leq 0.0001$. In the study, n = 10 mice in CDE-AP model. All mice were treated with the same batch of L&K-NPs.

120

4.2.6 Methods

Animal care. Mice were housed in an animal facility at the University of California San Diego (UCSD) under federal, state, local, and National Institutes of Health (NIH) guidelines. All animal experiments were performed in accordance with NIH guidelines and approved by the Institutional Animal Care and Use Committee (IACUC) of UCSD.

MΦ culture. Murine J774A.1 cell line (American Type Culture Collection, ATCC) was maintained in Dulbecco's Modified Eagle Medium (DMEM, Invitrogen) supplemented with 10% FBS (Hyclone) and 1% penicillin-streptomycin (Invitrogen). Human THP-1 cell line (ATCC) was maintained in RPMI 1640 (Gibco) supplemented with 10% FBS and 1% penicillin-streptomycin. Cell cultures were maintained at 37 °C in a humidified incubator with 5% CO_2 and regularly tested for mycoplasma contamination.

MΦ membrane derivation. The plasma membrane of MΦs was harvested by following a previously published protocol.[28] Briefly, J774A.1 cells were grown in T175 culture flasks to full confluency and detached with 3 mM ethylenediaminetetraacetic acid (EDTA, Sigma-Aldrich) in PBS. The cells were washed with 1× PBS three times (centrifugation at 800 ×g) and suspended in a hypotonic lysing buffer containing 30 mM Tris-HCl (pH = 7.5), 225 mM D-mannitol, 75 mM sucrose, 0.2 mM ethylene glycol-bis(β-aminoethyl ether)-(N,N,N',N'-tetraacetic acid (EGTA), and protease and phosphatase inhibitor cocktails (all from Sigma-Aldrich). Cells were then disrupted using a Dounce homogenizer with a tight-fitting pestle (20 passes). The homogenized solution was centrifuged at 20,000 ×g for 25 min at 4 °C. The pellet was discarded, and the supernatant was centrifuged again at 100,000 ×g for 35 min at 4 °C. Following the centrifugation,

membrane was collected as the pellet and washed twice with 0.2 mM EDTA in water. Membrane content was quantified by using a BCA protein assay kit (Pierce) in reference to a bovine serum albumin (BSA) standard. Approximately 1×10^8 MΦs were able to yield 1 mg of membrane material (protein weight). The membrane was suspended with 0.2 mM EDTA to a protein concentration of 10 mg/ml and stored at -80 °C for subsequent studies. To collect membrane from THP-1 cells, the cells were grown in T175 suspension flasks (Olympus Plastics) to a density of 1×10^6 cells/ml and washed three times in PBS (centrifugation at 800 $\times g$). The plasma membrane was then harvested following the same procedure.

Fabrication of MΦ-NPs. To synthesize nanoparticle cores, 0.4 ml poly(DL-lactic-*co*-glycolic acid) (50:50 PLGA, 0.67 dl/g, Lactel Absorbable Polymers) in acetone (20 mg/ml) was added dropwise into 1 ml water. The solution was placed below a vacuum aspirator until the acetone evaporated completely. To trace the nanoparticles, PLGA cores were prepared by co-dissolving PLGA with 0.1 wt% 1,1'-dioctadecyl-3,3,3',3'-tetramethylindotricarbocyanine iodide (DiR, excitation = 750 nm/emission = 780 nm, ThermoFisher Scientific). For coating, the MΦ membrane was mixed with PLGA cores at a polymer-to-membrane protein weight ratio of 2:1. The mixture was then sonicated in the bath sonicator for 2 min, resulting in MΦ-NPs.

Fabrication of MΦ-MJ-NPs. A lipid doping method was used to incorporate MJ-33 into the MΦ membrane. Briefly, MΦ membrane (4 mg/ml in water) was mixed with MJ-33 (0.04 – 1.28 mg/ml, corresponding to 1 – 32% membrane protein weight, dissolved in 100% ethanol, Cayman Chemicals) and sonicated with a bath sonicator (Fisher Scientific FS30D) for 30 s and incubated at 37 °C for 15 min. The same sonication-incubation cycle was repeated once. The suspension was

centrifuged at 20,000 ×*g* for 10 min and the MJ-33-loaded MΦ membrane was resuspended in water. To form nanoparticles, the MJ-33-loaded MΦ membrane was mixed with PLGA cores at a polymer-to-membrane protein weight ratio of 2:1. The mixture was then sonicated in the bath sonicator for 2 min for coating, resulting in MΦ-MJ-NPs. MΦ-MJ-NPs were then washed twice with centrifugation. MJ-33 input into the MΦ membrane was optimized by measuring the inhibitory capacity of the resulting MΦ-MJ-NPs against native bovine PLA2 (Creative Enzymes). Briefly, 160 μg/ml MΦ-MJ-NPs with increasing MJ-33 input was mixed with native bovine PLA2 (600 U/l in PBS) and incubated at 37 °C for 1 h before the PLA2 activity was measured. Native bovine PLA2 (600 U/l in PBS) incubated at 37 °C for 1 h served as a positive control. PLA2 activity was measured by the EnzChek[TM] Phospholipase A2 activity assay kit (ThermoFisher Scientific) with a calibration curve determined by measuring PLA2 standards with known enzymatic activity. PLA2 inhibition was calculated by subtracting the PLA2 activity of nanoparticle-PLA2 mixtures from that of the positive control sample. MJ-33 input that resulted in the maximum PLA2 inhibition (16% of membrane protein weight) was used for subsequent studies.

Fabrication of L&K-NPs. To fabricate L&K-NPs, 2 mg/ml MΦ-MJ-NPs was incubated with melittin (5 – 160 μg/ml, corresponding to 0.25 – 8% membrane protein weight, Sigma-Aldrich) at 37 °C for 30 min. L&K-NPs were then washed twice with centrifugation. Melittin input into MΦ-MJ-NPs was optimized by measuring the inhibitory capacity of the resulting L&K-NPs against native bovine PLA2. Briefly, L&K-NPs (160 μg/ml) with increasing melittin input was mixed with 600 U/l native bovine PLA2 and incubated at 37 °C for 1 h. PLA2 activity was measured to calculate PLA2 inhibition by L&K-NPs. PLA2 inhibition was calculated using the same method

as mentioned above. The melittin input that resulted in the maximum PLA2 inhibition (4% of membrane protein weight) was used to prepare L&K-NPs for all subsequent studies.

Quantitative analysis of MJ-33 loading yield in L&K-NPs. Freshly prepared MΦ-MJ-NPs or L&K-NPs (30 μL, 2 mg/mL) were centrifuged at 25,000 ×g for 10 min and resuspended in 100 μL ultrapure water. To extract cell membrane lipids, 200 μL methanol was added to the nanoparticle suspensions and the samples were vigorously vortexed for 30 s. Then 400 μL chloroform was added and the mixture was shaken at room temperature for 30 min. After that, the samples were centrifuged at 2,500 ×g for 5 min. The organic solvent at the bottom was collected, dried under nitrogen flow, and reconstituted in 100 μL methanol for HR-ESI-MS analysis. MΦ-NPs (30 μL, 2 mg/mL) were processed by following the same procedure and served as a control sample. MJ-33 content in the nanoparticle samples were derived from the relative abundance value (m/z = 491.3) from the nanoparticle sample using the MJ-33 calibration curve. MJ-33 loading yield was calculated as the weight percentage of MJ-33 in total membrane protein. Results were fitted by using linear regression function in Graphpad Prism 8.

Quantitative analysis of melittin loading yield in L&K-NPs. Melittin loading into L&K-NPs was derived by measuring hemolytic activity of melittin solution before and after the incubation with the MΦ-MJ-NPs. To quantify melittin loading into L&K-NPs, MΦ-MJ-NPs (final concentration 2 mg/ml) were mixed with melittin (final concentration 10 ~ 160 μg/mL) and incubated at 37 °C for 30 min. The mixture was diluted 10× in PBS and added to washed mouse RBCs (5 v/v%) in PBS and incubated at 37 °C for 30 min. Afterwards, the RBC suspension was centrifuged at 16,100 ×g for 5 min. Then 20 μL supernatant was added into 80 μL PBS in 96-well

plates. Hemoglobin absorption was measured at 540 nm. RBCs (5 v/v%) in PBS were disrupted with sonication and centrifuged at 16,100 ×*g* for 5 min. The supernatant of sonicated RBCs (5 v/v%) in PBS was taken as 100% hemolysis, and the supernatant of intact RBCs (5 v/v%) in PBS was taken as 0% hemolysis. Hemolysis (%) was defined as (A_{sample} − A_{intact}) / ($A_{sonicated}$ − A_{intact}) × 100%. Remaining melittin concentration after incubation with the nanoparticles was derived from the calibration curve for melittin-induced hemolysis. Melittin loading was calculated as the weight percentage of melittin in total membrane protein. Results were fitted by using non-linear fitting in Graphpad Prism 8.

Physicochemical properties, morphology, and colloidal stability of L&K-NPs. L&K-NPs were measured for hydrodynamic size and surface zeta potential with dynamic light scattering (DLS, ZEN 3600 Zetasizer, Malvern). To examine the intra-particle structure, nanoparticles were stained with uranyl acetate (0.2 wt%) and visualized with transmission electron microscopy (TEM, FEI 200kV Sphera). To study the long-term colloidal stability, L&K-NP suspensions were adjusted to 1× PBS or 0.5× FBS, at a final protein concentration of 0.5 mg/ml. Samples were stored at 37 °C and nanoparticle hydrodynamic size was measured and monitored once a day for 7 consecutive days.

Evaluation of L&K-NP cytotoxicity. J774A.1 MΦs were seeded in a 96-well tissue culture plate at a density of 5×10^4 cells/ml and cultured overnight. Cells were then added with various concentrations of free MJ-33 or L&K-NPs with equivalent MJ-33 content. Cells were then cultured for 24 h. Cell viability was determined by using a CellTiter Cell Proliferation assay (Promega) based on the manufacturer's instruction.

Mouse model of mild acute pancreatitis (CAE-AP). CAE-AP mouse model was established by following a previously published protocol.[37] Briefly, 6-week-old CD-1 female mice were fasted 12 h before pancreatitis induction and given ad libitum access to water. Mice received intraperitoneal injections of caerulein (VWR) at 50 μg/kg hourly for 8 h to induce acute pancreatitis (AP).

Inhibition of PLA2 in serum samples from CAE-AP mice and human AP patients. To collect serum from CAE-AP mice, the whole blood of mice was collected with submandibular bleeding into microtubes and allowed to clot at room temperature for 30 min. Samples were then centrifuged at 2,000 ×g for 6 min to collect serum from the supernatant. The serum was then lyophilized and reconstituted to 1/10 of its volume (equivalent to a 10× serum concentration). Serum samples collected from human AP patients were purchased from BioreclamationIVT. Aliquots of samples were stored at -80 °C and used within two weeks after the collection. In the study, mouse serum samples (0.1× final concentration) were mixed with L&K-NPs or control formulations (final concentrations ranging from 0.625 to 160 μg/ml). Samples were incubated at 37 °C for 1 h before PLA2 activity was measured. For studies with human serum samples, L&K-NPs made from membrane of THP-1 cells were used. In the study, patient serum samples (0.1× final concentration) were mixed with L&K-NPs or control formulations (final concentrations ranging from 0.016 to 4 mg/ml). Samples were incubated at 37 °C for 1 h before the PLA2 activity was measured. IC_{50} values were derived from the variable slope model using Graphpad Prism 8.

Pharmacokinetics and biodistribution of L&K-NPs. To characterize the pharmacokinetics and biodistribution of L&K-NPs *in vivo*, L&K-NPs were prepared from DiR-loaded PLGA cores. To study pharmacokinetics, 200 µl of 3 mg/ml fluorescently labeled nanoparticles were administered intravenously into 4-week-old CD-1 female mice. Blood samples were collected by submandibular bleeding at 3 min, 30 min, 1 h, 3 h, 7 h, 24 h, 48 h, and 72 h. Samples were then diluted 10× with PBS and the fluorescence intensity was measured (Tecan Infinite M200 multiplate reader). Pharmacokinetic parameters were calculated by fitting the curve with a two-compartment model. For the biodistribution study, 200 µl of 3 mg/ml fluorescently labeled nanoparticles were administered intravenously into 4-week-old CD-1 female mice. At 24, 48, and 72 h after the injection, organs, including the liver, kidneys, spleen, lungs, heart, blood, and pancreas, were collected from a randomly grouped subset of mice. Organs were weighed and then homogenized in PBS with a Mini-Beedbeater-16 (Biospec Products) for fluorescence measurement.

In vivo **toxicity of L&K-NPs.** To evaluate the toxicity, L&K-NPs were injected intravenously (80 mg/kg) through the tail vein into 4-week-old CD-1 female mice daily for 4 days. At 24 h after the last injection, approximately 250 µl of whole blood was collected into Eppendorf tubes and allowed to coagulate. Then the samples were centrifuged at 2,000 ×g for 6 min to collect serum for the comprehensive metabolic panel analysis. Meanwhile, 100 µl of whole blood was collected into an EDTA-coated microtube for the complete blood count. All blood samples were tested at the UCSD Animal Care Program Diagnostic Services Laboratory. Immediately after blood collection, mice were euthanized to collect major organs, including the liver, kidneys, spleen, lungs, heart, and pancreas. Organs were fixed in 10% formalin (Fisher Scientific), sectioned, and stained

with hematoxylin and eosin (H&E) for histological analysis. Histology slides were imaged with a Hamamatsu NanoZoomer 2.0-HT slide scanning system.

Determination of NF-κB nuclear translocation in MΦs. J774A.1 MΦs were seeded in Celltreat™ tissue culture-treated dishes with a glass bottom (Neta Scientific) at a density of 5 × 10^4 cells/ml and cultured for 24 h. Serum from CAE-AP mice was reconstituted with the culture medium to a final PLA2 activity of 600 U/l. Then, L&K-NPs or control nanoparticles were mixed with the culture medium to reach a final concentration of 400 μg/ml (membrane protein). The final volume in each culture dish was adjusted to 500 μl using the culture medium. Cells were incubated for 2 h at 37 °C and then washed with PBS 3 times. Washed cells were fixed with 10% formalin for 15 min, then permeabilized and blocked with a PBS solution containing 0.4% Triton X-100 (Fisher Scientific) and 2% BSA for 30 min at room temperature. Intracellular NF-κB was probed with anti-mouse NF-κB p65 antibody (clone A-8, 1:200 dilution in PBS, Santa Cruz Biotechnology) for 1 h at room temperature. Cells were then washed twice with PBS and FITC-anti-mouse IgG (1:500 dilution in PBS, Biolegend) was added to the cells for 20 min at room temperature. Cells were washed twice and stained with 0.1 μg/ml Hoechst 33342 (ThermoFisher Scientific) for 20 min at room temperature. Fluorescence was visualized using a Leica SP8 confocal microscope. Quantification of NF-κB nuclear translocation was performed by following a previously published protocol using ImageJ[39]. Briefly, the Hoechst-positive area was used to define the nuclear region of interest (ROI) for each nucleus. NF-κB-positive area encompassing each nuclear ROI was defined as the ROI for a whole cell. NF-κB signal within a nucleus was measured by the total fluorescence intensity within the nuclear ROI. NF-κB signal within a whole cell was measured by the total fluorescence intensity within the ROI of a whole cell. Nuclear translocation (%) was

defined as $Fluo_{nuclei} / Fluo_{whole\ cell} \times 100\ \%$. One hundred cells were measured individually for each group. Nuclear translocation histograms were fitted with Gaussian non-linear regression by using GraphPad Prism 8.

Measurement of MΦ cytokine production. J774.1 MΦs were seeded in 96-well tissue culture plates at a density of 8×10^4 cells/ml and cultured overnight. Serum from CAE-AP mice was reconstituted with the culture medium to a final PLA2 activity of 600 U/l. Afterward, L&K-NPs or control nanoparticles were mixed with the culture medium to reach final concentrations ranging from 3.125 to 400 μg/ml in membrane protein concentration. The final volume in each well was adjusted to 100 μl using the culture medium. Cells were incubated for 6 h at 37 °C and the culture medium was collected. Concentrations of inflammatory cytokines IL-6, TNF-α, and IL-1β in the culture medium was quantified by using the corresponding ELISA kits (Biolegend).

Isolation of pancreatic acini. Six-week-old healthy CD-1 mice were euthanized, and the pancreatic tissues were collected. Minced pancreatic tissues were dispersed in DMEM with Nutrient Mixture F-12 (DMEM/F12, Gibco) supplemented with 1.0 U/ml collagenase D from *C. histolyticum* and 0.25 mg/ml trypsin inhibitor from soybean (both from Roche Diagnostics). The pancreatic tissues were vigorously shaken at 200 rpm for 2 h at 37 °C. Digested tissue was filtered by using a cell strainer (100 μm pore size, Corning). Pancreatic acini retained by the cell strainer were transferred to a 24-well tissue culture plate and cultured overnight in DMEM/F12 medium supplemented with 5% FBS and 1% penicillin-streptomycin. Non-adherent pancreatic acini were then transferred into a new 48-well tissue culture plate and used immediately, while adherent contaminant cells were discarded.

Pancreatic acinar cell injury assay. Pancreatic acini were suspended in DMEM/F12 medium at a density of 800 acini/ml, and 100 µl pancreatic acini suspension was added to each well of a 48-well tissue culture plate. Serum from CAE-AP mice was first added to the acini suspension to a final PLA2 activity of 600 U/l. L&K-NPs or control nanoparticles were then added to the acini suspension to reach final concentrations ranging from 3.125 to 400 µg/ml in membrane protein concentration. The final volume in each culture dish was adjusted to 200 µl using the culture medium. Pancreatic acini were cultured for 24 h and washed three times with PBS. Cell viability was determined by using a CellTiter Cell Proliferation assay (Promega). To study the cell death pathway of PLA2-induced acinar cell injury, serum from CAE-AP mice was added to the acini suspension (800 acini/ml in 100 µl culture medium) to a final PLA2 activity of 600 U/l. Then, L&K-NPs or control nanoparticles were mixed with the acini suspension to reach a final concentration of 400 µg/ml in membrane protein concentration. The final volume in each well was adjusted to 200 µl using the culture medium. The mixtures were incubated for 24 h at 37 °C and then washed with PBS for 3 times. Pancreatic acinar cells were then stained with PE-labelled annexin-V (1:100 dilution, Biolegend) and propidium iodide (1:5000 dilution, Biolegend), and analysed with a Becton Dickinson FACSCanto-II flow cytometer. Results were analysed using FlowJo software.

Mouse model of choline-deficient diet with DL-ethionine (CDE diet)-induced acute pancreatitis (CDE-AP). CED-AP was established by following a previously published protocol[40]. Briefly, 4-week-old CD-1 female mice were fasted on day 0 and then fed with CDE-diet (MP Biomedicals) from days 1 to 3, followed by normal laboratory diet on day 4 to induce

lethal acute pancreatitis. Survival was monitored for 10 days. Throughout the CDE-AP studies, mice had access to water ad libitum.

Protocol to study L&K-NP treatment efficacy in CAE-AP and CDE-AP. In CAE-AP, 2 h after the initial caerulein administration, 200 µl of L&K-NPs (40 mg/kg) was administered intravenously through the tail vein. MΦ-NPs (40 mg/kg), MΦ-mel-NPs (40 mg/kg), MΦ-MJ-NPs (40 mg/kg), or 200 µl sterile PBS was administered intravenously to mice at the same time as controls. CAE-AP mouse whole blood was collected at 0, 2, 4, 8, 24 h after initial caerulein injection (~80 µl whole blood per mouse per timepoint) with submandibular bleeding into microtubes and allowed to clot at room temperature for 30 min. Samples were then centrifuged at 2,000 ×g for 6 min to collect serum from the supernatant. Serum samples were immediately frozen at -20 °C and analysed for PLA2 activity and cytokine concentration within 24 h. All mice were euthanized at 24 h after initial caerulein injection to collect pancreatic tissues for measurement of pancreatic tissue PLA2 activity and histological analyses. In CDE-AP studies, 200 µl of L&K-NPs (80 mg/kg) was administered intravenously through the tail vein on days 1, 2, and 3 of the studies. MΦ-NPs (80 mg/kg), MΦ-mel-NPs (80 mg/kg), MΦ-MJ-NPs (80 mg/kg), or 200 µl sterile PBS was administered intravenously to mice at the same time as controls. The whole blood of CDE-AP mice was collected on days 0, 1, 2, and 3 (~80 µl whole blood per mouse per timepoint). CDE-AP mouse serum samples were derived and stored following the aforementioned procedures. Pancreatic tissues were collected on day 3 of the CDE-AP studies for histological analyses.

Measurement of PLA2 activity and cytokine levels in serum. Serum samples from CAE-AP mice and CDE-AP mice were diluted 5× in PBS and serum PLA2 activity was quantified by using

the EnzChek^{TM} PLA2 assay kit. Serum cytokine concentrations were determined by using mouse IL-6, mouse TNF-α, and mouse IL-1β ELISA kits. To measure PLA2 activity in CAE-AP mouse pancreatic tissues, freshly collected mouse pancreas samples were homogenized with a Mini-Beedbeater-16 (Biospec Products). The homogenate was immediately diluted 10× in PBS and analysed for PLA2 activity. PLA2 activity results were normalized to the weight of pancreatic tissues.

Histological analysis of pancreatic tissues. For histological analyses, CAE-AP mouse and CDE-AP mouse pancreatic tissues were fixed, sectioned, and stained with H&E. H&E-stained sections were visualized by a Hamamatsu NanoZoomer 2.0-HT slide scanning system. Histopathological features including edema, necrotic acinar cells, hemorrhage, and CD45$^+$ cell infiltration were studied. To analyze parenchymal edema in the pancreatic tissue in CAE-AP and CDE-AP models, a representative 0.45 mm × 0.45 mm area was selected from each H&E-stained pancreatic section. The selected area was scored by a blinded subject who was unaware of the type of treatment administered to the animals. Score 0 = no edema; 0.5 = focal expansion of interlobular space; 1 = diffuse expansion of interlobular space; 1.5 = focal expansion of intralobular space; 2 = diffuse expansion of intralobular space; 2.5 = focal expansion of inter-acinar space; 3 = diffuse expansion of inter-acinar space; 3.5 = focal expansion of intercellular space; 4 = diffuse expansion of intercellular space. To quantify the necrotic cells in the pancreatic parenchyma in CAE-AP and CDE-AP models, five 0.15 mm × 0.15 mm areas were randomly selected from each H&E-stained pancreatic section. Necrotic cells in each area were counted. To study the extent of hemorrhage in the CDE-AP model, a representative 0.6 mm × 0.6 mm area was selected from each pancreatic section. The hemorrhagic area was defined as the area containing extravasated erythrocytes and

quantified using Adobe Photoshop. Counts of necrotic acinar cells and hemorrhagic area results were normalized to the area occupied by the pancreatic tissue. To study CD45$^+$ cell infiltration into the pancreas, pancreatic tissues were sectioned and stained with a rabbit anti-mouse CD45 antibody (Abcam). Biotinylated anti-rabbit IgG was used as the secondary antibody for chromagen development. Sections were counter-stained with haematoxylin to visualize cell nuclei and were scanned by a Hamamatsu NanoZoomer 2.0-HT slide scanning system. A 0.15 mm × 0.15 mm area in each anti-CD45-stained pancreatic section was selected to quantify CD45$^+$ cell infiltration using ImageJ. Briefly, RGB images of anti-CD45-stained pancreatic sections were converted to 16-bit grayscale images. A standard threshold was applied to exclude CD45$^-$ cells. Remaining CD45$^+$ cells were counted by using ImageJ Particle Analyzer. Counts of CD45$^+$ cells were normalized to the area occupied by the pancreatic tissue.

Statistical analysis. Statistical analyses of serum biomarkers were performed using a repeated-measure one-way ANOVA with Dunnett's post hoc analysis. Statistical difference in edema scores was analyzed by Kruskal-Wallis non-parametric test with Dunnett's post hoc analysis. Necrotic cell counts, tissue PLA2 activity, and CD45$^+$ cell counts were analyzed by using one-way ANOVA with Dunnett's post hoc analysis. Animal survival data were analysed by using the log-rank (Mantel-Cox) test. In the CAE-AP study, n = 10 mice in all groups. In CDE-AP studies, n = 10 mice in all groups. Replicates represent different mice subjected to the same treatment.

4.2.7 Conclusions

In summary, we exploited the susceptibility of MΦs to pancreatitis-associated PLA2 and designed a biomimetic nanoparticle with a 'lure and kill' mechanism for safe and effective

133

inhibition of PLA2. In this design, nanoparticles were made by wrapping with natural MΦ membranes doped with melittin, a PLA2 attractant, and MJ-33, a PLA2 inhibitor. The membrane coating, together with melittin, acts as a decoy to lure PLA2 for enzymatic digestion. Upon the attack, PLA2 is exposed to MJ-33 that effectively kills the enzymatic activity. Such design uses the biomimetic feature of MΦ membrane and further exploits the membrane-binding characteristics of PLA2 attractant and inhibitor. The resulting L&K-NPs eliminate the toxicity associated with the free form of these molecules. When tested in pancreatitis models, L&K-NPs were shown to inhibit PLA2 activity and PLA2-induced pancreatic injury. Their administration into mice with AP showed protective effects against AP-induced inflammation, tissue damage, and lethality. Notably, in different diseases such as cardiovascular disease, cancer, and autoimmune disorders, systemic PLA2 activity is positively correlated with disease severity and PLA2 inhibition is a desirable strategy.[41-43] In atherosclerosis, PLA2 is known to be responsible for remodeling low-density lipoprotein particles, promoting the aggregation of modified lipoproteins and the generation of foam cells.[44] PLA2 modulates cancer cell proliferation through the arachidonic acid metabolic pathway.[42] In autoimmune disorders such as rheumatoid arthritis, cytosolic PLA2 produces precursor for the synthesis of leukotriene and prostaglandin, which are known to contribute to disease progression.[45] Meanwhile, PLA2 isoforms show unique origins, substrate selectivity, and tissue distribution.[12] To address such complexity, L&K-NPs can be formulated by coating with membranes from cells sensitive to specific isoforms [28, 46]. In addition, the cell membrane could be further functionalized with unique compounds that either attract or inhibit PLA2.[47, 48] With such high level of versatility, L&K-NP design can be finely tailored to precisely target a specific PLA2 in the target disease. These design features

together make L&K-NPs a platform technology with superior engineering flexibility as a promising candidate for treating PLA2-mediated diseases.

Chapter 4.2, in full, is a reprint of the material in preparation for submission to *Nature Biomedical Engineering*, 2020, Qiangzhe Zhang, Julia Zhou, Jiarong Zhou, Ronnie H. Fang, Weiwei Gao, and Liangfang Zhang. The dissertation author was the primary author of this manuscript.

4.2.8 References

1. Lee, P.J. and Papachristou, G.L., *New insights into acute pancreatitis.* Nature Reviews: Gastroenterology & Hepatology, 2019. **16**(8): p. 479-496.

2. Manohar, M., Verma, A.K., Venkateshaiah, S.U., Sanders, N.L., and Mishra, A., *Pathogenic mechanisms of pancreatitis.* World journal of gastrointestinal pharmacology and therapeutics, 2017. **8**(1): p. 10-25.

3. Bakker, O.J., Issa, Y., van Santvoort, H.C., Besselink, M.G., Schepers, N.J., Bruno, M.J., Boermeester, M.A., and Gooszen, H.G., *Treatment options for acute pancreatitis.* Nature Reviews: Gastroenterology & Hepatology, 2014. **11**(8): p. 462-469.

4. Krishna, S.G., Kamboj, A.K., Hart, P.A., Hinton, A., and Conwell, D.L., *The Changing Epidemiology of Acute Pancreatitis Hospitalizations A Decade of Trends and the Impact of Chronic Pancreatitis.* Pancreas, 2017. **46**(4): p. 482-488.

5. Besselink, M., van Santvoort, H., Freeman, M., Gardner, T., Mayerle, J., Vege, S.S., Werner, J., Banks, P., McKay, C., Fernandez-Del Castillo, C., French, J., Gooszen, H., Johnson, C., Sarr, M., Takada, T., Windsor, J., Saluja, A., Liddle, R., Papachristou, G., Singh, V., Runzi, M., Wu, B., Singh, V., Bollen, T., Morgan, D., Mortele, K., Mittal, A., En-Qiang, M., de Waele, J., Petrov, M., Dellinger, P., Lerch, M.M., Anderson, R., McClave, S., Hartwig, W., Bruno, M., Oria, A., Baron, T., Fagenholz, P., Horvath, K., van Baal, M., Nealon, W., Andren-Sandberg, A., Bakker, O., Bassi, C., Buchler, M., Boermeester, M., Bradley, E., Chari, S., Charnley, R., Connor, S., Dervenis, C., Deviere, J., Dudeja, V., Fockens, P., Forsmark, C., Friess, H., Isaji, S., Isenmann, R., Klar, E., Levy, P., Lillemoe, K., Liu, X., Lohr, C.M., Mayumi, T., Mossner, J., Neoptolemos, J., Nordback, I., Olah, A., Padbury, R., Parks, R., Radenkovic, D., Rau, B., Rebours, V., Seewald, S., Seifert, H., Shimosegawa, T., Siriwardena, A., Steinberg, W., Sutton, R., Tanaka, M., Takeda, K., Tse, F., van Goor, H., Warshaw, A., Wang, C., Whitcomb, D., Zhao, Y., Zyromski, N., and Working Grp, I.A.P.A.P.A.A., *IAP/APA evidence-based guidelines for the management of acute pancreatitis.* Pancreatology, 2013. **13**(4): p. E1-E15.

6.   Whitcomb, D.C., *Acute pancreatitis.* New England Journal of Medicine, 2006. **354**(20): p. 2142-2150.

7.   Hackert, T. and Werner, J., *Antioxidant Therapy in Acute Pancreatitis: Experimental and Clinical Evidence.* Antioxidants and Redox Signaling, 2011. **15**(10): p. 2767-2777.

8.   Saluja, A.K., Lerch, M.M., Phillips, P.A., and Dudeja, V., *Why does pancreatic overstimulation cause pancreatitis?* Annual Review of Physiology, 2007. **69**: p. 249-269.

9.   Al Mofleh, I.A., *Severe acute pancreatitis: Pathogenetic aspects and prognostic factors.* World Journal of Gastroenterology, 2008. **14**(5): p. 675-684.

10.   Shrivastava, P. and Bhatia, M., *Essential role of monocytes and macrophages in the progression of acute pancreatitis.* World Journal of Gastroenterology, 2010. **16**(32): p. 3995-4002.

11.   Logsdon, C.D. and Ji, B.A., *The role of protein synthesis and digestive enzymes in acinar cell injury.* Nature Reviews: Gastroenterology & Hepatology, 2013. **10**(6): p. 362-370.

12.   Murakami, M., Taketomi, Y., Sato, H., and Yamamoto, K., *Secreted phospholipase A(2) revisited.* Journal of Biochemistry, 2011. **150**(3): p. 233-255.

13.   Browne, G.W. and Pitchumoni, C.S., *Pathophysiology of pulmonary complications of acute pancreatitis.* World Journal of Gastroenterology, 2006. **12**(44): p. 7087-7096.

14.   Elder, A.S.F., Saccone, G.T.P., and Dixon, D.L., *Lung injury in acute pancreatitis: Mechanisms underlying augmented secondary injury.* Pancreatology, 2012. **12**(1): p. 49-56.

15.   Ong, W.-Y., Farooqui, T., Kokotos, G., and Farooqui, A.A., *Synthetic and Natural Inhibitors of Phospholipases A(2): Their Importance for Understanding and Treatment of Neurological Disorders.* Acs Chemical Neuroscience, 2015. **6**(6): p. 814-831.

16.   Nicholls, S.J., Kastelein, J.J.P., Schwartz, G.G., Bash, D., Rosenson, R.S., Cavender, M.A., Brennan, D.M., Koenig, W., Jukema, J.W., Nambi, V., Wright, R.S., Menon, V., Lincoff, A.M., Nissen, S.E., and Investigators, V.-. *Varespladib and Cardiovascular Events in Patients With an Acute Coronary Syndrome The VISTA-16 Randomized Clinical Trial.* Jama-Journal of the American Medical Association, 2014. **311**(3): p. 252-262.

17.   Zeiher, B.G., Steingrub, J., Laterre, P.F., Dmitrienko, A., Fukiishi, Y., Abraham, E., and Grp, E.S., *LY315920NA/S-5920, a selective inhibitor of group IIA secretory phospholipase A(2), fails to improve clinical outcome for patients with severe sepsis.* Critical Care Medicine, 2005. **33**(8): p. 1741-1748.

18.   Zhang, K.J., Zhang, D.L., Jiao, X.L., and Dong, C., *Effect of phospholipase A2 silencing on acute experimental pancreatitis.* European Review for Medical and Pharmacological Sciences, 2013. **17**(24): p. 3279-3284.

19.   Yarla, N.S., Bishayee, A., Vadlakonda, L., Chintala, R., Duddukuri, G.R., Reddanna, P., and Dowluru, K., *Phospholipase A(2) Isoforms as Novel Targets for Prevention and Treatment of Inflammatory and Oncologic Diseases.* Current Drug Targets, 2016. **17**(16): p. 1940-1962.

20.   *Varespladib.* American Journal of Cardiovascular Drugs, 2011. **11**(2): p. 137-143.

21.   Hour, M.J., Tsai, S.C., Wu, H.C., Lin, M.W., Chung, J.G., Wu, J.B., Chiang, J.H., Tsuzuki, M., and Yang, J.S., *Antitumor effects of the novel quinazolinone MJ-33: Inhibition of metastasis through the MAPK, AKT, NF-kappa B and AP-1 signaling pathways in DU145 human prostate cancer cells.* International Journal of Oncology, 2012. **41**(4): p. 1513-1519.

22.   Gowda, R., Dinavahi, S.S., Iyer, S., Banerjee, S., Neves, R.I., Pameijer, C.R., and Robertson, G.P., *Nanoliposomal delivery of cytosolic phospholipase A(2) inhibitor arachidonyl trimethyl ketone for melanoma treatment.* Nanomedicine, 2018. **14**(3): p. 863-873.

23.   Pardeike, J., Schmidt, C., Volz, I., and Mueller, R.H., *Nanostructured lipid carriers as delivery system for the phospholipase A(2) inhibitors PX-18 and PX-13 for dermal application.* Pharmazie, 2011. **66**(5): p. 357-361.

24.   Liu, M.-S., Liu, C.-H., Wu, G., and Zhou, Y., *Antisense inhibition of secretory and cytosolic phospholipase A(2) reduces the mortality in rats with sepsis.* Critical Care Medicine, 2012. **40**(7): p. 2132-2140.

25.   O'Brien, J., Lee, S.-H., Onogi, S., and Shea, K.J., *Engineering the Protein Corona of a Synthetic Polymer Nanoparticle for Broad-Spectrum Sequestration and Neutralization of Venomous Biomacromolecules.* Journal of the American Chemical Society, 2016. **138**(51): p. 16604-16607.

26.   O'Brien, J. and Shea, K.J., *Tuning the Protein Corona of Hydrogel Nanoparticles: The Synthesis of Abiotic Protein and Peptide Affinity Reagents.* Accounts of Chemical Research, 2016. **49**(6): p. 1200-1210.

27.   Zhou, X., Cao, X., Tu, H., Zhang, Z.R., and Deng, L., *Inflammation-Targeted Delivery of Celastrol via Neutrophil Membrane-Coated Nanoparticles in the Management of Acute Pancreatitis.* Molecular Pharmaceutics, 2019. **16**(3): p. 1397-1405.

28.   Thamphiwatana, S., Angsantikul, P., Escajadillo, T., Zhang, Q., Olson, J., Luk, B.T., Zhang, S., Fang, R.H., Gao, W., Nizet, V., and Zhang, L., *Macrophage-like nanoparticles concurrently absorbing endotoxins and proinflammatory cytokines for sepsis management.* Proc Natl Acad Sci U S A, 2017. **114**(43): p. 11488-11493.

29. Hu, C.-M.J., Fang, R.H., Copp, J., Luk, B.T., and Zhang, L., *A biomimetic nanosponge that absorbs pore-forming toxins.* Nature Nanotechnology, 2013. **8**(5): p. 336-340.

30. Hu, C.M., Zhang, L., Aryal, S., Cheung, C., Fang, R.H., and Zhang, L., *Erythrocyte membrane-camouflaged polymeric nanoparticles as a biomimetic delivery platform.* Proc Natl Acad Sci U S A, 2011. **108**(27): p. 10980-5.

31. Jakkampudi, A., Jangala, R., Reddy, B.R., Mitnala, S., Nageshwar Reddy, D., and Talukdar, R., *NF-kappaB in acute pancreatitis: Mechanisms and therapeutic potential.* Pancreatology, 2016. **16**(4): p. 477-88.

32. Tsukahara, Y., Morisaki, T., Horita, Y., Torisu, M., and Tanaka, M., *Phospholipase A(2) mediates nitric oxide production by alveolar macrophages and acute lung injury in pancreatitis.* Annals of Surgery, 1999. **229**(3): p. 385-392.

33. Kaiser, A.M., Saluja, A.K., Sengupta, A., Saluja, M., and Steer, M.L., *Relationship between severity, necrosis, and apoptosis in 5 models of experimental acute-pancreatitis.* American Journal of Physiology: Cell Physiology, 1995. **269**(5): p. C1295-C1304.

34. Jacob, T.G., Raghav, R., Kumar, A., Garg, P.K., and Roy, T.S., *Duration of injury correlates with necrosis in caerulein-induced experimental acute pancreatitis: implications for pathophysiology.* International Journal of Experimental Pathology, 2014. **95**(3): p. 199-208.

35. Schmidt, J., Lewandrowski, K., Castillo, C.F., Mandavilli, U., Compton, C.C., Warshaw, A.L., and Rattner, D.W., *Histopathologic correlates of serum amylase activity in acute experimental pancreatitis.* Digestive Diseases and Sciences, 1992. **37**(9): p. 1426-1433.

36. Makela, A., Kuusi, T., Nuutinen, P., and Schroder, T., *Phospholipase A2 activity in body fluids and pancreatic tissue in patients with acute necrotising pancreatitis.* European Journal of Surgery, 1999. **165**(1): p. 35-42.

37. Ren, Z., Li, H., Zhang, M., Zhao, Y., Fang, X., Li, X., Chen, W., Zhang, H., Wang, Y., Pan, L.-L., and Sun, J., *A Novel Derivative of the Natural Product Danshensu Suppresses Inflammatory Responses to Alleviate Caerulein-Induced Acute Pancreatitis.* Frontiers in Immunology, 2018. **9**: p. 2513.

38. Niederau, C., Luthen, R., Niederau, M.C., Grendell, J.H., and Ferrell, L.D., *Acute experimental hemorrhagic-necrotizing pancreatitis induced by feeding a choline-deficient, ethionine-supplemented diet. Methodology and standards.* European Surgical Research, 1992. **24**: p. 40-54.

39. Noursadeghi, M., Tsang, J., Haustein, T., Miller, R.F., Chain, B.M., and Katz, D.R., *Quantitative imaging assay for NF-kappaB nuclear translocation in primary human macrophages.* J Immunol Methods, 2008. **329**(1-2): p. 194-200.

40.   Lombardi, B., Estes, L.W., and Longnecker, D.S., *Acute hemorrhagic pancreatitis (massive necrosis) with fat necrosis induced in mice by DL-ethionine fed with a choline-deficient diet.* American Journal of Pathology, 1975. **79**(3): p. 465-480.

41.   Cook, N.R., Paynter, N.P., Manson, J.E., Martin, L.W., Robinson, J.G., Wassertheil-Smoller, S., and Ridker, P.M., *Clinical Utility of Lipoprotein-Associated Phospholipase A(2) for Cardiovascular Disease Prediction in a Multiethnic Cohort of Women.* Clinical Chemistry, 2012. **58**(9): p. 1352-1363.

42.   Scott, K.F., Sajinovic, M., Hein, J., Nixdorf, S., Galettis, P., Liauw, W., de Souza, P., Dong, Q.H., Graham, G.G., and Russell, P.J., *Emerging roles for phospholipase A(2) enzymes in cancer.* Biochimie, 2010. **92**(6): p. 601-610.

43.   Cunningham, T.J., Yao, L.H., Oetinger, M., Cort, L., Blankenhorn, E.P., and Greenstein, J.I., *Secreted phospholipase A2 activity in experimental autoimmune encephalomyelitis and multiple sclerosis.* Journal of Neuroinflammation, 2006. **3**.

44.   Talmud, P.J. and Holmes, M.V., *Deciphering the Causal Role of sPLA2s and Lp-PLA2 in Coronary Heart Disease.* Arteriosclerosis Thrombosis and Vascular Biology, 2015. **35**(11): p. 2281-2289.

45.   Leslie, C.C., *Thematic Review Series: Phospholipases: Central Role in Lipid Signaling and Disease Cytosolic phospholipase A(2) : physiological function and role in disease.* Journal of Lipid Research, 2015. **56**(8): p. 1386-1402.

46.   Zhang, Q., Dehaini, D., Zhang, Y., Zhou, J.L., Chen, X.Y., Zhang, L.F., Fang, R.H., Gao, W., and Zhang, L., *Neutrophil membrane-coated nanoparticles inhibit synovial inflammation and alleviate joint damage in inflammatory arthritis.* Nature Nanotechnology, 2018. **13**(12): p. 1182-+.

47.   Kokotou, M.G., Limnios, D., Nikolaou, A., Psarra, A., and Kokotos, G., *Inhibitors of phospholipase A(2) and their therapeutic potential: an update on patents (2012-2016).* Expert Opinion on Therapeutic Patents, 2017. **27**(2): p. 217-225.

48.   Mingarro, I., Perezpaya, E., Pinilla, C., Appel, J.R., Houghten, R.A., and Blondelle, S.E., *Activation of bee venom phospholipase A(2) through a peptide-enzyme complex.* Febs Letters, 1995. **372**(1): p. 131-134.

Chapter 5
Conclusions

5.1 Neutrophil membrane-coated nanoparticles suppress synovial inflammation and ameliorate joint destruction in inflammatory arthritis

This chapter covered the design, synthesis, and characterization of a biomimetic nanodecoy as a broad-spectrum anti-inflammatory therapy against inflammatory arthritis. By fusing neutrophil membrane onto polymeric cores, we prepared neutrophil membrane-coated nanoparticles that inherit the antigenic exterior and associated membrane functions of the source cells, which made them ideal decoys of neutrophil-targeted biological molecules. We showed that these nanoparticles could neutralize proinflammatory cytokines, suppress synovial inflammation, target deep into the cartilage matrix, and provide strong chondroprotection against joint damage. Using a classic mouse model of collagen-induced arthritis and a human transgenic mouse model of arthritis, the neutrophil membrane-coated nanoparticles showed significant efficacy by ameliorating joint damage and suppressing overall arthritis severity. Overall, this work extends cell membrane-coated detoxification platforms from erythrocytes to neutrophils, a type of leukocyte, for function-driven detoxification in the treatment of inflammatory disorders. This application of nanoengineering in anti-inflammatory therapy holds great potential for application in other inflammatory diseases driven by similar inflammatory pathways. The abundance of neutrophils in human peripheral blood warrants excellent translational prospect of this work to become a personalized and effective inflammation mitigation strategy.

5.2 Macrophage-like nanoparticles concurrently absorbing endotoxins and proinflammatory cytokines for sepsis management

This chapter reported the development of a macrophage-like biomimetic nanoaprticles for the management of sepsis. Sepsis, resulting from uncontrolled inflammatory responses to bacterial infections, continues to cause high morbidity and mortality worldwide. Currently, effective sepsis treatments are lacking in the clinic, and care remains primarily supportive. We prepared macrophage-like nanoparticles by wrapping polymeric cores with cell membrane derived from macrophages. The resulting nanoparticles acted as macrophage decoys to bind and neutralize endotoxins that would otherwise trigger immune activation. In addition, these macrophage-like nanoparticles sequestered proinflammatory cytokines and inhibited their ability to potentiate the sepsis cascade. In a mouse Escherichia coli bacteremia model, treatment with macrophage mimicking nanoparticles reduced proinflammatory cytokine levels, inhibited bacterial dissemination, and ultimately conferred a significant survival advantage to infected mice. Overall, this work demonstrates the versatility of leukocyte membrane-coated nanodecoys for function-driven anti-inflammatory therapy. Employing these macrophage-like nanoparticles as a biomimetic detoxification strategy shows promise for improving patient outcomes, potentially shifting the current paradigm of sepsis management.

5.3 A biomimetic nanoparticle to 'lure and kill' phospholipase A2

This chapter presented a unique biomimetic nanoparticle specifically designed to 'lure and kill' phospholipase A2. Inhibition of PLA2 has long been considered promising to treat various diseases associated with an elevated activity of PLA2. However, safe and effective PLA2 inhibitors remain unavailable. In the first section of this chapter, we report a biomimetic nanoparticle design that enables a 'lure and kill' mechanism designed for PLA2 inhibition (denoted 'L&K-NP'). Specifically, the L&K-NPs are made with polymeric cores wrapped with modified red blood cell membrane that is inserted with two key components: melittin and oleyloxyethyl phosphorylcholine (OOPC). Melittin acts as a PLA2 attractant that works together with the membrane lipids to 'lure' in-coming PLA2 for attack. Meanwhile, OOPC acts as an inhibitor that 'kills' PLA2 upon the enzymatic attack. Both compounds are integrated into L&K-NP structure, which voids toxicity associated with free molecules. In the study, L&K-NPs effectively inhibit PLA2-induced hemolysis. In mice administered with a lethal dose of venomous PLA2, L&K-NPs also inhibit hemolysis and confer a significant survival benefit. Furthermore, L&K-NPs show no obvious toxicity in mice. Overall, L&K-NP design provides a platform technology for a safe and effective anti-PLA2 approach.

Encouraged by the results in the first generation of L&K-NP, we adopted this design strategy towards inhibition of inflammatory PLA2 in acute pancreatitis (AP). AP is a disease associated with a high lethality and great suffering. However, the disease mechanism remains elusive and treatment options for AP are limited. In this section, biomimetic nanoparticles were leveraged to treat AP through their cell membrane coating and a built-in 'lure and kill' mechanism (denoted "L&K-NPs"). Specifically, L&K-NPs were made with polymeric cores wrapped with

natural macrophage membrane. The cell membrane was inserted with two key components: melittin and MJ-33. Melittin acts as a PLA2 attractant that works together with the membrane lipids to 'lure' in PLA2 for attack. Meanwhile, MJ-33 acts as an inhibitor that 'kills' PLA2 upon the enzymatic attack. Both compounds were integrated into the L&K-NP structure, which voided the toxicity associated with their free forms. L&K-NPs were shown to inhibit PLA2 activity in the sera of mice and human patients with acute pancreatitis. In mouse models of mild and severe acute pancreatitis, L&K-NPs conferred protection against AP-associated inflammation, tissue damage, and lethality. Overall, L&K-NP nanomedicine platform offers an anti-PLA2 approach with potential of treating various inflammatory disorders.